School of Doctoral Studies in Biological Sciences

University of South Bohemia in České Budějovice

Faculty of Science

Biology of the Mitochondrial Contact Site and Cristae Organizing System in Trypanosomatids

Ph.D. Thesis

Iosif Kaurov

Supervisor: Doc. Hassan Hashimi, Ph.D.

Biology Centre, Institute of Parasitology, Czech Academy of Sciences, and

University of South Bohemia, Faculty of Sciences, České Budějovice, Czech Republic

České Budějovice 2019

This thesis should be cited as: Kaurov I., 2019: Biology of the Mitochondrial Contact Site and Cristae Organizing System in Trypanosomatids. Ph.D. Thesis. University of South Bohemia, Faculty of Science, School of Doctoral Studies in Biological Sciences, České Budějovice, Czech Republic.

Annotation

This study describes Mitochondrial Contact Site and Cristae Organization System (MICOS) in unicellular parasitic protist *Trypanosoma brucei*. This is the first study of MICOS outside of canonical model organisms belonging to the supergroup Opisthokonta. Nine subunits of the complex were purified and characterized. Their role in cristae biogenesis and interaction with other mitochondrial protein complexes was demonstrated. Further investigation revealed a hierarchical organization of *T. brucei* MICOS and the existence of two subcomplexes. One of MICOS subunits, TbMic20, facilitates protein import into mitochondrial intermembrane space, which is one of the novel features of *T. brucei* MICOS. The role of TbMic20 in oxidative protein folding was demonstrated and the mechanism of this process in *T. brucei* was addressed.

Declaration

I hereby declare that I did all the work presented in this thesis by myself or in collaboration with co-authors of the presented papers and only using the cited literature.

České Budějovice, ... Iosif Kaurov

PROHLÁŠENÍ

Prohlašuji, že svoji disertační práci jsem vypracoval samostatně pouze s použitím pramenů a literatury uvedených v seznamu citované literatury.

Prohlašuji, že v souladu s § 47b zákona č. 111/1998 Sb. v platném znění souhlasím se zveřejněním své disertační práce, a to v úpravě vzniklé vypuštěním vyznačených částí archivovaných Přírodovědeckou fakultou elektronickou cestou ve veřejně přístupné části databáze STAG provozované Jihočeskou univerzitou v Českých Budějovicích na jejích internetových stránkách, a to se zachováním mého autorského práva k odevzdanému textu této kvalifikační práce. Souhlasím dále s tím, aby toutéž elektronickou cestou byly v souladu s uvedeným ustanovením zákona č. 111/1998 Sb. zveřejněny posudky školitele a oponentů práce i záznam o průběhu a výsledku obhajoby kvalifikační práce. Rovněž souhlasím s porovnáním textu mé kvalifikační práce s databází kvalifikačních prací Theses.cz provozovanou Národním registrem vysokoškolských kvalifikačních prací a systémem na odhalování plagiátů.

České Budějovice, ... Iosif Kaurov

This thesis originated from a partnership between the Faculty of Science, University of South Bohemia, and Institute of Parasitology, Biology Centre of the Czech Academy of Sciences, supporting doctoral studies in the Molecular and Cell biology and Genetics study program.

Přírodovědecká
fakulta
Faculty
of Science

INSTITUTE OF PARASITOLOGY
Biology Centre CAS

Financial support

This work was supported by Grant agency of the University of South Bohemia in České Budějovice (grant 046/2016/P to Iosif Kaurov), Czech Science Foundations grants 17-24036S to Hassan Hashimi and 16-18699S to Julius Lukeš. This work was also supported by project Centre for research of pathogenicity and virulence of parasites r.n.: CZ.02.1.01/0.0/0.0/16_019/0000759, funded by the European Regional Development Fund (ERDF) and the Ministry of Education, Youth and Sport, Czech Republic (MEYS). We obtained the group research grant 147/2016/P from the Grant Agency of the University of South Bohemia. A travel stipend 103-2110 RVO from the Department of molecular biology and genetics, travel grant S201907 from the Biology Centre of the Czech Academy of Science were awarded to Iosif Kaurov.

Acknowledgements.

During my work on the thesis I got help from many people. First of all, I would like to thank my supervisor Hassan Hashimi. He helped me from the time I performed the first Western blot in the lab to the last steps in preparation of the thesis. He put lot of time and effort into my progress as a scientist and was always ready to discuss any problem I had. “My door is always open”, he used to say. The level of his time management skills and attention to small details is something I hope to approach one day.

Thanks to Julius Lukeš I got the opportunity to start this long way of Ph.D. student in his laboratory. His passion to science and personal charisma are well-known. He encouraged everybody, especially us students, to work hard, but also was eager to participate in team-building informal recreation. He made his lab a desired place to work at. Thank you, Julius, for your friendliness and support.

Recently I was lucky enough to visit the laboratory of Prof. André Schneider in the University of Bern. I thank him and all his team for the warm welcome and for giving me the opportunity to improve my skills in this excellent lab. I especially thank Moritz Niemann and Bernd Schimanski who taught me some of the sophisticated techniques they utilize.

I thank the members of our small MICOS group, especially Jiři Heller and L. Rudy Cadena, for excellent collaboration we have. I also thank all other members of our “Tritryp lab” for their help and positive atmosphere.

List of papers and author's contribution

The thesis is based on the following papers (listed chronologically):

I. Kaurov, I., Vancová, M., Schimanski, B., Cadena, L.R., Heller, J., Bílý, T., Potěšil, D., Eichenberger, C., Bruce, H., Oeljeklaus, S., Warscheid, B., Zdráhal, Z., Schneider, A., Lukeš, J., Hashimi, H., 2018. The Diverged Trypanosome MICOS Complex as a Hub for Mitochondrial Cristae Shaping and Protein Import. Current Biology 28, 3393-3407.e5. https://doi.org/10.1016/j.cub.2018.09.008

Iosif Kaurov participated in cell cultivation, producing genetically changed cell lines, crude mitochondria preparation, observations on light and electron microscope, immunoprecipitation experiments, cell growth rate measurements, proteinase K protection assays.

II. Eichenberger, C., Oeljeklaus, S., Bruggisser, J., Mani, J., Haenni, B., Kaurov, I., Niemann, M., Zuber, B., Lukeš, J., Hashimi, H., Warscheid, B., Schimanski, B., Schneider, A., 2019. The highly diverged trypanosomal MICOS complex is organized in a nonessential integral membrane and an essential peripheral module. Molecular Microbiology mmi.14389. https://doi.org/10.1111/mmi.14389

Iosif Kaurov participated in cell cultivation and isotonic mitochondria isolation, performed the synthesis of radiolabeled import substrates and in vitro import assay.

III. Thioredoxin-like MICOS subunit TbMic20 promotes intermembrane space protein import (unpublished study).

Iosif Kaurov designed the constructs for expression of TbMic20 isoforms, produced transgenic cell lines, performed cell cultivation and growth rate measurements, Western blotting, data analysis.

Doc. Hassan Hashimi, Ph.D. _____

Table of Contents

Abbreviations:

ER – endoplasmic reticulum

IM – inner membrane

OM – outer membrane

IBM – inner boundary membrane

CS – contact sites

CJ – crista junction

IMS – intermembrane space

LECA – last eukaryotic common ancestor

TOM – translocase of the outer mitochondrial membrane

SAM – sorting and assembly machinery

MIB - mitochondrial intermembrane space bridging complex

VDAC – voltage dependent anion channel

PAM – presequence translocase-associated motor

CL – cardiolipin

OXPHOS – oxidative phosphorylation

ETC – electron transport chain

ROS – reactive oxygen species

GSH – glutathione

GSSG – glutathione disulfide

GRX – glutaredoxin

MICOS – mitochondrial contact site and cristae organizing system

MISS/ITS – mitochondrial IMS sorting/IMS targeting signal

ERV – essential for respiration and viability

MIA – mitochondrial sorting and assembly machinery

Summary.

The mitochondrion is an organelle of endosymbiotic origin. The acquisition of mitochondria happened before the divergence of modern eukaryotes. Since that remote symbiogenesis event, the integration of former alphaproteobacterium into the host cell had gone very far. For instance, mitochondria lost most of their genome and became dependent on the import of proteins encoded in the nucleus and translated in the cytosol. On the other hand, performing oxidative phosphorylation and many other indispensable functions, mitochondria are vitally important for virtually all eukaryotic organisms.

Nearly all existing knowledge about mitochondria has been obtained from a few opisthokont (*e.g.* animals and fungi) and plant species. Studies presented in this thesis were performed on the excavate *Trypanosoma brucei*. This unicellular parasite is easily cultivated and genetically manipulated. Knowledge obtained from this distant relative of more common model species can broaden our understanding of mitochondrial biogenesis and organelle evolution.

The thesis comprises an introduction and three chapters. In the introduction relevant information about mitochondrial morphology and biochemistry is summarized. Two main aspects of mitochondrial biogenesis are discussed more in-depth, namely cristae biogenesis, organized by MICOS complex, and mitochondrial protein import. The peculiarities of *Trypanosoma brucei* as a model species are also addressed in the introduction.

The first chapter represents our study of MICOS complex in *T. brucei*. TbMICOS consists of nine subunits, most of which are not present in opisthokonts. Their localization and depletion phenotypes on morphology and cell viability were addressed. The characterized TbMICOS revealed some conserved features, such as crucial role in cristae biogenesis and interaction with TbSAM50, a protein responsible for protein insertion into the mitochondrial outer membrane. Among the unexpected findings was the role of a thioredoxin-like subunit named TbMic20 in the import of intermembrane space (IMS) proteins (Kaurov *et al.*, 2018, Curr. Biol.).

In the second chapter interactions within TbMICOS complex are thoroughly studied and the hierarchy of subunits is revealed. TbMICOS consists of two subcomplexes, similar to opisthokont MICOS. However, TbMICOS subcomplexes are organized in a different way. The network of several integral inner membrane proteins is likely responsible for cristae formation, and the subcomplex of peripheral proteins, which includes TbMic20, maintains mitochondrial

protein import. The role of TbMic20 in protein import was directly addressed *in vitro* (Eichenberger *et al.*, 2019, Mol. Microbiol.).

In the third chapter the mechanism of how TbMic20 promotes intermembrane space protein import was addressed. TbMic20 has CIPC motif, which we hypothesize is a functional analog of the CPC motif in opisthokont oxidoreductase Mia40. Mutations of the cysteine residues in the CIPC motif affected cell viability and IMS protein import. In another experiment, TbMic20 targeted to bacterial periplasm was able to complement deletion of *dsbA*, an oxidoreductase that folds proteins in the periplasm. These experiments support our hypotheses that TbMic20 may be a Mia40 analog and shed light on the mechanism it performs protein import (unpublished study).

Aims of the study:

- Immunopurification of TbMic10 paralog interaction partners from the mitochondria of *T. brucei*.
- Determination of submitochondrial localization of TbMICOS subunits.
  Functional analysis of TbMICOS: characterization of TbMICOS subunit depletion phenotypes.
- Reveal interactions with mitochondrial proteins that are not part of MICOS, *e.g.* Sam50. Define the subcomplex architecture of TbMICOS. Demonstrate TbMic20 import activity *in vitro* and *in vivo*.
- Investigate the role of the CIPC motif of TbMic20 in the IMS protein import.
- Determine whether TbMic20 is truly an analog of Mia40, the central catalyst of the IMS protein
- Test TbMic20 capacity for oxidative protein folding in the periplasm of the alphaproteobacterium *E. coli*.

1. Introduction

1.1. General information about mitochondria

1.1.1. Key points in mitochondria research

Mitochondria were discovered in the mid-1800s, not long after the discovery of the nuclei (Flemming, 1882). Already early observations by light microscopy suggested that mitochondria were membrane-bound (Ernster and Schatz, 1981). By the end of the 19th century, mitochondria were recognized as the structures of ubiquitous occurrence and the name mitochondrion was introduced (Benda, 1898). Their resemblance to bacteria inspired the first suggestions about their endosymbyotic origin (Altmann, 1890). In 1930s, the first purifications of mitochondria by differential centrifugation were performed (Bensley and Hoerr, 1934). The development of purification methods facilitated functional and biochemical studies of mitochondria. It was subsequently demonstrated that mitochondria contain enzymes needed for respiration and the respiratory chain was reconstituted (Hatefi et al., 1962; Keilin and King, 1958).

The implementation of electron microscopy techniques allowed observation of mitochondrial ultrastructure in the early 1950s. Already the first high resolution electron micrographs of the organelle revealed membrane folds and the existence of double membrane around the organelle (Palade, 1952; Sjostrand, 1953). The inner membrane folds were initially named cristae mitochondriales (Palade, 1952). Two important discoveries were made in 1960's: both DNA (Nass, 1963) and ribosomes similar to those of bacteria (Kuntzel and Noll, 1967) were found in the mitochondria. These findings revitalized the endosymbiotic hypothesis (Sagan, 1967). Sequencing of the first mitochondrial genome in 1981 was a major achievement at that time (Anderson et al., 1981). Years later, the genome of alphaproteobacterium *Rickettsia prowazekii*, the obligate intracellular parasite that is the causative agent of the epidemic typhus, was sequenced (Andersson et al., 1998). Comparison of the obtained sequence with mitochondrial genome revealed a high degree of similarity between them, indicating alphaproteobacteria are the closest relatives of mitochondria.

1.1.2. The origin of mitochondria

Nowadays the origin of mitochondria through the integration of an alphaproteobacterial endosymbiont in a host cell of archaeal origin is undoubted (Archibald, 2015; Gray, 2012). Despite the general acceptance of endosymbiotic theory, some of its aspects remain disputable, even to this day (Koonin, 2010). Initially, it was not absolutely clear whether all modern eukaryotes primarily possessed mitochondria. Certain organelles (mitosomes, hydrogenosomes) found in anaerobic protists were not always recognized as homologs of mitochondria and sometimes overlooked (Lindmark and Muller, 1973; Tovar et al., 2003). With the accumulation of genomic and proteomic data, the monophyletic origin of mitochondria, mitosomes and other similar organelles was demonstrated (Gray, 2012). Thus, the common ancestor of all modern eukaryotes possessed mitochondria. The only truly amitochondriate eukaryote *Monocercomonoides sp*. observed thus far is most probably an example of the secondary loss of the organelle (Karnkowska et al., 2016).

Some controversy still exists about the timing of the endosymbiotic event. Two competing scenarios exist, the archezoan and the symbiogenesis hypotheses (Koonin, 2010). The archezoan hypothesis claims that by the time of the acquisition of the mitochondrion, the host of archaeal ancestry gained significant complexity, perhaps it was a primitive amitochondrial eukaryote. The symbiogenesis scenario postulates that uptake of the alphaproteobacterial symbiont predated and caused subsequent compartmentalization and evolution of the nucleus. The symbiogenesis scenario has strong support (Gray, 2012; Koonin, 2010), though full consensus is not yet achieved (Pittis and Gabaldón, 2016). Recent success in isolation of an Asgard archaeon allowed the study of its morphology and metabolism (Imachi et al., 2019). Asgard archaea are considered to share common ancestry with eukaryotes (Zaremba-Niedzwiedzka et al., 2017). The obtained data allowed the authors to propose a new evolutionary model for eukaryogenesis from archaea. This Entangle-Engulf-Enslave (E^3) model suggests the syntrophic interaction of an archaeon with O_2-scavenging pre-mitochondrial alphaproteobacterium. Physical interaction of the archaeon with alphaproteobacterium through membrane vesicles and protrusions led to engulfment of the latter and emergence of pre-LECA symbiotic organism. ATP generation was delegated to alphaproteobacterium as the symbiotic relationship maturated and the symbiont was gradually becoming an organelle (Imachi et al., 2019). A third syntrophic organism, a sulphate-reducing bacterium, participated in this symbiosis but was not engulfed.

1.1.3. Basic description of function and structure of mitochondria

1.1.3.1. Gross morphology and integration into the cell

Usually mitochondria in diverse eukaryotes are numerous tubular-like structures, often interconnected and forming a network. The degree of fragmentation and branching of the mitochondria depends on the balance between fission and fusion in these highly dynamic organelles (Zhao et al., 2013). Besides fission and fusion, mammalian mitochondria are able to move in the cytosol by interacting with microtubules (Campello and Scorrano, 2010) or intermediate filaments (Summerhayes et al., 1983). In yeast, mitochondria are tethered to actin filaments, unlike in mammals and other multicellular eukaryotes (Simon et al., 1995).

Another organelle that mitochondria interact with tightly is the endoplasmic reticulum (ER) (Wu et al., 2018). The existence of these mitochondria-ER contacts was detected during electron microscopy observations (Perkins et al., 1997), and the interaction between two organelles was supported biochemically (Voelker, D. R., 1990). These sites of close proximity between mitochondria and the ER are important for lipid transport and biosynthesis (Phillips and Voeltz, 2016; Voelker, D. R., 1990). The ER is also involved in mitochondrial fission and fusion in plants, yeast and mammals (Friedman et al., 2011; Jaipargas et al., 2015; Murley et al., 2013). A third function of mitochondria-ER interactions is Ca^{2+} transmission from ER to mitochondria (de Brito and Scorrano, 2010). The Ca^{2+} level regulates the activity of enzymes involved in mitochondrial metabolism, such as α-ketoglutarate, isocitrate dehydrogenases and pyruvate dehydrogenase of the citric acid cycle. Mobilization of Ca^{2+} from ER to mitochondria plays a role in apoptosis (Szalai et al., 1999).

1.1.3.2. Basic compartments of the mitochondrion

The inner membrane (IM) separates the inner volume of the mitochondrion into the intermembrane space (IMS) and matrix (Fig. 1). The part of the IM parallel to the OM and not folded within cristae is named the inner boundary membrane (IBM).

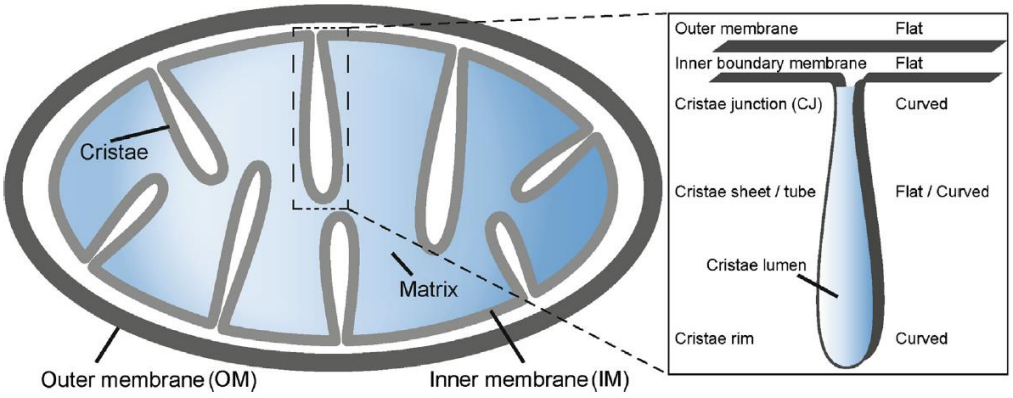

Fig. 1. Schematic illustration of mitochondrial ultrastructure (Barbot and Meinecke, 2016).

The inner volume of a crista is referred to as crista lumen or intracrista space. Initially after their discovery, cristae were considered to be simple invaginations in the mitochondrial IM (Palade, G. E., 1953). At the same time the model of cristae as a closed space without any connection to the IM was proposed (Sjostrand, 1953). A compromise model suggested a connection with the IM by thin tubules called "*pediculi cristae*" (Daems and Wisse, 1966). Electron microscopy at that time could not help to resolve this debate. The implementation of electron tomography finally and definitively demonstrated the presence of thin ~20 nm in the diameter tubular connections of cristae with the IM. They were named crista junctions (Perkins et al., 1997). A lamellar crista can possess more than one crista junction. Bridges exist between IM and OM, named contact sites (CS) that become apparent after treatment of isolated mitochondria with hypertonic buffer and consequent shrinking of the IM (Hackenbrock, 1968; Harner et al., 2011). The existence of CS was also demonstrated biochemically when the translocases of the OM and IM were co-purified together with imported preprotein (Dekker, 1997). It was shown that some CS do not overlap with CJs (Perkins et al., 1997), although there is evidence that CJs do also contact OM (Harner et al., 2011).

1.1.3.3. Mitochondrial composition and metabolism

IM and OM are composed of phospholipid bilayers that proteins, ions and water molecules cannot cross. Pores are needed to allow protein import and metabolite exchange between mitochondria and the cytosol. The OM is rich with β-barrel proteins such as porins (TOM40, SAM50), which allow unrestricted diffusion of molecules up to ~5 kDa.

The IM isolates the matrix space completely so that even small molecules and ions cannot diffuse through it without the participation of protein carriers. Also the IM is exceptionally protein rich, with the protein: lipid ratio approximately 3:1 (Ardail et al., 1990).
Non-bilayer forming phospholipids, such as phosphatidylethanolamine or the glycerophospholipid cardiolipin (CL), also play important role in the mitochondrial function and biogenesis (Barbot and Meinecke, 2016; Gohil et al., 2005; Osman et al., 2011). CL is considered the signature phospholipid of the mitochondria, and in particular, the IM. CL is present mostly in the IM (Gebert et al., 2009). Cardiolipin was stably co-purified with complex V (Eble, K. S et al., 1990) and is considered essential for the assembly or maintenance of respiratory complexes (Schlame and Haldar, 1993). Respiratory complexes tend to aggregate and form supercomplexes in mitochondria. Supercomplex formation is dependent on CL (Bazán et al., 2013). CL is also involved in membrane bending and therefore is one of the factors defining cristae morphology (Huang and Ramamurthi, 2010).

1.1.3.4. OXPHOS and respiratory chain

The best known mitochondrial function is the production of ATP by oxidative phosphorylation (OXPHOS). It is performed by several multiprotein complexes, integrated into the crista membrane (Davies and Daum, 2013). The electron carrier NADH brings electrons produced by the tricarboxylic acid (TCA) cycle to NADH-ubiquinone oxidoreductase (complex I) of the respiratory chain (Fig. 2). The lipophilic electron carrier ubiquinol transfers electrons to cytochrome *c* reductase (complex III). The only soluble electron carrier cytochrome *c* is responsible for the electron flow between complex III and complex IV (cytochrome *c* oxidase). Additional electrons enter the ETC through complex II (succinate dehydrogenase), also a part of the TCA cycle. The final electron acceptor is the oxygen (Kühlbrandt, 2015). The energy of electrons moving along the respiratory chain is used for pumping protons from the matrix into the IMS by complexes I, III and IV. The proton gradient is created across the IM. Potential energy, accumulated in proton motive force, is utilized by F_1-F_O ATP synthase (complex V) for ATP synthesis.

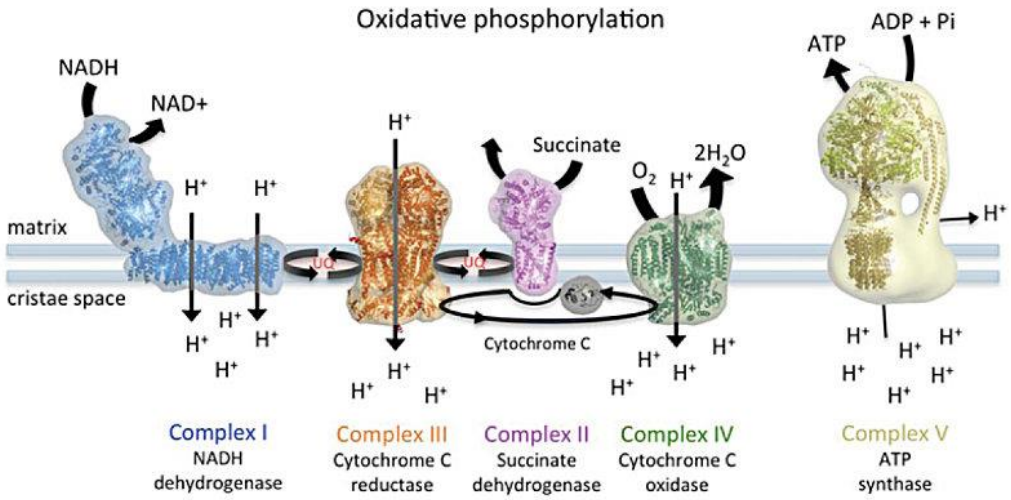

Fig. 2. Electron transport chain in mitochondria (Davies and Daum, 2013).

The respiratory chain, especially complexes I and III, produce reactive oxygen species (ROS) as a byproduct. The most abundant ROS species is the superoxide anion (O_2^-), which is rapidly converted into hydrogen superoxide H_2O_2, spontaneously and enzymatically, by superoxide dismutase SOD1 (Herrmann and Riemer, 2010; Murphy, 2009). ROS, especially H_2O_2, are signaling molecules, but can also be toxic byproducts capable of damaging proteins and lipids. Several protective systems exist in the IMS, including glutathione redox buffer, cytochrome *c* peroxidase and superoxide dismutase (Herrmann and Riemer, 2010).

Glutathione (GSH) is the most important redox regulator in eukaryotes (Schafer and Buettner, 2001). During its interaction with ROS, GSH is oxidized to glutathione disulfide (GSSG). To restore the reduced state of GSSG, glutathione reductase and several other enzymes are utilized, including glutaredoxin (GRX) (Herrero et al., 2006) and thioredoxin (Pedrajas et al., 1999). The GSH:GSSH ratio defines the redox state of a given compartment.

1.1.3.5 Cristae, their shape and function

The majority of the aerobic mitochondria possess cristae (Muñoz-Gómez et al., 2015a). Variable shapes of cristae were traditionally classified into tubular, discoidal and lamellar morphologies (Taylor, 1999). Both lamellar and discoidal cristae are flattened; discoidal ones are usually

described as flat with pinched bases or paddle-like. Tubular cristae may be long or bleb-shaped and may be branching. The shape of CJ opening is predominantly tubular, though slot-like shapes were also detected in yeast (Davies et al., 2011). Attempts were made to use cristae morphology to distinguish large systematic groups of eukaryotes (Cavalier-Smith, 1997; Taylor, 1999). The development of phylogenomics and accumulation of ultrastructural data proved that no correlation exists between cristae shape and the species position on the tree of life (Muñoz-Gómez et al., 2015a). Moreover, variations in cristae shape were shown to exist within different tissues in the same organism, such as humans (Vafai and Mootha, 2012; Zick et al., 2009).

The shape of cristae membrane is defined by several membrane-bending agents. Strong positive curvature at crista rims is produced by oligomers of complex V. For negative curvature observed at cristae junctions, MICOS subunits are responsible, described in-depth in chapter 2.2. Aforementioned CL forms dimers of conical shape, which, embedded into the IM, cause negative curvature. CL can influence cristae morphology directly, bending IM at CJs together with MICOS, or indirectly, playing a role in stabilizing MICOS sub-complexes (Barbot and Meinecke, 2016). One more protein involved in orchestrating mitochondrial morphology in metazoans is Opa1. It is responsible for cristae remodeling during apoptosis (Frezza et al., 2006). Mutations in OPA1 result in distorted cristae structure and impaired respiratory function (Agier et al., 2012). If the respiration impairment reveals the role of OPA1 in arranging respiratory complexes or it is the secondary effect of cristae shape alterations, is not yet clear (Cogliati et al., 2016). One more function of OPA1 is mediating IM fusion. This also has relation to cristae shape, since it was shown that yeast lamellar cristae are formed in the process of mitochondrial fusion (Harner et al., 2016). Yeast have functional analog of Opa1, named Mgm1, which is required for mitochondrial fusion and maintenance of cristae (Meeusen et al., 2006). The formation of tubular cristae is independent from mitochondrial fusion, but both processes require complex V dimers and MICOS subunits (Harner et al., 2016).

Controversy existed about the degree of separation of crista lumen from the rest of the IMS and the IMS from the cytosol. Some predominantly *in vitro* studies indicate that in spite of the presence of porins the OM is not fully penetrable even for small molecules (Herrmann and Riemer, 2010). Studies exist claiming that the pH in the IMS may differ from that of the cytosol (Porcelli et al., 2005) and the redox environment in the IMS is more oxidizing than in the cytosol

or matrix (Hu et al., 2008). On the other hand, it was demonstrated that glutathione pools of the IMS and cytosol are interconnected, unlike the IMS and matrix (Kojer et al., 2012). Cytosolic glutathione reductase determines the redox state of glutathione also in the IMS, and this state is likely similar in both compartments and is reducing. It was unclear, how oxidative protein folding could happen in the reducing environment of the IMS. But in this compartment, a limited amount of GRXs, enzymes that use GSH as a cofactor to reduce other substrates, is enough to prevent disulfide bond reduction. Thus, a balanced amount of GRX activity allows oxidative folding to happen in the IMS (Kojer et al., 2015).

Electron microscopy data indicate that CJs are narrow enough to create diffusion barrier between crista lumen and IMS (Mannella et al., 2001). Functional studies demonstrated that at least some important metabolites, such as cytochrome *c*, are concentrated in the crista lumen (Scorrano et al., 2002). The crista membrane and the IBM are differentially populated with the membrane proteins: the crista membrane is enriched with respiratory chain complexes, whereas IBM is enriched with TIM complexes (Vogel et al., 2006; Wurm and Jakobs, 2006). This indicates that CJs provide barrier not only for the diffusion in and out of the crista lumen, but also for lateral IM protein diffusion.

A direct relationship exists between cristae and the respiration. It can be observed on several levels of organization. In individual cells ablation of mitochondrial DNA, encoding the respiratory chain subunits, prevents cristae formation. Yeast and human cells mutated in this way are unable to respire and therefore can survive only in the presence of fermentable carbon sources (Chen and Clark-Walker, 1999; Gilkerson et al., 2000). The inner mitochondrial morphology, at least in yeast, changes drastically depending on the presence of fermentable substrates in the medium (Entian and Barnett, 1992). In multicellular organisms high number of cristae is usually observed in the cells with high level of respiration (*e.g.* muscle cells, neurons) (Fawcett, 1981; Frey and Mannella, 2000). During the course of evolution organisms living in anaerobic conditions, such as parasitic protists *Giardia intestinalis* or *Blastocystis hominis* tend to lose cristae (Jedelský et al., 2011; Santos et al., 2018). Their mitochondria are reduced and lose the ability to perform OXPHOS. Thus, the role of cristae as a hosting space for respiratory chain complexes is well established.

1.2. MICOS

1.2.1. Discovery and characterization of MICOS

In 2005 it was demonstrated that mitofilin, a mitochondrial protein of previously unknown function, is responsible for maintenance of the mitochondrial ultrastructure in mammalian cells (John et al., 2005). Subsequently mitofilin was discovered in yeast and named Fcj1 (Rabl et al., 2009). According to suggested unified nomenclature mitofilin was renamed Mic60 (Pfanner et al., 2014).

Yeast Mic60 is enriched in cristae and especially CJs. Clusters of Mic60 co-localized with CJs were observed in yeast and mammalian cells (Jans et al., 2013; Stoldt et al., 2019). Mic60 is embedded in the IM via its single N-terminal transmembrane domain. The bulk of the protein extends into the IMS (Rabl et al., 2009). The Mic60 domain structure includes a coiled coil domain and conserved mitofilin domain localized near the C-terminal end (Fig. 3). Between coiled-coil domain and mitofilin domain two amphipathic helical regions were detected (Hessenberger et al., 2017). They were named lipid-binding sites 1 and 2 (LBS1 and LBS2) since they, especially LBS1, are critical for membrane binding.

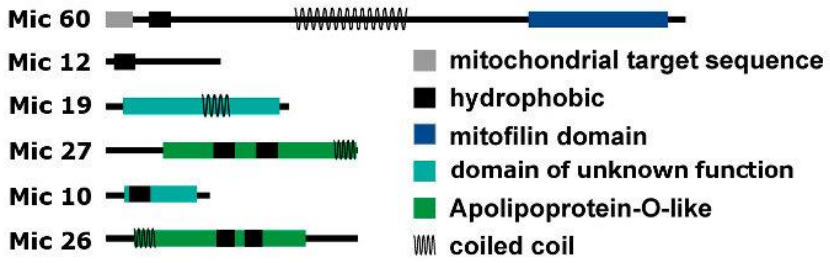

Fig. 3. Domain architecture of yeast MICOS subunits (Hoppins et al., 2011).

Mic60 was shown to determine the number and architecture of CJs (John et al., 2005; Rabl et al., 2009). Deletion of Mic60 leads to loss of CJs and abnormalities in cristae morphology. Yeast growth on non-fermentable media is compromised, which indicates impairment of respiration, likely a consequence of cristae deformation. In mammalian cells, increased membrane potential and the amount of ROS was detected, which may have led to the increased level of apoptosis (John et al., 2005). Mic60 membrane-bending activity was verified also by experiments *in vitro* (Hessenberger et al., 2017; Tarasenko et al., 2017). Mic60 bound the artificial lipid bilayer

vesicles, called liposomes. The binding of Mic60 caused liposomes to change their shape from spheres into long thin tubular structures. When expressed in prokaryotic cells, Mic60 causes cristae-like invaginations of the plasma membrane (Tarasenko et al., 2017).

In search for the proteins that define cristae shape together with Mic60 various methods were utilized: isolation of CS with subsequent proteomic analysis (Harner et al., 2011), affinity purification of Mic60 interaction partners (von der Malsburg et al., 2011) and a genetic interaction screen (Hoppins et al., 2011). The outputs of all three studies were consistent and revealed the existence of six subunit protein complex in yeast (Fig. 3, Fig. 4). The complex was named Mitochondrial Contact Site and Cristae Organizing System (MICOS) (Harner et al., 2011; Hoppins et al., 2011; von der Malsburg et al., 2011).

One of the characterized MICOS subunits, Mic10, demonstrated pronounced depletion phenotype similar to the depletion phenotype of Mic60 (Harner et al., 2011). It also has membrane-bending activity *in vivo* and *in vitro* (Barbot et al., 2015; Bohnert et al., 2015). Yeast Mic10 molecule contains two transmembrane domains and spans the IM two times (Bohnert et al., 2015). The transmembrane domains contain glycine-rich motifs, which are required for the formation of homo-oligomers (Alkhaja et al., 2012; Barbot et al., 2015; Bohnert et al., 2015). Mic10 oligomerization promotes CJ formation in yeast and membrane-bending activity *in vitro* (Barbot et al., 2015; Bohnert et al., 2015).

Other subunits of yeast MICOS are Mic12, Mic19, Mic26, Mic27 (Fig. 4). All subunits are enriched at CJs (Harner et al., 2011). Mic12 is anchored in the IM with its single transmembrane domain. Mic26 and Mic27 have two transmembrane domains. Only Mic19 is the peripheral protein which is not directly connected to the IM (Harner et al., 2016; van der Laan et al., 2016).

Detailed studies revealed the hierarchy of MICOS subunits. MICOS exists as two sub-complexes: the one of Mic60, including Mic19/Mic25, and Mic10 sub-complex, including Mic12, Mic26 and Mic27 (Anand et al., 2016; Friedman et al., 2015; Guarani et al., 2015). Yeast Mic19 was supposed to promote the interaction of MICOS sub-complexes (Friedman et al., 2015), but later this role was assigned to Mic12 (Zerbes et al., 2016). In mammals the protein Mic13/Qil1 plays the role of intermediate between Mic10 and Mic60 sub-complexes (Anand et al., 2016; Guarani et al., 2015).

Mic60 interacts with Mic19 via mitofilin domain, and the interaction enhances membrane remodeling and regulates Mic60 distribution within mitochondria (Friedman et al., 2015; Hessenberger et al., 2017). Mic19 contains coiled-coil helix coiled-coil helix (CHCH) domain. The presence of CHCH domain indicates that Mic19 can exist in the oxidized state, when two disulfide bonds are formed between cysteine residues, and the reduced unfolded state. The oxidized state is preferable for Mic19-Mic60 interaction (Sakowska et al., 2015). Thus, Mic19 is proposed to be a redox sensor modulating cristae formation. Deletion of Mic19 resulted in significant loss of CJs, and, additionally, bizarre cristae that were often branching (Darshi et al., 2011; Harner et al., 2011).

Mic26 and Mic27 are paralogs that belong to apolipoprotein O family (Huynen et al., 2016; Muñoz-Gómez et al., 2015a). CL binding activity was shown for yeast Mic27 *in vivo* (Friedman et al., 2015) and for human Mic27 *in vitro* (Weber et al., 2013). Mic27 stabilizes Mic10 homooligomers and Mic26 have destabilizing effect on them (Rampelt et al., 2018). Cardiolipin is also involved in this interplay and increases the stability of Mic10 oligomers. Deletion phenotype of Mic12, Mic26 and Mic27 was relatively mild.

MICOS subunits were proved to interact with other mitochondrial proteins that do not belong MICOS. The mitofilin domain of Mic60 facilitates its interaction with the OM protein SAM50 in yeast and mammals (Huynen et al., 2016; Körner et al., 2012; Xie et al., 2007). In humans a stable supercomplex exists called the mitochondrial intermembrane space bridging complex (MIB), connecting SAM50 with Mic60 via Mic19 (Huynen et al., 2016; Ott et al., 2012; Tang et al., 2019). Mic60 also interacts with TOM, a complex responsible for protein import through the OM (Huynen et al., 2016; Michaud et al., 2016; von der Malsburg et al., 2011), VDAC and Ugo1, a part of mitochondrial fusion machinery (Zerbes et al., 2012). Transient interaction of Mic60 with Mia40, the key protein of the IMS import pathway was detected. Therefore MICOS was proposed to facilitate IMS import (von der Malsburg et al., 2011). Thus the other important role of MICOS is supporting OM-IM contact sites and therefore protein import in the mitochondria (Wiedemann and Pfanner, 2017). Besides protein import contact sites are also proposed to play a role in lipid exchange between OM and IM (Aaltonen et al., 2016; Michaud et al., 2016).

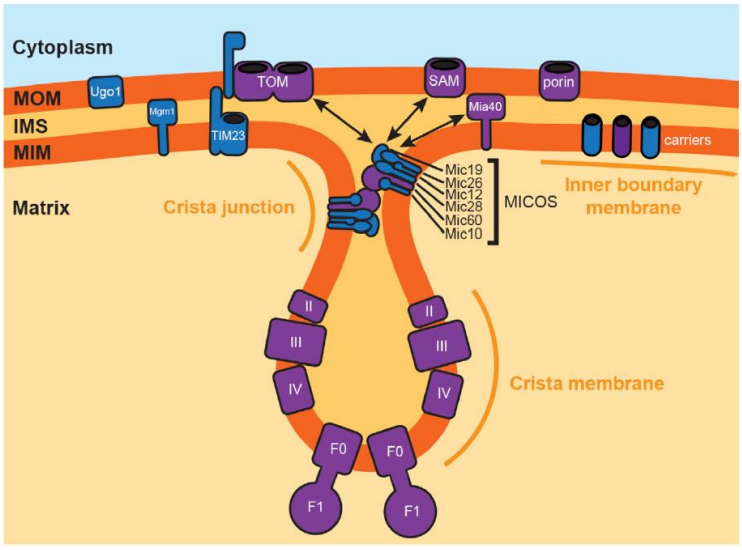

Fig. 4. MICOS composition (Muñoz-Gómez et al., 2015a)

1.2.2. Evolution of MICOS

Besides yeast and mammals, MICOS subunits were characterized in fellow opisthokonts such as *Caenorabditis elegans* (Head et al., 2011) and *Drosophila melanogaster* (Guarani et al., 2015). How are MICOS subunits distributed in other eukaryotic supergroups remained unknown. Until recently, the origin and evolution of cristae, crista junctions and the proteins shaping these important structures was obscure. To elucidate this problem, an attempt was made to search for the MICOS homologs using BLAST (Altschul et al., 1997) and hidden Markov models (Finn et al., 2011) algorithms. This search through sequence databases allowed mapping of the distribution of MICOS subunits among eukaryotic lineages (Fig. 5) (Huynen et al., 2016; Muñoz-Gómez et al., 2015a).

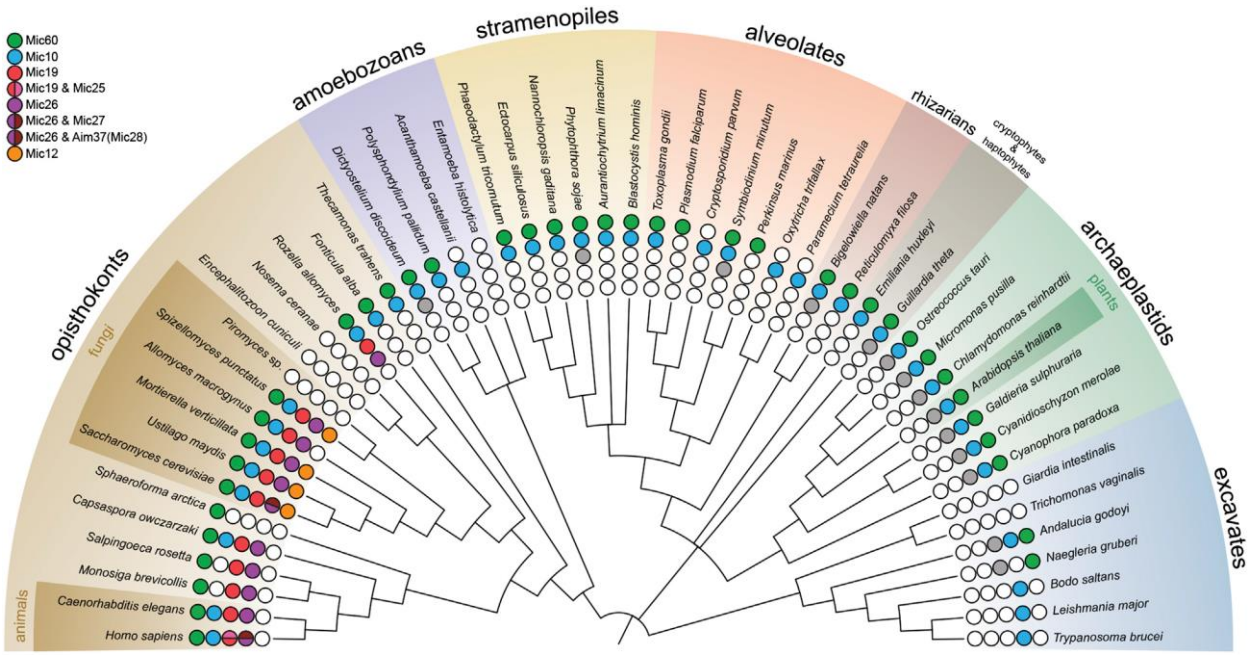

Fig. 5. Distribution of MICOS subunits across the eukaryotic tree (Muñoz-Gómez et al., 2015a).

Only the core Mic10 and Mic60 subunits are widely distributed outside of opisthokonts. They co-occur with the presence of the cristae and aerobic mitochondria in various organisms. This distribution pattern supports the key role of MICOS in cristae formation. The presence of the core subunits in all eukaryotic supergroups indicates the ancient origin of the complex, predating the divergence of these supergroups ~2 Ga (Eme et al., 2014).

Mic19 is also present outside opisthokonts, but since the protein is small, there is not enough information in its primary structure to detect Mic19 homologs with certainty (Huynen et al., 2016; Muñoz-Gómez et al., 2015a). Although the presence of MICOS correlates very well with the presence of cristae, the presence or absence of certain subunits reveals no correlation with cristae shape (Huynen et al., 2016; Muñoz-Gómez et al., 2015a).

Homologs of Mic60 were also detected in alphaproteobacteria, the lineage that gave rise to mitochondria (Huynen et al., 2016; Muñoz-Gómez et al., 2015a). Prokaryotic Mic60 retains a conserved mitofilin domain. Not only is the sequence conserved, but also its membrane-bending activity (Tarasenko et al., 2017). These results let us hypothesize the pre-endosymbiotic origin of

some MICOS subunits and that cristae may have evolved from membranous protrusions in the bacterial cytoplasm (intracytoplasmic membranes) of prokaryotes (Muñoz-Gómez et al., 2017, 2015b). Similar to cristae, intracytoplasmic membranes increase the membrane area in the cell to provide space for enzymatic complexes responsible for anoxygenic photosynthesis or nitrite oxidation.

1.3. Protein import into the mitochondria

About 1000 proteins were detected in the mitochondria of yeast, humans and *Trypanosoma brucei* (Morgenstern et al., 2017; Pagliarini et al., 2008; Panigrahi et al., 2009) (Fig. 6). Due to the reduction of the mitochondrial genome, only about 1% of these proteins are synthetized within the organelle (Wiedemann et al., 2004a). The vast majority is nuclear-encoded, translated in the cytosol and then imported into the mitochondria (Jensen and Dunn, 2002).

1.3.1. Mechanism of the mitochondrial protein import

As was already mentioned, the OM contains three porins, which have a β-barrel structure: VDAC, TOM40 and SAM50 (Wiedemann and Pfanner, 2017). Translocase of the outer mitochondrial membrane (TOM), with its central β-barrel subunit TOM40 , is a multi-protein complex that serves as the only gate proteins can pass through the OM (Gabriel, 2003). The sorting and assembly machinery pore forming subunit (SAM50) is responsible for insertion of β-barrel proteins into the OM (Höhr et al., 2015; Kozjak et al., 2003). Small TIM chaperones are required for their OM insertion after they go through TOM (Hoppins and Nargang, 2004; Wiedemann et al., 2004b). Monomers of small TIMs assemble into hexameric structures, forming a cavity that shields the hydrophobic part of the precursor (Beverly et al., 2008; Webb et al., 2006) and this way deliver the substrates to SAM50 or the IM insertase TIM22. Voltage-dependent anion channel (VDAC) is the most abundant β-barrel OM protein (Bayrhuber et al., 2008). It is responsible for the flux of metabolites through the OM and plays key role in release of mitochondrial apoptotic factors.

Protein precursors enter the mitochondrion through the TOM and are distributed to one of four main destinations: OM, IM, IMS and matrix (Fig. 6) (Chacinska et al., 2009). Their destination is defined based on their targeting signal. This can be a cleavable sequence, usually N-terminal (presequence, matrix targeting signal), or non-cleavable internal signal (Neupert and Herrmann, 2007).

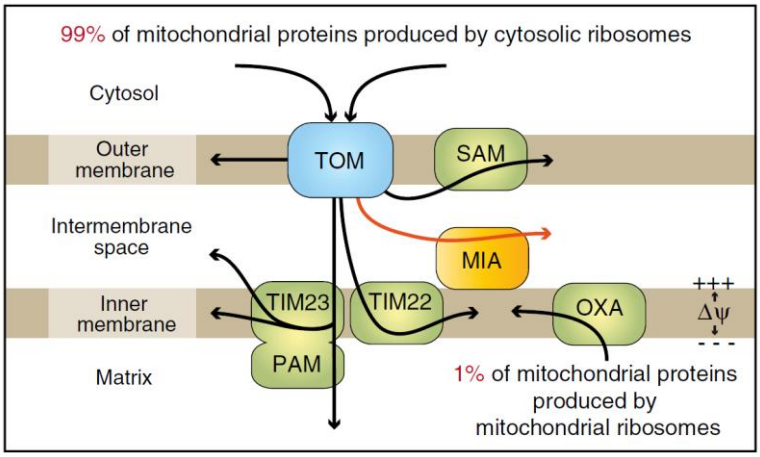

Fig. 6. Protein import pathways in mitochondria (Stojanovski et al., 2012).

After translocation through the OM the proteins, targeted to the IM or matrix, interact with one of the translocase of the inner membrane (TIM) machineries: TIM22 or TIM23. Hydrophilic preproteins targeted to the matrix cross the IM through TIM23, utilizing also the presequence translocase-associated motor (PAM) (Mokranjac and Neupert, 2010; Truscott et al., 2003). Matrix targeting signals are eventually cleaved by the mitochondrial processing peptidase (MPP).

Both TIM22 and TIM23 can release proteins into the lipid bilayer of the IM. TIM22 does this with integral multidomain proteins in membrane potential-dependent manner. (Rehling et al., 2004). Since such proteins are hydrophobic, they are brought through IMS bound to small TIM chaperones. Many proteins are embedded in the IM by TIM23. They have matrix targeting signal and a single transmembrane domain. The majority of proteins going this pathway are embedded

in the IM with their C-terminal end facing IMS. The example of such proteins is yeast Mia40 (Chatzi et al., 2013). Matrix targeting sequence is cleaved by mitochondrial processing peptidase. A fraction of Tim23 substrates is released to the IMS after protease cleavage of the hydrophobic sequence, such as cytochrome b2, which is further processed by the inner membrane peptidase (Glick et al., 1992; van der Laan et al., 2010). The majority of soluble IMS proteins requires oxidative folding to stay in the IMS. This pathway, independent of TIM23, is named mitochondrial sorting and assembly machinery (MIA), and is described more in-depth in the next sub-chapter.

1.3.2. Description of the MIA pathway

The majority of the proteins localized in the IMS go through the mitochondrial import and assembly machinery (MIA) pathway, which was characterized in yeast at first (Gabriel et al., 2007; Stojanovski et al., 2008). Unlike other mitochondrial import pathways, MIA involves oxidative folding of the substrates due to formation of covalent disulfide bonds between cysteine residues (Deponte and Hell, 2009; Mordas and Tokatlidis, 2015; Stojanovski et al., 2008). Thus the protein is folded and trapped in the IMS. Apparently, at least one pair of cysteine residues is required for this mechanism to work as it was shown for humans (Hofmann et al., 2002; Roesch, 2002). Transport through the MIA pathway is energetically favorable, not requiring neither ATP hydrolysis nor membrane potential (Mordas and Tokatlidis, 2015).

The key components of the MIA pathway are the oxidoreductase Mia40 and sulfhydryl oxidase ERV1 (an abbreviation of "essential for respiration and viability") (Fass, 2008). Mia40 contains six cysteine residues in the CPC-C(X_9)C-C(X_9)C arrangement (Banci et al., 2009). The N-terminal pair of cysteines makes the conserved redox-active CPC motif. It is required for the formation of the disulfide bridge with the substrate. The other cysteines contained in a twin C(X_9)C motif are responsible for maintenance of the overall protein shape. Mia40 in the active conformation has a hydrophobic binding site, which is required for substrate protein docking (Dudek et al., 2013; Stojanovski et al., 2012). The second cysteine of the CPC motif is the key one. It is exposed and is in close proximity to the hydrophobic cleft (Fig. 7).

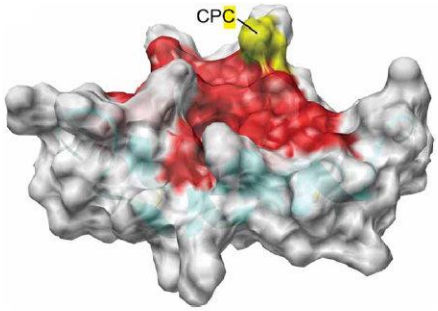

Fig. 7. Mia40 structure. Hydrophobic cleft shown in red, the active cysteine of the CPC motif in yellow (Banci et al., 2009).

The representatives of the proteins imported through MIA pathway are small TIMs and peripheral complex IV subunits, for instance COX17 and COX19 (Chacinska et al., 2009; Gabriel et al., 2007). The cysteines of MIA substrates are usually organized into double C(x_3)C or C(x_9)C motifs. The mitochondrial IMS sorting/ IMS targeting signal (MISS/ITS) was detected close to these cysteines (Fig.8).

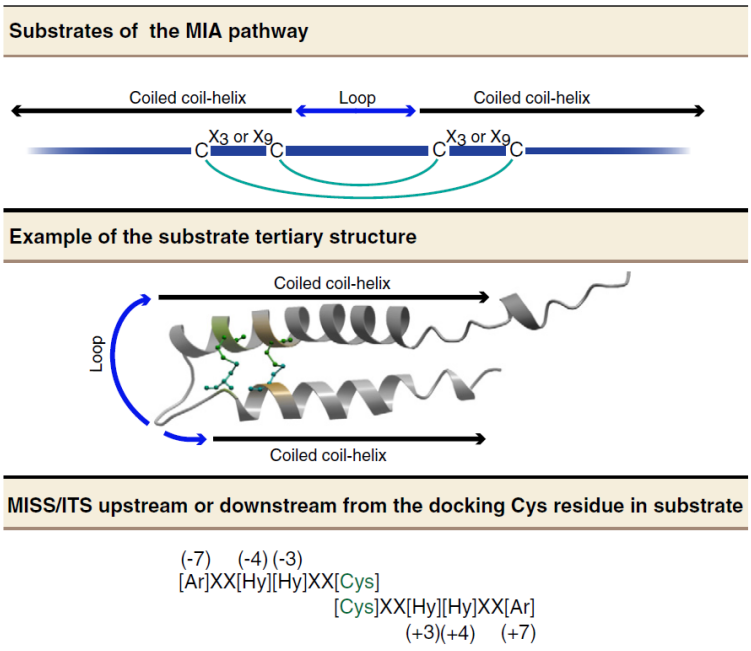

Fig. 8. C(x_{3-9})C motifs in MIA substrates, tertiary structure and MISS/ITS motif of MIA substrates (Stojanovski et al., 2012).

MISS/ITS consists of the docking cysteine, the one that first forms the disulfide bond with Mia40, and 8 amino acids up-or downstream. Analysis of MISS/ITS sequences revealed the importance of position -7 in relation to the cysteine residue, where the presence of aromatic amino acid is required. The presence of hydrophobic residues in position -4 and -3 is also important (Fig.8). It was shown for yeast proteins that MISS/ITS form a helix in which the hydrophobic and aromatic residues and docking cysteine are on the same side (Milenkovic et al., 2009; Sideris et al., 2009). This conformation is necessary for proper positioning of the substrate with Mia40.

The interaction of protein precursors with Mia40 happens in two steps. First, the non-covalent interaction of MISS/ITS motif with Mia40 hydrophobic cleft takes place (Fig.9). This interaction positions the substrate in a way that allows the disulfide bond to form between the active cysteine in the Mia40 CPC motif and the docking cysteine of the substrate in the second step (Milenkovic et al., 2009; Mordas and Tokatlidis, 2015; Sideris et al., 2009). In small TIMs, the docking cysteine is the most N-terminal one in the twin C(x_3)C motif, though in the other MIA substrate COX17, unrelated to TIMs, the third cysteine of twin C(x_9)C motif is probably responsible for the docking (Fig. 8). (Sideris et al., 2009). Docking is followed by the formation of the disulfide bond between two cysteine residues of the substrate.

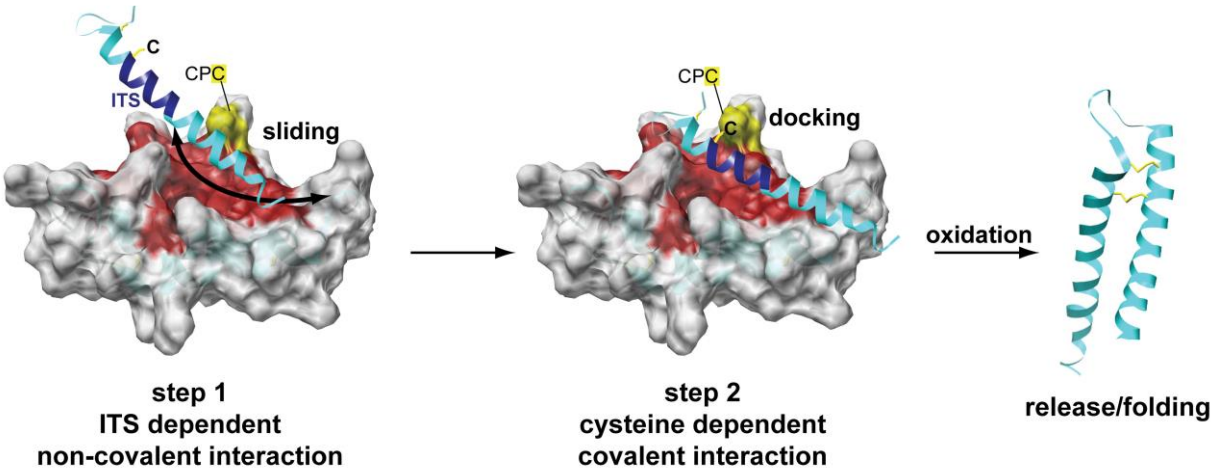

Fig. 9. Main steps of substrate-Mia40 interaction (Sideris et al., 2009).

Subsequent steps of Mia40-substrate interaction are not fully resolved. According to one of the models the substrate is released after the formation of the first intramolecular disulfide bridge, and the formation of the other disulfide bridge happens in Mia40-independent way, since the

cysteine residues are now in proximity (Banci et al., 2010). Another model suggests the simultaneous formation of both disulfide bridges prior to substrate release (Chacinska et al., 2009). Erv1 is involved in the disulfide bond formation and was reported to form ternary complex with Mia40 and substrate (Stojanovski et al., 2008).

The MISS/ITS motif is sufficient for targeting the protein to the IMS (Stojanovski et al., 2012). This indicates that other cysteines and the twin $C(X_{3-9})C$ motif are not necessary for targeting the substrate to the IMS. They are required just for retaining of folded protein in the IMS. Some novel MIA substrates with non-canonical pattern of cysteine residues and MISS motif were discovered, indicating that the range of the substrates is broader than was expected (Kallergi et al., 2012; Reddehase et al., 2009; Terziyska et al., 2007; Wrobel et al., 2013).

The oxidized substrate is then trapped in the IMS due to its folded conformation. Reduced Mia40 is reoxidized by ERV1 dimer, from which electrons are passed to the cytochrome *c* and the electron transport chain (Stojanovski et al., 2012). The ability of Mia40 to be oxidized by ERV1 was also demonstrated *in vitro* (Grumbt et al., 2007).

Additional proteins may take part in the MIA pathway, like Hot13 or Mic60 (mitofilin) (Curran et al., 2004; Mesecke et al., 2008; von der Malsburg et al., 2011). Hot13, a zinc-binding conserved protein, interacts with Mia40 and stimulates its oxidation by ERV1, thus enhancing IMS import. Mic60 transiently interacts with Mia40 and also interacts with TOM. Presumably its role is to bring Mia40 in proximity with TOM to facilitate the interaction of the substrate and Mia40 right after the substrate goes through TOM (von der Malsburg et al., 2011). The interaction of redox sensor protein Gpx3 with Mia40 was shown *in organello* and *in vitro*. Gpx3 is capable of oxidizing reduced Mia40 and maintains the redox state of Mia40 (Kritsiligkou et al., 2017).

1.3.3. Disulfide bonds formation in different organisms.

The details of the MIA pathway discussed above were determined in yeast and humans. The IMS import pathway is conserved and therefore the principles of the disulfide bond formation are similar in various lineages of prokaryotes and eukaryotes. Enzymes responsible for introducing

disulfide bonds share certain common features throughout the whole tree of life (Sato and Inaba, 2012). The details of the system are highly variable though, and the reasons of such variability are not yet perfectly clear.

In prokaryotes, the first disulfide bond introducing enzymes were found in *E. coli*. In this organism the pathway consists of two proteins: DsbA and DsbB. DsbA is a thioredoxin homologue with CPHC motif (Bardwell et al., 1991). In the active state the motif is oxidized. It interacts with the cysteine residues of the substrates, removing electrons which leads to the formation of the disulfide bond between substrate cysteines (Landeta et al., 2018). The function of the second enzyme, DsbB, is the maintenance of DsbA in the oxidized state. Gained electrons are passed to quinones and then on to the respiratory chain (Bader et al., 1999). It was shown that only one of the two DsbA cysteine residues, the most N-terminal, is exposed and reactive (Zapun et al., 1994), resembling the exposed docking cysteine in the CPC motif of Mia40. DsbA substrates are periplasmic proteins such as flagella P-ring component FlgI (Dailey and Berg, 1993). Mutations or deletions in the Dsb system lead to inability of FlgI to fold properly. Flagellar assembly and therefore cell motility are impaired in *dsbA* mutants (Dailey and Berg, 1993; Hizukuri et al., 2006).

The disulfide relay is functionally conserved in mammals, fungi and plants. Plant ERV1 is unable to oxidize yeast Mia40 (Peleh et al., 2017). On the other hand, it is capable of performing import and oxidative folding of substrates in Mia40-independent way, unlike ERV1 homologs in animals and fungi. In land plant *Arabidopsis thaliana* Mia40 (AtMia40) is involved in the disulfide relay, but is not essential. AtERV1 is essential (Carrie et al., 2010).

1.4. Mitchondrial biogenesis in trypanosomatids

1.4.1. Trypanosomatids as a model for studying mitochondria

As already mentioned, the ancestor of all eukaryotes possessed mitochondria. So far, though, there are just a few species in which mitochondria are thoroughly studied. They are yeast, humans, *Neurospora crassa*, *Caenorhabditis elegans and Arabidopsis thaliana*. All of them excluding *Arabidopsis* belong to the opisthokont supergroup, which is just a minority in the variety of eukaryotes (Fig. 10). One perspective model species to expand our knowledge about

mitochondria biogenesis is the parasitic protist *Trypanosoma brucei*. This species diverged with opisthokonts ~2 Ga ago (Eme et al., 2014) and therefore is very distantly related to them.

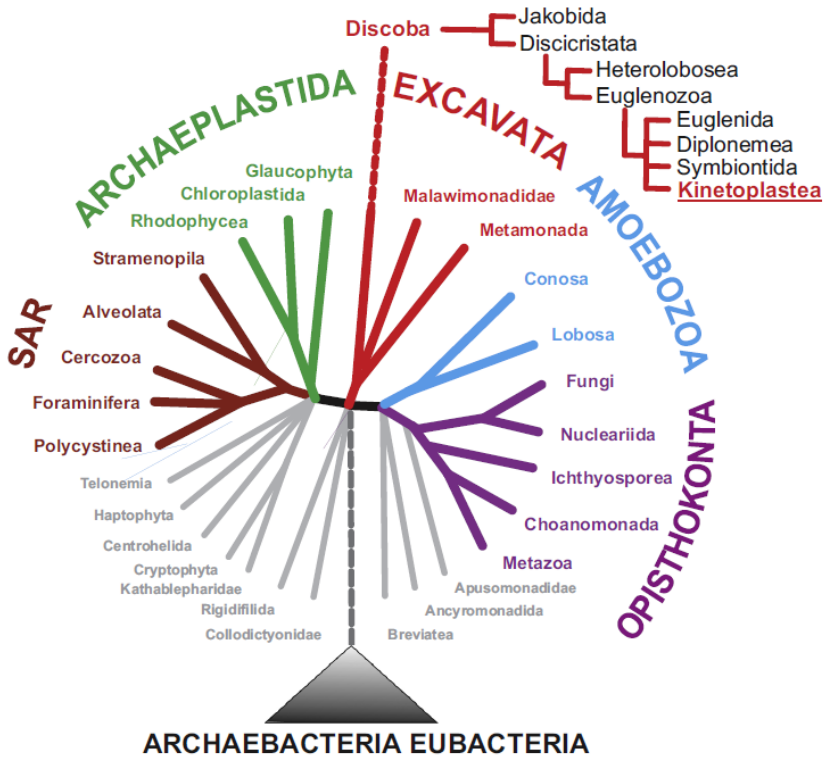

Fig. 10. Eukaryote phylogeny with the position of Kinetoplastea highlighted (Lukeš et al., 2014).

Trypanosomatids belong to the class Kinetoplastea, also referred to as kinetoplastids (Adl et al., 2018). Many kinetoplastid species are parasites, in contrast to the members of sister clades (Euglenida, Symbiontida, Diplonemea) known so far (Lukeš et al., 2014). As causative agents of many diseases, kinteoplastids have been thoroughly studied since the end of 19th century (Steverding, 2008). *T. brucei*, the causative agent of African sleeping sickness, is the best studied kinetoplastid species. It is easily cultured, amenable to many methods of forward and reverse genetics, and therefore is widely used as a model species (Matthews, 2015). *T. brucei* has a complex life cycle, which involves two hosts: mammals and the tsetse fly vector (Fig. 11).

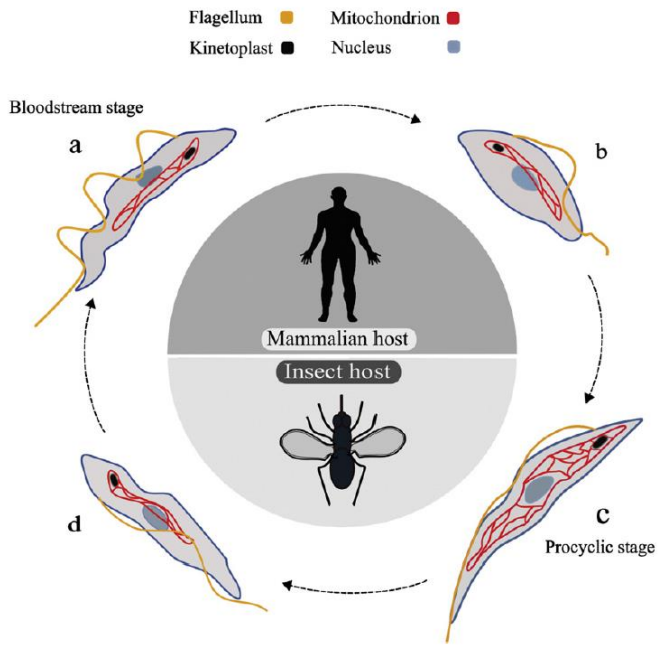

Fig. 11. Life cycle of *Trypanosoma brucei*. Simplified depiction of life cycle includes **(a)** proliferative long slender bloodstream stage, **(b)** non-dividing short stumpy form, **(c)** proliferative insect procyclic stage and **(d)** non-dividing metacyclic form (Lukeš and Basu, 2015).

While *T. brucei* goes through different life cycle stages, its overall morphology and ultrastructure are remodeled and its metabolism is changed (Brown et al., 1973; Smith et al., 2017). In the mammalian host, *T. brucei* populate the bloodstream and, at later stages of the infection, the brain. Recently a third reservoir for trypanosomes in mammalian host was discovered, which is adipose tissue (Trindade et al., 2016). Parasites living there are capable of β-oxidation of fatty acids. Except for this fact, nothing else is currently known about their metabolism and for this reason only traditional bloodstream and procyclic forms are discussed here.

Living in the mammalian bloodstream, *T. brucei* rely on glycolysis as a way to produce energy. They do not perform oxidative phosphorylation because electron transport chain (ETC) complexes III and VI are absent. During the process of differentiation to the insect (procyclic) stage, oxidative phosphorylation becomes predominant. The mitochondrion is extensively remodeled, new cristae are formed and populated with respiratory complexes. These changes make *T.brucei* especially attractive model for studying mitochondrial and *de novo* cristae biogenesis. In pleomorphic cell lines the differentiation from slender bloodstream forms to

procyclic can be induced *in vitro* and thus cristae biogenesis can be thoroughly and relatively easily studied. Changes in gene expression can be traced in parallel with morphological changes. The genetic amenability of *T. brucei* allows us to manipulate gene expression of proteins putatively responsible for mitochondrial development on different life stages and track the results. Procyclic stage can be easily cultivated with or without fermentable carbon sources to address their metabolic and respiration capacities.

1.4.2. MICOS in trypanosomatids

Until recently the only known MICOS subunit in trypanosomatids was the Mic10 orthologue, detected bioinformatically (Huynen et al., 2016; Muñoz-Gómez et al., 2015a). We performed a study in attempt to detect other MICOS subunits and address their functions. Unlike opisthokont species characterized so far, trypanosomatids have two Mic10 paralogs (Huynen et al., 2016; Kaurov et al., 2018; Muñoz-Gómez et al., 2015a). They both have two transmembrane domains, like the other members of Mic10 family. The functions of Mic10 paralogs were determined to be redundant in procyclic *T. brucei* grown *in vitro* (Kaurov et al., 2018). But together they perform the same function as opisthokont Mic10: namely cristae shaping and CJ biogenesis. Opisthokonts and trypanosomatids are very distantly related groups, and conservation of Mic10 function between them is remarkable.

Since Mic10 paralogs were the only MICOS subunits detected in trypanosomatids, one of the first goals of the study was to find out if the multisubunit MICOS complex exists in these organisms, like in opisthokonts. We used Mic10 paralogs as bait to immunoprecipitate their possible interaction partners. This way seven novel TbMICOS subunits were identified. This study revealed a mixture of conserved and novel features compared with opisthokont MICOS.

Neither sequence nor domain structure are conserved between opisthokont and TbMICOS subunits. Exceptions are TbMic10 and putative TbMic60, which lacks the characteristic mitofilin domain, but retains the rest of the domain architecture of Mic60 (Kaurov et al., 2018; Muñoz-Gómez et al., 2015a). TbMICOS subunits are predominantly co-localized with cristae membranes, but only four of them are membrane-embedded. Depletion of several TbMICOS subunits causes alteration in cristae shape and abundance, which resembles opisthokont MICOS depletion phenotype.

Addressing the depletion phenotype of TbMICOS allowed us to reveal surprising properties of another subunit, TbMic20. This thioredoxin-like protein appears to be involved in IMS protein import to some capacity. It may represent the putative functional analog of Mia40, the protein responsible for the IMS import in various eukaryotes but missing in trypanosomatids (Haindrich et al., 2017; Muñoz-Gómez et al., 2015b).

Our latest study revealed the hierarchy of TbMICOS subunits and existence of two subcomplexes (Eichenberger et al., 2019). Opisthokont MICOS also exists in two subcomplexes, but the principle of subcomplex organization is different. Opisthokont MICOS subcomplexes are assembled around the most conserved subunits Mic10 and Mic60. One TbMICOS subcomplex comprises integral and mostly non-essential proteins (TbMic10-1, TbMic10-2, TbMic16, TbMic60), and the other one consists of soluble and essential proteins (TbMic20, TbMic32, TbMic34, TbMic40). It should be noted that in our previous study, depletion of TbMic60 resulted in cell growth arrest (Kaurov et al., 2018). This difference between the two studies is hard to explain. Presumably, the reason is in different efficiency of RNAi constructs, which were produced independently, in the use of two different *T. brucei* strains in each of the studies.

Similar to opisthokont MICOS, TbMICOS interacts with the OM insertase SAM50, though the mechanism of interaction remains unknown so far. This indicates that a role in establishing contact sites between IM and OM is conserved.

The study of TbMICOS revealed both conserved and novel features of the complex. Main conserved features are the role of TbMICOS in formation of cristae and CJs, maintenance of OM-IM contact sites due to interaction with SAM50 and bipartite nature of the complex. On the other hand, the primary structure of TbMICOS is not conserved. The absence of mitofilin domain in putative Mic60 and especially the import activity of thioredoxin-like subunit are novel diverged features. Whether they have distribution in other eukaryotes outside trypanosomatids, still remains to be answered.

1.4.3. MIA pathway in trypanosomatids

Mitochondrial protein import pathways are functionally conserved in eukaryotes (Eckers et al., 2012). However, trypanosomatids lack the key component of the MIA pathway, Mia40, whose homologs are detected in fungi, amoebae, plants, and animals (Allen et al., 2008; Deponte and Hell, 2009; Haindrich et al., 2017; Muñoz-Gómez et al., 2015b). Small cysteine-containing

substrates of the MIA pathway are present in trypanosomatids. The other key protein of the pathway, ERV1, is also detected. Several speculations can be made to explain the absence of the key component of the conserved pathway. One of them is the redundancy of Mia40 in some eukaryotic lineages, leading to the loss of this protein. The sequence of original Mia40 could undergo significant changes in the course of evolution so it can be too difficult to detect it *in silico*. Some unknown protein could have performed the function of this central oxidoreductase in the past, and later replaced with Mia40 in the most but not all eukaryotic lineages (Eckers et al., 2012).

To maintain redox balance in the cell, the majority of eukaryotic species utilize GSH and glutaredoxin. Trypanosomatids lack the ubiquitous glutathione/glutathione reductase system. Instead they have specific redox system based on thiolpolyamine conjugate trypanothione (Krauth-Siegel et al., 2003). Trypanothione is reduced by the NADPH-dependent flavoenzyme trypanothione reductase. This trypanothione/trypanothione reductase system is analogous to GSH system. Not only their functions are similar, but the initial steps of synthesis pathways (Fairlamb, 1992). Redox potentials of trypanothione and glutathione are quite similar, but trypanothione is more reactive (Dormeyer, 2001; Krauth-Siegel et al., 2003). Some parts of other redox systems are retained in *T. brucei*, for instance, thioredoxins and glutaredoxins. Since oxidative protein folding is tightly connected with the redox state of the cell, and the *T.brucei* redox system is noticeably different from other eukaryotes, we presume that these differences may influence *T.brucei* IMS protein folding machinery. It seems probable that this may underlie the absence of a *bona fide* Mia40 orthologue in trypanosomatids. So far though, no exact mechanism of such interconnection is known, and further studies are required to elucidate this question.

2.

Chapter 1. The diverged trypanosome MICOS complex as a hub for mitochondrial cristae shaping and protein import

Article

Current Biology

The Diverged Trypanosome MICOS Complex as a Hub for Mitochondrial Cristae Shaping and Protein Import

Graphical Abstract

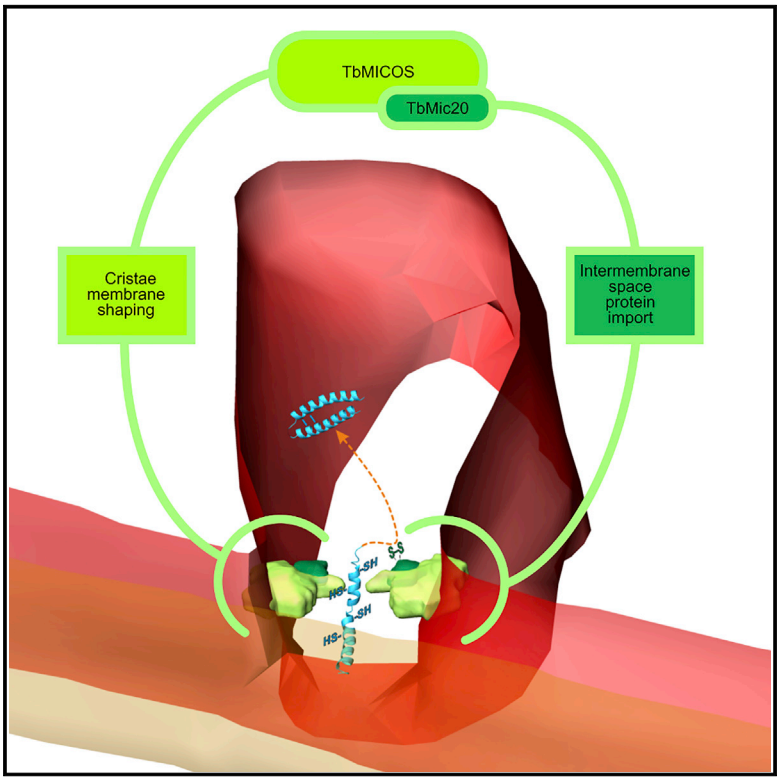

Authors

Iosif Kaurov, Marie Vancová, Bernd Schimanski, ..., André Schneider, Julius Lukeš, Hassan Hashimi

Correspondence

hassan@paru.cas.cz

In Brief

The mitochondrial contact site and cristae organizing system (MICOS) is a conserved feature of mitochondria. Kaurov et al. identify and characterize MICOS proteins outside of opisthokonts in the kinetoplastid parasite *Trypanosoma brucei*. TbMICOS plays a conserved role in mitochondrial cristae shaping and harbors several unique features as well.

Highlights

- First study of MICOS outside opisthokonts verifies a conserved role in shaping cristae
- Trypanosome MICOS novelties include two distinct Mic10s and an atypical Mic60
- TbMICOS features a novel thioredoxin-like subunit called TbMic20
- TbMic20 appears to be a catalyst for intermembrane space protein import

Kaurov et al., 2018, Current Biology *28*, 1–15
November 5, 2018
https://doi.org/10.1016/j.cub.2018.09.008

CellPress

Current Biology
Article

The Diverged Trypanosome MICOS Complex as a Hub for Mitochondrial Cristae Shaping and Protein Import

Iosif Kaurov,[1,2] Marie Vancová,[1,2] Bernd Schimanski,[3] Lawrence Rudy Cadena,[2] Jiří Heller,[1] Tomáš Bílý,[1,2] David Potěšil,[4] Claudia Eichenberger,[3] Hannah Bruce,[2,7] Silke Oeljeklaus,[5] Bettina Warscheid,[5,6] Zbyněk Zdráhal,[4] André Schneider,[3] Julius Lukeš,[1,2] and Hassan Hashimi[1,2,8,*]

[1]Institute of Parasitology, Biology Center, Czech Academy of Sciences, 37005 České Budějovice, Czech Republic
[2]Faculty of Science, University of South Bohemia, 37005 České Budějovice, Czech Republic
[3]Department of Chemistry and Biochemistry, University of Bern, 3012 Bern, Switzerland
[4]Central European Institute of Technology, Masaryk University, 62500 Brno, Czech Republic
[5]Faculty of Biology, Biochemistry and Functional Proteomics, Institute of Biology II, University of Freiburg, 79104 Freiburg, Germany
[6]BIOSS Centre for Biological Signaling Studies, University of Freiburg, 79104 Freiburg, Germany
[7]Present address: Genome Research, Ltd., Wellcome Sanger Institute, Wellcome Genome Campus, Hinxton, Cambridge, UK
[8]Lead Contact
*Correspondence: hassan@paru.cas.cz
https://doi.org/10.1016/j.cub.2018.09.008

SUMMARY

The mitochondrial contact site and cristae organization system (MICOS) is a multiprotein complex responsible for cristae formation. Even though cristae are found in all mitochondria capable of oxidative phosphorylation, only Mic10 and Mic60 appear to be conserved throughout eukaryotes. The remaining 4 or 5 known MICOS subunits are specific to the supergroup Opisthokonta, which includes yeast and mammals that are the only organisms in which this complex has been analyzed experimentally. We have isolated the MICOS from *Trypanosoma brucei*, a member of the supergroup Excavata that is profoundly diverged from opisthokonts. We show that it is required for the maintenance of the unique discoidal cristae that typify excavates, such as euglenids and kinetoplastids, the latter of which include trypanosomes. The trypanosome MICOS consists of 9 subunits, most of which are essential for normal growth. Unlike in opisthokonts, it contains two distinct Mic10 orthologs and an unconventional putative Mic60 that lacks a mitofilin domain. Interestingly, one of the essential trypanosomatid-specific MICOS subunits called TbMic20 is a thioredoxin-like protein that appears to be involved in import of intermembrane space proteins, including respiratory chain complex assembly factors. This result points to trypanosome MICOS coordinating cristae shaping and population of its membrane with proteins involved in respiration, the latter via the catalytic activity of TbMic20. Thus, trypanosome MICOS allows us to define which of its features are conserved in all eukaryotes and decipher those that represent lineage-specific adaptations.

INTRODUCTION

Cristae are mitochondrial inner membrane (MIM) invaginations that are the organelle's morphological hallmark. They are distributed throughout eukaryotes, inherited from the last eukaryotic common ancestor (LECA) [1, 2]. Cristae assume different forms, with lamellar ones found in the best-studied supergroup Opisthokonta, which encompasses yeast and animals. Tubular-shaped cristae typify the unicellular supergroup SAR, containing stramenopiles, alveolates, and rhizarians. Euglenid members of the protistan supergroup Excavata generally have discoidal cristae, which exhibit a paddle-like morphology. Thus, cristae have evolved different morphologies that may represent adaptions to the multifarious cellular milieus of diverse eukaryotes.

Cristae occurrence correlates with an aerobic lifestyle mediated by mitochondria. This is because cristae membranes are enriched with respiratory chain complexes that perform oxidative phosphorylation (OXPHOS) [3–5]. Such a configuration boosts OXPHOS capacity by increasing the surface area for this process and concentrating the soluble electron carrier cytochrome *c* in the lumen enclosed by the cristae membrane [6, 7].

Pioneering studies in yeast identified a key multiprotein complex for cristae biogenesis called the mitochondrial contact site and cristae organizing system (MICOS) [8–10]. In this and other opisthokonts, the MICOS complex has been shown to maintain cristae junctions (CJs), narrow necks attaching cristae to the MIM [11–13]. The evolutionarily conserved core subunits Mic10 and Mic60 catalyze formation of negative curvature at CJs [14–16]. MICOS also forms contacts with mitochondrial outer membrane (MOM) proteins via Mic60's conserved C-terminal mitofilin domain. This domain is an intermembrane space (IMS) extension that interacts with the β-barrel protein sorting and assembly machinery subunit Sam50 and the protein translocase of the outer membrane (TOM) [17–19]. Furthermore, the mitofilin domain has been reported to augment the mitochondrial IMS import and assembly (MIA) pathway in yeast by interaction with the central MIA catalyst Mia40 [10].

By an oxidative folding mechanism, MIA sequesters small cysteine-rich proteins bearing twin CX_3C or CX_9C motifs [20, 21]. Mia40 catalyzes this folding through its reactive CPC motif, forming an intermolecular disulfide bond with a thiol group of a reduced and unfolded IMS precursor [22]. With Erv1, an IMS sulfhydryl oxidase, two intramolecular disulfide bridges linking each of the dual $CX_{3,9}C$ motifs are formed, creating a hairpin fold that traps substrate proteins within the IMS. During this process, Erv1 reoxidizes Mia40 for another round of translocation.

The mechanistic model of MICOS function has been proposed based on data gained solely from opisthokonts [11–13]. However, the majority of identified MICOS subunits are restricted to this clade. Only the Mic10 and Mic60 core subunits have a wide distribution overlapping with the occurrence of cristae [1, 2]. This strongly indicates that the ancestor of MICOS was already present in LECA. Mic60 may even pre-date MICOS, supported by evidence that it originates from the proteobacterial endosymbiont giving rise to mitochondria [1, 2]. Hitherto unidentified supernumerary MICOS subunits interacting with the ancient core may contribute to the diverse cristae morphologies of eukaryotes.

Thus, true insight into how the ancient and ubiquitous MICOS shapes cristae in eukaryotes requires mechanistic studies outside of the single opisthokont clade. The discipline of evolutionary cell biology postulates that a comparative approach to examining a biological system in different organisms can reveal chemical and physical constraints to their evolution [23]. Conversely, this approach can also identify a system's more flexible attributes, from which novelties may potentially emerge in certain lineages. The *in silico* approach to address the evolutionary cell biology of MICOS has reached saturation, necessitating functional data from other eukaryotic groups.

To this end, we have undertaken the first study of MICOS composition and function outside of opisthokonts. We have chosen the pathogen *Trypanosoma brucei* as our model, not only for its robust genetic toolkit but also because of its suitability for tackling the evolutionary cell biology of MICOS. *T. brucei* is a kinetoplastid belonging to the supergroup Excavata and therefore has an extended independent evolutionary history [24]. Its single mitochondrion undergoes massive remodeling during its life cycle [25]. The procyclic stage (PS) infecting the tsetse fly midgut has a mitochondrion with extensive discoidal cristae and OXPHOS capacity and thus is the focus here. The long slender bloodstream stage (BS) infecting mammalian hosts lacks both cristae and OXPHOS. Furthermore, *Mic10* was the only MICOS ortholog found in *T. brucei* by bioinformatics methods alone [1, 2], hinting at the tantalizing possibility of its MICOS bearing novel properties.

RESULTS

Trypanosomatids Have Two Mic10 Paralogs

Trypanosomatid Mic10 is made up of two well-supported clades [1] (Figure 1A). In *T. brucei*, these paralogs are represented by TbMic10-1 and TbMic10-2 (TbMic10-1/2) (Figure 1B). Mic10 duplication does not pre-date the emergence of trypanosomatids, because there is only one Mic10 ortholog found in the *Euglena gracilis* [26] and *Bodo saltans* genomes [27], representing their free-living sister groups. Although *B. saltans* Mic10 clearly belongs to the TbMic10-1 clade, the *E. gracilis* homolog cannot be assigned to either with high confidence.

As Mic10 family members, each *T. brucei* paralog contains two transmembrane domains (TMDs) (Figure 1B). The C-proximal TMD2 has a highly conserved GxGxGxG motif, which mediates Mic10 oligomerization required for membrane bending in yeast [14, 16]. The motif is conserved in the TbMic10-1 clade, whereas it is abbreviated to 3 alternating Gs in the TbMic10-2 clade (Figures 1B and S1A).

Both paralogs share some features that distinguish them from the best-characterized *Saccharomyces cerevisiae* Mic10 (Figure S1A). The TMD1 glycine-rich motif essential for Mic10 oligomerization is dramatically reduced in TbMic10-1/2. Furthermore, the *T. brucei* paralogs lack the positively charged KRR loop between the TMDs needed for MIM targeting of the yeast homolog [16]. Surprisingly, the KKR loop is absent in Mic10 orthologs of all eukaryotes outside the opisthokonts (Figure S1A). This fact underscores the need to study MICOS in other organisms like *T. brucei*.

TbMic10 Paralogs Shape Cristae

C-terminal V5-epitope-tagged TbMic10 paralogs show a patchy mitochondrial localization by indirect immunofluorescence (Figure 1C). To further investigate whether TbMic10-1/2 associate with cristae, immunogold labeling of the V5 epitopes on Tokuyasu cryosections were viewed by transmission electron microscopy (TEM) or electron tomography (ET). Nanoparticles (NPs) immunodecorating TbMic10-1-V5 and TbMic10-2-V5 were mainly observed at cristae membranes (Figure 1D; Video S1).

Next, we addressed whether TbMic10-1/2 are involved in shaping cristae. Initial attempts to delete either *TbMic10-1* or *TbMic10-2* by gene knockout did not yield any obvious phenotype, suggesting their functional redundancy. Thus, we generated cells in which both paralogs were ablated simultaneously by tetracycline-inducible RNAi silencing of TbMic10-2 in a TbMic10-1 deletion background (Figure S2). Cryosections derived from *ΔTbMic10-1*:TbMic10-2↓ 1 and 4 days post-induction (dpi) of RNAi were examined by TEM. At 4 dpi, cristae were significantly elongated compared to the parental cell line, sometimes as stacked semi-circles or arcs (Figure 2A). The severity of this phenotype correlates with time of induction, as it is less pronounced yet present at 1 dpi (Figure 6C).

Stacking of elongated cristae was also observed in yeast Mic10 deletion mutants in conjunction with CJ loss [8–10]. Because the slender CJs of discoidal cristae are difficult to observe on ultrathin cryosections, a 3D reconstruction of serial TEM cryosections was performed on *ΔTbMic10-1*:TbMic10-2↓ 4 dpi, which allows better assessment of CJ loss thanks to a broad z axis (Figures 2B and 2C; Video S2). The aberrant cristae were barrel shaped with finger-like projections extending from one end. CJs were not observed along the examined ~700 nm. In conclusion, the TbMic10 paralogs function synergistically in shaping of cristae and CJ biogenesis in PS *T. brucei*, thus confirming its hypothetical role outside of opisthokonts.

TbMic10 Paralogs Are Part of a Multi-protein Complex

Blue native PAGE of digitonin-solubilized mitochondrial membranes resolved a >1-MDa complex containing TbMic10-1, likely corresponding to *T. brucei* MICOS, with potential intermediates

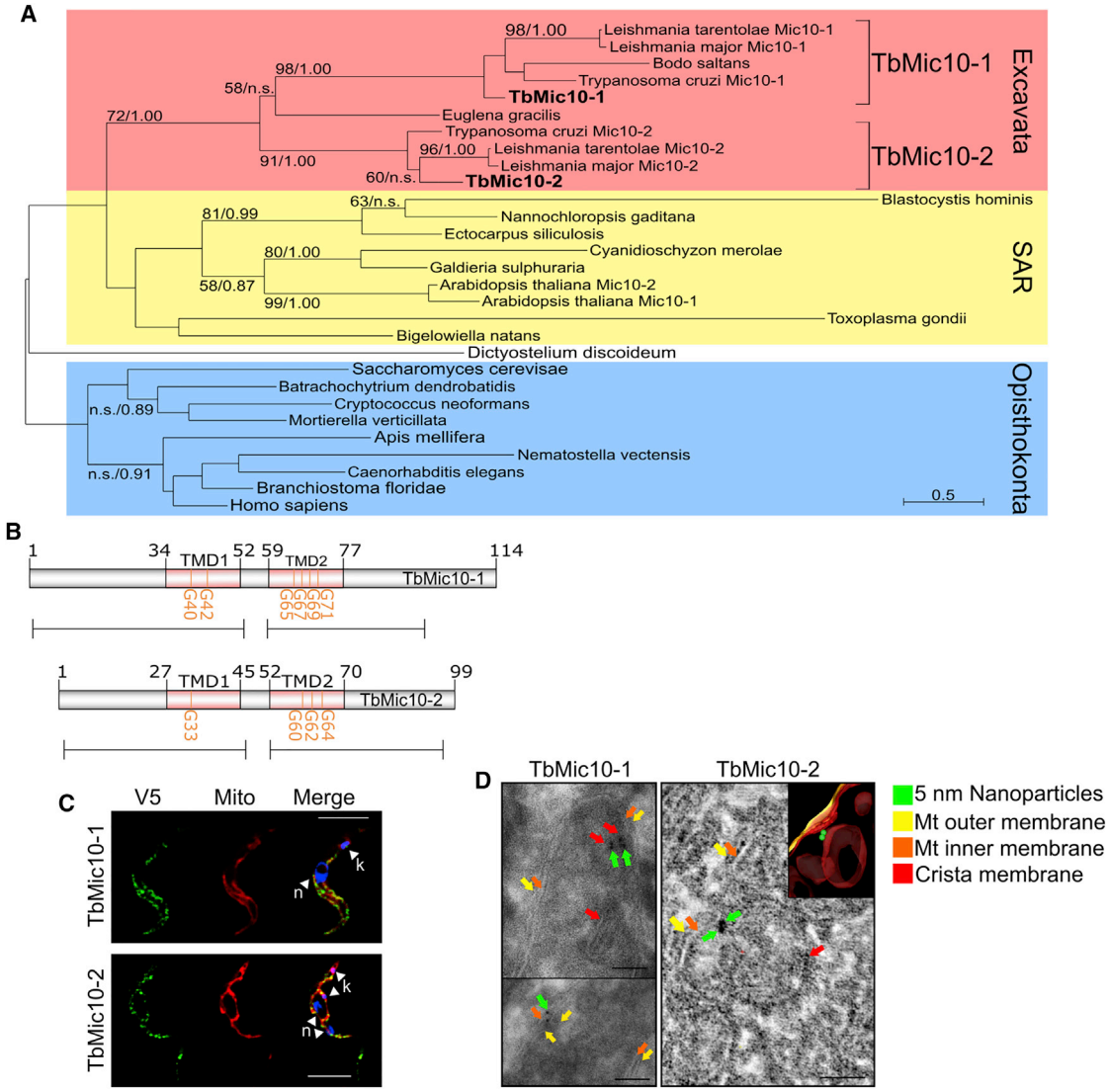

Figure 1. *T. brucei* Has Two Mic10 Paralogs that Localize to Cristae Membranes

(A) Maximum-likelihood tree of Mic10 orthologs from Excavata, SAR, and Opisthokonta. Branches well supported by bootstrap/posterior probabilities are indicated, and "n.s." signifies no support. Scale bar, substitutions/site. Alignment used for the tree is shown in Figure S1A.

(B) Scheme of TbMic10-1 and TbMic10-2. Each transmembrane domain (TMD) is shown in pink with conserved G residues demarked by orange bars. Scale bars indicate LC-MS/MS peptide coverage as in Figure 4B.

(C) Indirect immunofluorescence of TbMic10-1/2. k, kDNA (i.e., mitochondrial genome); n, nucleus. Scale bar, 5 μm.

(D) TbMic10-1-V5 and TbMic10-2-V5 immunogold labeling. Inset, tomography model. Colored arrow key is on right. Scale bars, 50 nm.

See also Video S1.

and/or subcomplexes migrating at ~440 and ~200 kDa (Figure 3A). To immunocapture proteins interacting with TbMic10-1/2, we used TbMic10-1/2-V5 as affinity handles in the *T. brucei* 927 strain. Solubilized hypotonically isolated mitochondria (Figure 3B) were incubated with mouse α-V5 antibody cross-linked to Protein G Dynabeads to immunoprecipitate (IP) the tags. After extensive washing, eluted proteins that coIP with TbMic10-1/2 were trypsinized and identified by liquid chromatography-tandem mass spectroscopy (LC-MS/MS). A mock IP was done with mitochondria from the parental cell line without V5 epitope to discriminate any non-specific binding to the anti-body-bead adduct. TbMic10-1/2-V5 IPs performed in triplicate invariably isolated the same complement of 11 proteins (named using the established MICOS nomenclature) [28], none of which were detected in the mock control (Figure 3C; Data S1A and S1B). All the identified subunits exhibited high peptide coverage (Figure 4B).

These interactions were verified by IP of the subunit we designated TbMic60 (explained in the next section), which was reciprocally tagged with a C-terminal hemagglutinin (HA) epitope. LC-MS/MS analysis revealed the same complement of TbMICOS subunits in triplicate TbMic60 IPs (Figure 3C; Data S1C). The

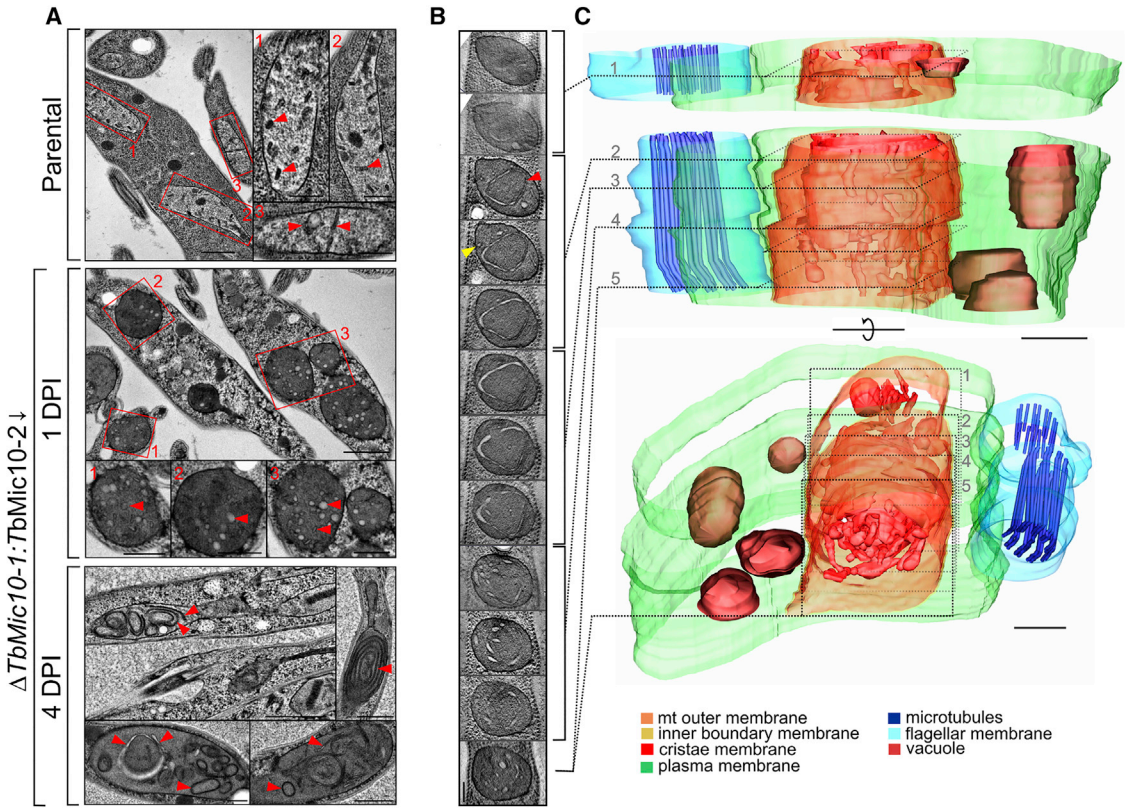

Figure 2. Simultaneous TbMic10-1/2 Ablation Results in Altered Cristae

(A) Representative TEM images from parental and *ΔTbMic10-1*/TbMic10-2↓ 1 and 4 days post-induction (DPI) *T. brucei*. Insets from the former two samples indicate close ups of the boxed and numbered mitochondria in the main images. Scale bars, 1 μm and 500 nm (insets). Representative cristae are indicated by red arrowheads. See also Figure S2.

(B) Serial TEM cryosections of *ΔTbMic10-1*/TbMic10-2↓ 4 DPI. Red and yellow arrows point to crista and inner mitochondrial membranes, respectively. Scale bars, 200 μm.

(C) 3D reconstruction of serial TEM cryosections in (B). Approximate location of sections is numbered and points to its respective section in (B). Key is on bottom. Scale bars, 200 μm.

See also Video S2.

only significant difference was detection of a single peptide from TbSAM50.

TbMICOS composition was also studied in the *T. brucei* 427 strain using a stable isotope labeling by/with amino acids in cell culture (SILAC)-based approach. Four cell lines expressing epitope-tagged versions of putative MICOS subunits TbMic10-1, TbMic10-2, TbMic20, and TbMic34 were subjected to IP using anti-tag antibodies (Figure 3D). The eluted proteins from a mixture of differentially labeled cells either expressing or lacking the tagged bait protein were analyzed by quantitative MS in triplicate to determine protein abundance ratios. In these four IPs, a set of proteins was recovered that were enriched >5-fold. Strikingly, this set was essentially identical to the one recovered in the 927 strain, with the difference of TbMic75 and TbSAM50 not being detected (Figures 3E–3G). However, TbSAM50 was enriched 2.6-fold in the TbMic10-2 IP.

Thus, by using two different IP protocols of 5 different baits in two *T. brucei* strains, we observe the same set of 9 proteins (Figure 4A). This result provides strong evidence that they constitute TbMICOS subunits. To further investigate this hypothesis, each candidate was C-terminally HA-tagged *in situ* in the 927 strain already bearing TbMic10-V5, except TbSAM50, which was N-terminally tagged. TbMic75 was not amenable to tagging and, given its absence in SILAC-IPs, was not pursued further. All TbMICOS subunits plus TbSAM50 were confirmed to assemble into the >1-MDa complex (Figure S3), consistent with their interaction as stable subunits of a single complex or an interaction partner in the case of Sam50.

TbMICOS Coincides with Cristae and Contains Novel Subunits

We determined whether TbMICOS subunit expression levels coincide with the occurrence of cristae via two high-throughput SILAC LC-MS/MS studies comparing the *T. brucei* PS and BS proteomes [29, 30] (Figure 4A). In at least one of these studies, most TbMICOS subunits are more expressed in PS compared to BS, the latter of which lack cristae. Intriguingly, TbMic17 is the sole exception, reported to be downregulated in PS.

Most TbMICOS subunits are well conserved among kinetoplastids (Figure 4A), which agrees with their presumptive association with such basic structures as cristae. Only *B. saltans* lacks

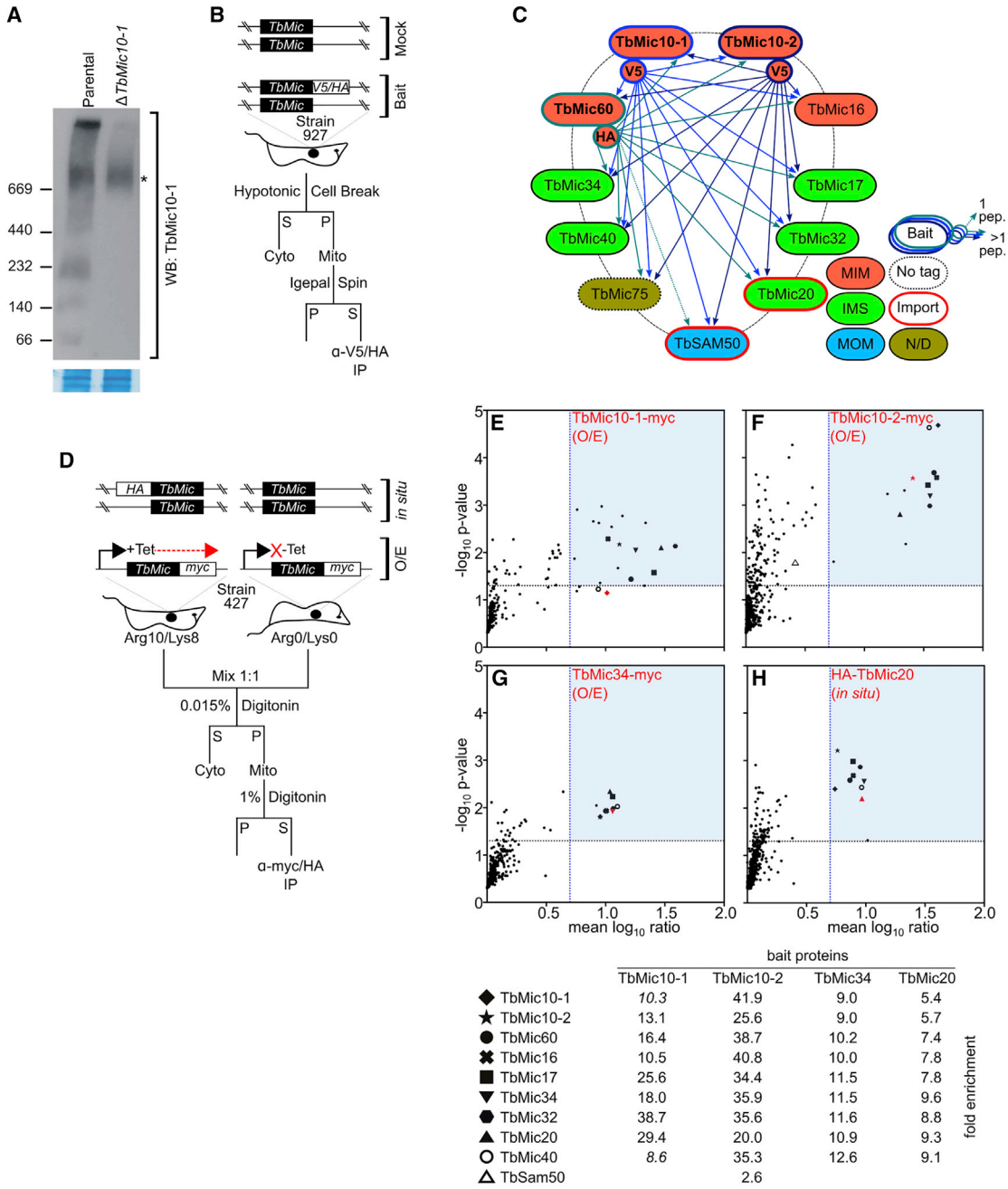

Figure 3. TbMICOS Subunit Composition

(A) Blue native (BN)-PAGE resolution of TbMICOS visualized on a western blot (WB) with anti-TbMic10-1 antibody. *, non-specific band. (Lower panel) Coomassie staining of F_1F_O-ATP synthase as a loading control is shown. Native protein size markers are on left.

(B) Scheme of 927 strain IP mitochondrial isolation and solubilization. (Top) Genetic background of parental cell line (mock) and tagged cell lines (bait) is shown. P, pellet; S, supernatant.

(C) Summary of 927 IPs. Affinity handles for TbMic10-1/2 (V5) and TbMic60 (HA) bait proteins point to co-IP proteins. Key is on right; N/D, sub-organellar localization not determined. Mass spectroscopy data used to make scheme are in Data S1.

(D) Scheme of 427 SILAC-IP as in (B), with genetic background of overexpression (O/E) and *in situ* tagged cell lines depicted at the top.

(E–H) SILAC-IP of epitope-tagged TbMic10-1 (E), TbMic10-2 (F), TbMic34 (G), and TbMic20 (H). x axis, the mean Log_{10} enrichment ratios of replicate bait IPs (n = 3), whose data point is marked in red; y axis, the corresponding Log_{10} p values. Blue quadrant highlights proteins that achieved the threshold of both values. Key to data point shape and fold enrichment for each protein is shown at the bottom.

See also Data S2 and Figure S3.

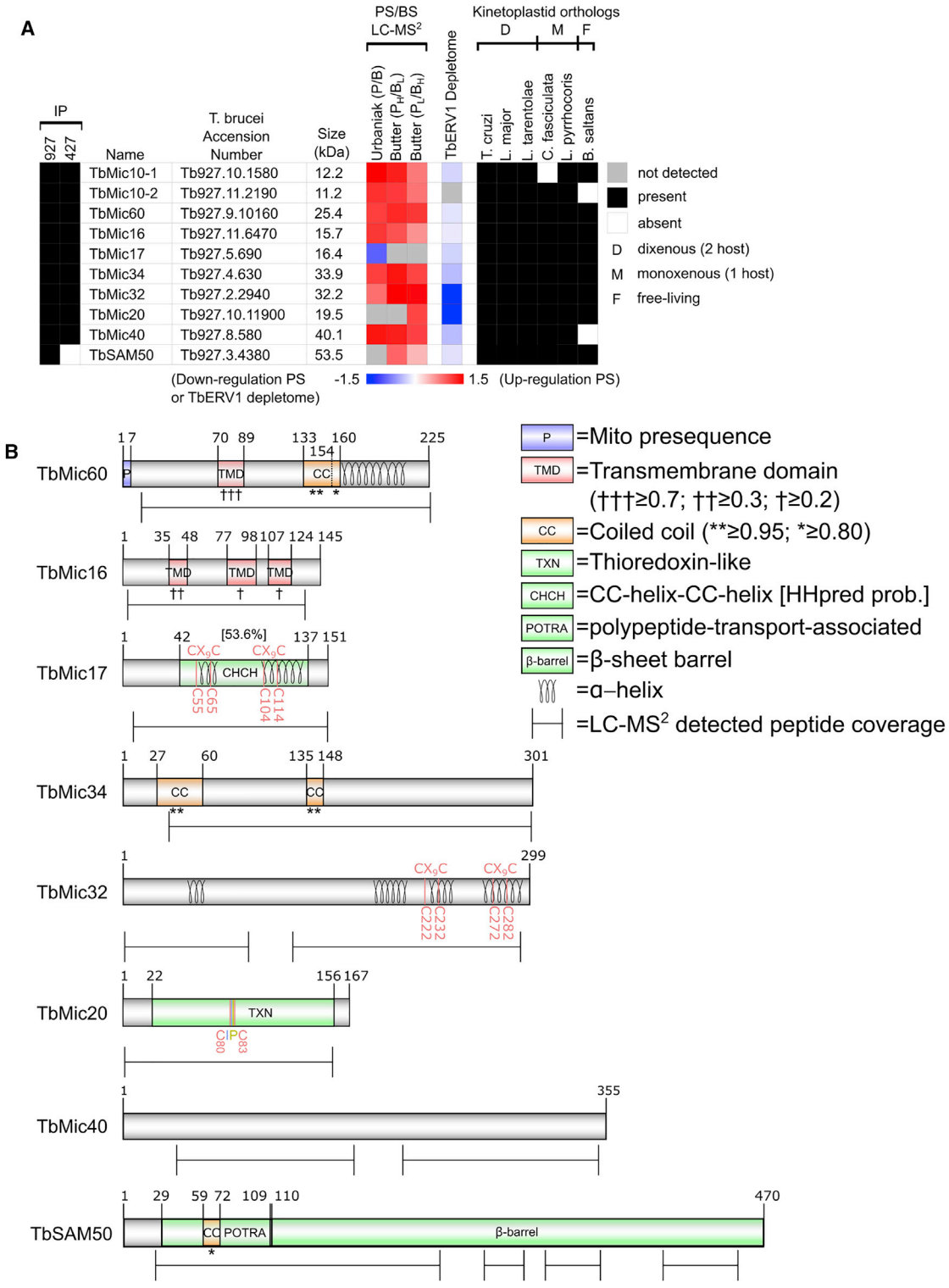

Figure 4. TbMICOS Subunit Analysis

(A) Summary of TbMICOS subunits: presence in IPs; SILAC LC-MS/MS determined expression levels in PS (P) and BS (B) by SILAC proteomics in Urbaniak [29] and Butter [30] studies with labeling indicated in subscripts (H, heavy; L, light); levels in TbERV1 depletome [31]; ortholog presence in other kinetoplastids. Relative protein abundance scale is shown below relevant columns. Key is on right. Accession numbers of kinetoplastid orthologs are in Table S1.

(B) Domain architecture and presence of α helices. Key to color-coding of motifs is on right. Probability scores from CC and TMD prediction software are indicated by * and †, respectively. Scale bars indicate LC-MS/MS peptide coverage as in Figure S1.

See also Figures S1B and S1C.

a homolog of TbMic40. Interestingly, the monoxenous trypanosomatid *Crithidia fasciculata* appears to have lost TbMic10-2.

Because these subunits are restricted to kinetoplastids, we investigated their domain architecture *in silico* to gain insight into their possible function. We designate a 25-kDa protein TbMic60 despite it missing the C-terminal mitofilin domain, which has been thus far this protein family's defining character [1]. However, TbMic60 has the same domain architecture of the N-terminal half of other Mic60 orthologs: a predicted mitochondrial presequence [32] that is consistent with observed LC-MS/MS peptide coverage (Figure S1B); a single TMD; a coiled coil (CC) domain; an α helix interspersed with conserved charged; and aromatic amino acids [33] (Figure S1C).

TbMic16 has 3 predicted TMDs, and TbMic34 has 2 putative CC domains. TbMic17 and TbMic32 have a pair of CX_9C motifs within predicted α helices, an IMS protein signature. TbMic17 has a degenerated CHCH domain that is detected by HHpred structure prediction [34], a feature also found in opisthokont Mic19. Interestingly, TbMic20 is a thioredoxin-like protein, complete with a CIPC motif that may catalyze redox reactions.

Association of TbMICOS with Cristae Membranes

The sub-organellar localization of TbMICOS was undertaken next. To facilitate comparison of all TbMICOS subunits, TbMic10-1/2 were also *in situ* HA tagged. The molecular weight of each tagged protein, with an extra ~5 kDa from the epitope, was confirmed by western blot analysis. The tagged proteins also served as proxies to estimate steady-state levels of TbMICOS subunits (Figure S4A). Consistent with aforementioned high-throughput proteomics data, TbMic17-HA was the least expressed subunit. Also, TbMic60-HA and TbMic34-HA exhibit similar levels (Figure S4B).

Next, hypotonically isolated mitochondria from the tagged TbMICOS cell lines were fractionated into matrix and membrane parts, the latter being further separated into peripheral and integral MIM fractions using an established pipeline [35] (Figure S4C). These fractions were probed with mitochondrial HSP70 [36] as a marker for matrix and peripheral MIM fractions. Expectedly, TbMic10-1-V5 and TbMic10-2-HA ended up in fractions having the integral MIM component prohibitin [37], confirming these are membrane proteins (Figure S4D). As each cell line contained TbMic10-1-V5, it was subsequently used as an integral membrane protein marker. TbMICOS subunit localization agreed with *in silico* predictions: TbMic60 and TbMic16 are integral proteins and the rest are in the MIM periphery (Figure S4D).

The sub-organellar localization of the soluble epitope-tagged TbMICOS subunits and integral subunit topology were subsequently addressed. Mitoplasts derived from these cell lines were subjected to a proteinase K protection assay (Figure S4E). Persistence of the C-terminal epitope indicates its localization in the matrix face of the intact MIM. The presence of matrix HSP70 and degradation of IMS TbERV1 confirmed the functionality of the assay. TbMic10-1-V5 served as a control after its topology had been verified (Figure S4F). In all cases, the C-terminal tag was degraded, indicating presence of the corresponding protein in the IMS.

Then, we asked whether the MICOS subunits are enriched within cristae *in vivo*. To address this question qualitatively, immunogold labeling of HA epitopes was employed in all TbMICOS cell lines, viewed by ET for integral subunits or TEM for the rest. As seen in Figures 5A–5T and Video S1, NPs mostly decorate cristae membranes, with some signal observed at the inner boundary membrane. Quantitative immunogold TEM revealed that HA-binding NPs were concentrated in mitochondria in comparison with the parental cell line lacking the epitope (Figure 5U). In all cases except TbMic20, more than half of NPs label cristae and all show significant inner boundary membrane localization (Figure 5V). This pattern is in contrast to the parental cell line, in which most NPs associate with undefined mitochondrial structures. Interestingly, HA-binding NPs often appear in clusters (Figures 5A–5D), suggesting a multimeric stoichiometry of the tagged protein within TbMICOS. This phenomenon was quantified by NP pairs that were <30 nm apart, revealing that most tagged subunits formed clusters with median ~10-nm distances (Figure 5W). Such clustering was vastly underrepresented in the negative control parental cells. In summary, we have shown that the TbMICOS subunits localize to cristae membranes in a way suggesting their multimerization.

Depletion of TbMICOS Subunits Alters Cristae

After establishing that TbMICOS localizes to cristae membranes, we asked whether some subunits have a role in shaping cristae, as was shown by concurrent ablation of TbMic10-1/2. Each cell line was transfected with a construct for inducible RNAi targeting a specific TbMICOS subunit or TbSAM50. An HA-tagged copy of each subunit allowed us to follow silencing of the target proteins using α-HA antibody and a consequent effect on TbMic10-1-V5. Over 6 days of RNAi induction, each cell line exhibited downregulation of its target subunit compared to HSP70 (Figure 6A).

Afterward, we examined whether depletion of each TbMICOS subunit compromised cell growth in a glucose-rich medium. We observed that all RNAi knockdowns except TbMic16 resulted in slower growth compared to mock-treated cell lines, usually 2 or 3 dpi (Figure 6B). This result was unexpected because growth was not inhibited in either *ΔTbMic10-1*:TbMic10-2↓ *T. brucei* (Figure S2C) or in MICOS yeast mutants grown on fermentable substrates [39]. Cell growth in glucose-poor medium, in which PS proliferation relies on OXPHOS [40], was not more severely affected (Figure S5A). Therefore, almost all TbMICOS subunits are essential for normal growth, irrespective of the mitochondrial bioenergetic state.

Cristae morphology was then observed in ultrathin cryosections of cells depleted of individual TbMICOS subunits at RNAi time points just before acute growth arrest (Figure S5B). TbMic40 RNAi stands out due to massive mitochondrial blebbing. TbMic60 and TbMic20 RNAi silencing exhibited phenotypes resembling those of *ΔTbMic10-1*:TbMic10-2↓4 dpi (Figure 2), with elongated cristae assuming an arc-like or circular morphology. To quantify this phenomenon, we measured cristae lengths of selected RNAi-silenced subunits, *ΔTbMic10-1*:TbMic10-2↓ and the parental strain (Figure 6C). These results correlated with qualitative observations, in which TbMic60 and TbMic20 RNAi displayed elongated cristae on par with *ΔTbMic10-1*:TbMic10-2↓. Furthermore, downregulation of TbMic34 resulted in a lesser degree of elongation similar to that of *ΔTbMic10-1*:TbMic10-2↓ 1 dpi. Other morphological parameters were also measured. *ΔTbMic10-1*:TbMic10-2↓ and TbMic60 RNAi exhibited an increase in mitochondrial area

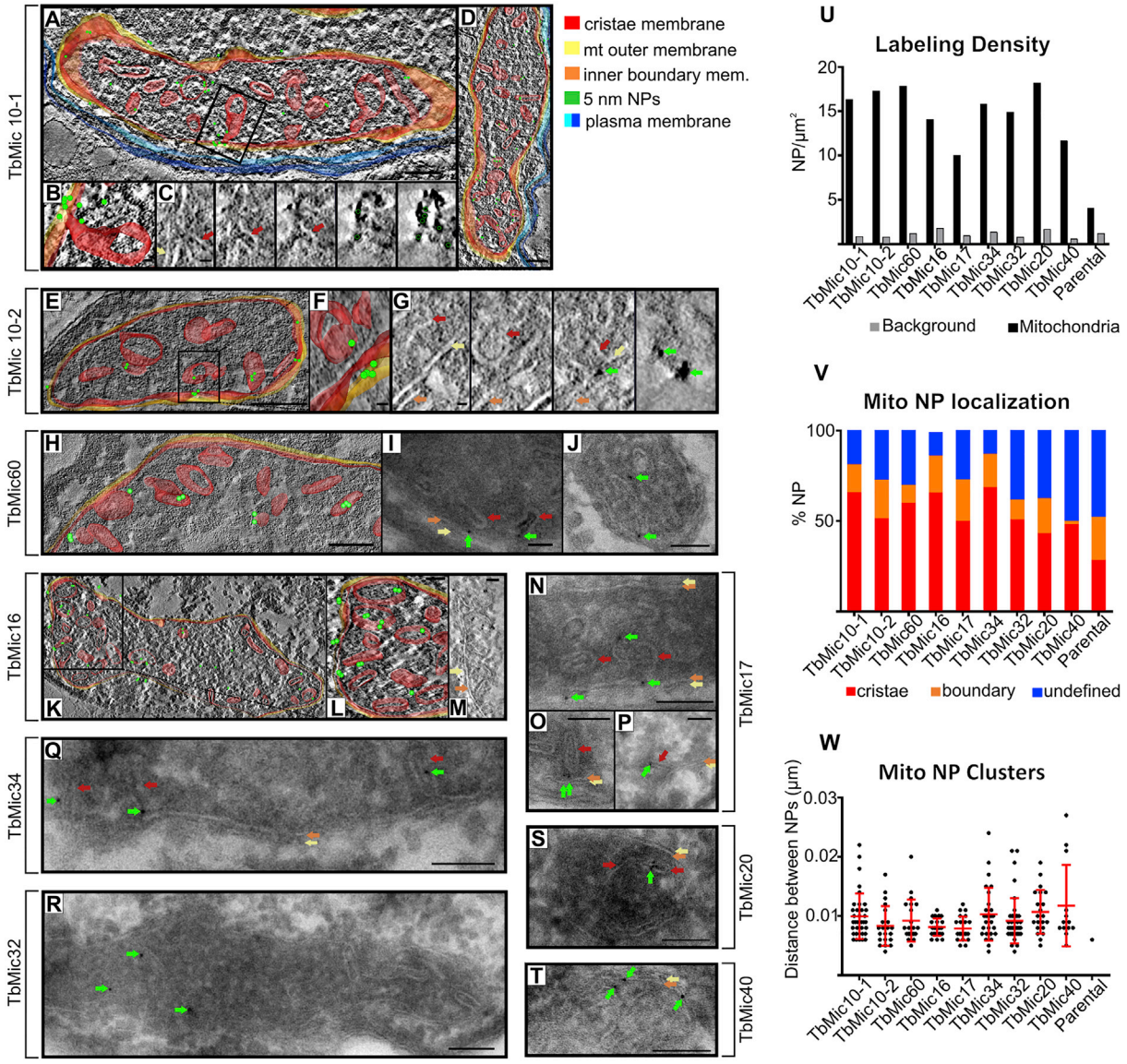

Figure 5. TbMICOS Localization in Cristae Membranes

(A–T) Representative electron tomography (A–M) and transmission electron microscopy (N–T) of subunits indicated on left (A–M, Q, and R) and right (N–P, S, and T) of brackets. Key on upper right classifies colors of structures (membranes and nanoparticles [NPs]) or arrows pointing to structures. C and G show electron tomography tilt series. Scale bars, 200 µm. See also Video S1.

(U) Labeling density of NPs in mitochondria (black bars) or background (gray bars). Statistical analyses of the labeling density by measuring relative labeling index [38] are given in Table S2, which contains total surface areas of mitochondria and background (i.e., rest of cell) examined in all analyses in (U)–(W).

(V) Localization of NPs within mitochondrial subcompartments. Red, cristae; orange, inner boundary membrane; blue, undefined.

(W) NP cluster analysis. Each dot represents measured distance (y axis) between 2 NPs. Median and interquartile range of these distances are in red. See also Figure S4.

(Figure 6D), correlating with the appearance of elongated cristae. There is a statistically significant increase in cristae per mitochondria in *ΔTbMic10-1*:TbMic10-2↓, and TbMic32 and TbMic20 displayed less of them, as compared to the parental control (Figure 6C). We have thus established that a subset of TbMICOS subunits, including TbMic60, shapes cristae.

Because the effect of TbMICOS ablation on *T. brucei* growth does not seem to correlate with altered cristae morphology, an effect on proteins of different mitochondrial compartments was examined in the RNAi cells (Figure 6A). Downregulation of all TbMICOS subunits except TbMic17 exhibited a subsequent depletion of TbMic10-1-V5. The voltage-dependent ion channel (VDAC) [41] was only affected upon TbSAM50 ablation. F_OF_1-ATP synthase β subunit was not decreased in any of the cell lines. However, we observed an unexpected significant drop in the abundance of the IMS protein TbERV1 [42] following RNAi against TbMic16, TbMic32, and TbMic20. To summarize, TbMic10-1 stability seems to depend on the presence of the

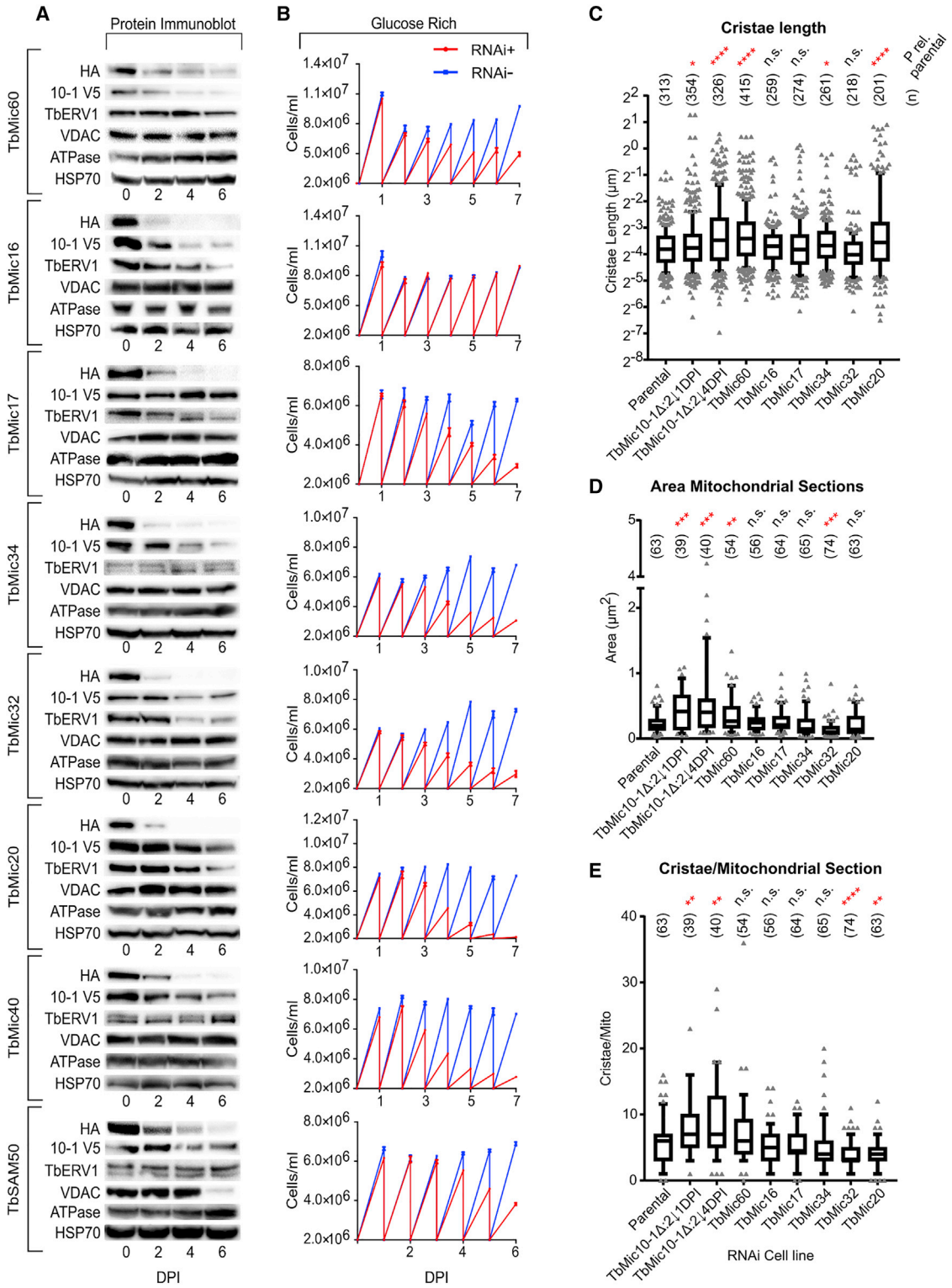

Figure 6. TbMICOS Subunit RNAi Phenotypes

(A) Immunoblot of RNAi cell lines (left of brackets) with antibody indicated on left. Days post-induction (DPI) are shown below panel.

(B) Measurement of TbMICOS RNAi growth in glucose-rich medium in which cells are diluted to 2 × 10^6 cells/mL every day (n = 3; error bars, SD). Cell density, y axis; DPI, x axis.

(C–E) Cristae properties in indicated RNAi cell lines.

(C) Cristae length measurement; y axis $\log_2$ transformed.

(legend continued on next page)

other TbMICOS subunits plus TbSAM50. Moreover, TbERV1 decreases upon depletion of some TbMICOS subunits, an intriguing phenomenon we further explored.

Thioredoxin-like TbMic20 Affects the Import of IMS Proteins

The downregulation of the IMS protein TbERV1 upon RNAi silencing of 3 TbMICOS subunits suggested that the complex may participate in the MIA pathway. TbERV1 is a key component of MIA, as evidenced by its knockdown in PS resulting in IMS protein downregulation [31]. Indeed, 2 of the 3 proteins affecting TbERV1 in our study, TbMic20 and TbMic32, were among those in the TbERV1 depletome (Figure 4A). However, an enzyme catalyzing IMS import in trypanosomes, in a way akin to opisthokont Mia40, remains unidentified [43].

We turned our attention to TbMic20 as a possible functional analog of Mia40. Along with it being affected by TbERV1 ablation, this hypothesis is supported by it having elements as a thioredoxin-like protein that could facilitate oxidative folding of $CX_{3,9}C$ IMS proteins. A TbMic20 homology model templated onto thioredoxin predicts that the CIPC reaction center occurs on a loop adjacent to an α helix, resulting in a structural motif similar to that of the human Mia40 CPC reaction center [22] (Figure S6A).

To address empirically whether TbMic20 is involved in MIA, we tested whether its depletion would result in reduced IMS protein abundance and thus phenocopy TbERV1 RNAi. Equal amounts of mitochondria were isolated from duplicate uninduced and 4 dpi TbMic20 RNAi cells. Proteins were extracted with ionic detergent, and their trypsin-derived peptides were labeled with tandem mass tags for sample discrimination after mixing them in equal parts before LC-MS/MS. In parallel, the same experiment was done for TbMic60.

A $\geq$1.6-fold threshold in both biological duplicates was set for detection of up- and downregulated proteins (Data S2A and S2B [TbMic20] and S2C and S2D [TbMic60]). Verified and predicted IMS proteins comprised 51% of the TbMic20 depletome (Figures 7A and S6B). Of these, over half overlap with those from the TbERV1 depletome (Figures 7A and 7B) [31]. Strangely, a ubiquinol-cytochrome *c* reductase that was decreased in the TbERV1 depletome was reproducibly the most upregulated protein upon TbMic20 RNAi silencing (Figures 7C and S6B). The other TbMic20 depletome IMS proteins belong to two categories: those identified by homology or experimentally (IMS) and those predicted to have a twin $CX_{3,9}C$ motifs (CxC). Notably, TbERV1 was not significantly affected by TbMic20 depletion 4 dpi, indicating that the phenotype is a direct effect (Figure 7C). Furthermore, such an effect on IMS proteins was not observed in the 4 dpi TbMic60 depletome analyzed in parallel. Thus, we provide evidence that TbMic20 participates in MIA.

Many of the affected IMS proteins are annotated as respiratory chain complex assembly factors (Figures 7C and S6B). Two of the most significantly downregulated proteins in the TbMic20 depletome are the respiratory complex III Rieske iron-sulfur protein and a complex I subunit (Figures S6B and S7). Given that cristae membranes are enriched in OXPHOS complexes [3], we interrogated the TbMic20 depletome for a preferential effect on respiratory chain components over matrix proteins, using the annotation of Zíková et al. [25]. Indeed, respiratory chain subunits were generally decreased in the 4 dpi TbMic20 depletome, and no such effect occurs in that of TbMic60 (Figure S7). Only the aforementioned pair of complex I and III subunits crossed the 1.6-fold threshold, suggesting the decline in the other OXPHOS subunits is a secondary effect of IMS-localized $CX_{3,9}C$ OXPHOS assembly factor depletion. Furthermore, the TbMic20-depletome more severely affects OXPHOS complex subunits, with the exception of complex II, than matrix proteins (Figure 7D). This finding suggests that TbMic20 association with cristae may facilitate population of its membrane with OXPHOS components.

We also examined how TbMic20 and TbMic60 RNAi depletion affected the TbMICOS subunits (Figure 7C). Although not significant, TbMic34, TbMic32, and TbMic40 were most affected by TbMic20 ablation. Among the 32 proteins downregulated by $\geq$1.6-fold in the TbMic60 RNAi cells are the target and TbMic16. TbMic10-1 appeared to be affected as well, confirming aforementioned western blot data (Figure 6A). Whether this differential effect of TbMic20 and TbMic60 depletion reflects a subcomplex architecture, as has been reported for yeast MICOS [39, 44, 45], remains to be determined.

DISCUSSION

Defining Conserved Features of MICOS

This study represents the first isolation and characterization of a MICOS complex outside of opisthokonts. As a highly diverged excavate unrelated to opisthokonts, *T. brucei* is well positioned to help identify highly conserved and relaxed features of MICOS that mediate CJ biogenesis and cristae shaping. The fundamental architecture of MICOS appears to be conserved, with novel supernumerary subunits attached to a MIM embedded core represented by Mic10 and Mic60 [11–13], albeit with diverged qualities that will be discussed later. Furthermore, some TbMICOS subunits appear to be multimeric, as has been observed in opisthokonts.

The association of MICOS with ancient Sam50 is conserved. The yeast Mic60 mitofilin domain mediates interaction with Sam50 [17–19] to form the even larger mitochondrial IMS bridging complex [2, 46]. Despite TbMic60 lacking the mitofilin domain, this interaction between TbMICOS and TbSAM50 was confirmed by its co-IP with TbMic10-1/2 and TbMic60. Furthermore, TbSAM50 assembles in a >1-MDa complex that was also observed in TbMICOS. Finally, TbSAM50 RNAi leads to TbMic10-1 downregulation.

In yeast, Cox17 and Aim24 have been shown to be peripheral MICOS interaction partners [47, 48]. It is possible that some of the TbMICOS subunits whose RNAi silencing does not yield the scored elongated cristae phenotype may represent such auxiliary factors. However, a counterargument to this idea is the tight association of the 9 TbMICOS subunits in 7 IPs performed under 2

(D) Mitochondrial section area measurement.

(E) Cristae per mitochondrial section in RNAi cell lines.

Boxplots show median and interquartile range. Whiskers demark data points in the 10–90 percentiles. Statistical significance of differences between each RNAi cell line and parental control is shown on top with population size (n): ****p < 0.0001; ***p < 0.001; **p < 0.01; *p < 0.05; n.s., not significant. See also Figure S5.

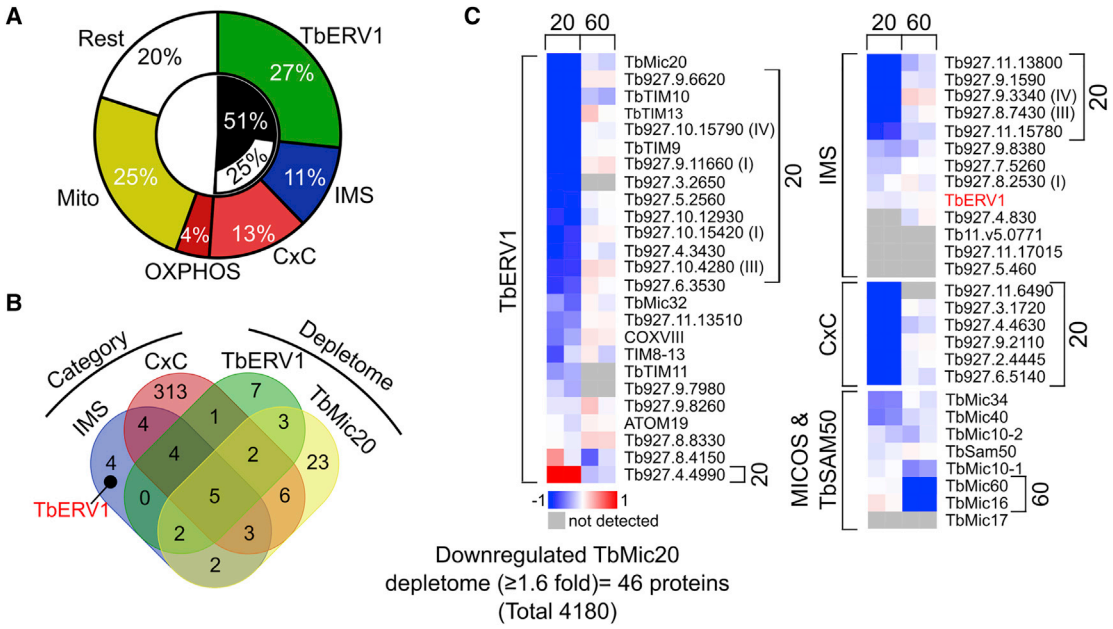

Downregulated TbMic20 depletome (≥1.6 fold)= 46 proteins (Total 4180)

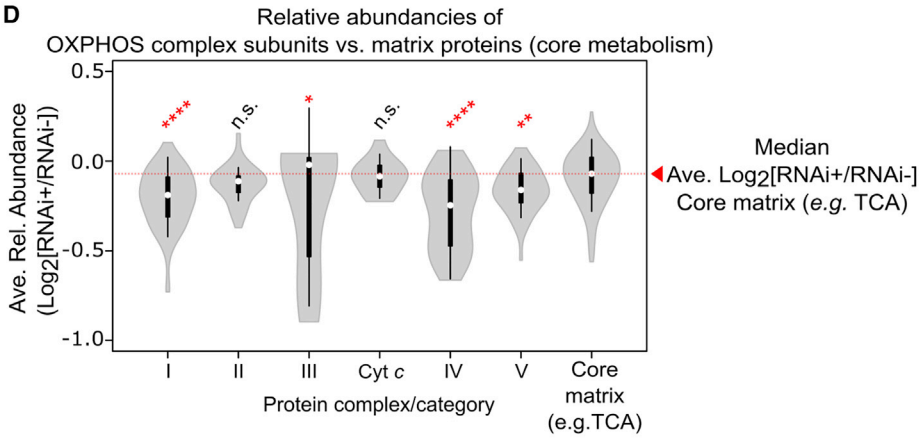

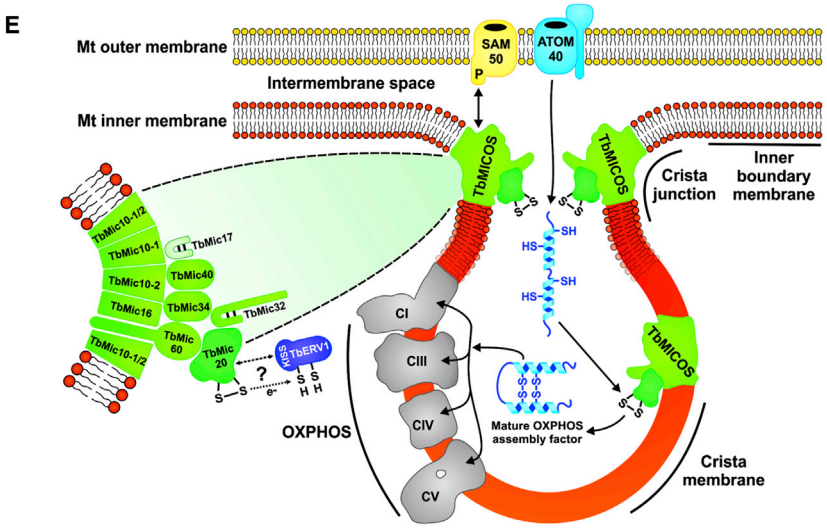

(legend on next page)

conditions. This is similar to the interconnection of yeast MICOS subunits upon their initial biochemical purification in 3 studies, none of which contained later identified peripheral proteins [8–10]. Furthermore, RNAi depletions of some human MICOS subunits also do not yield altered cristae [46], a similar result to ours. In the case of TbMICOS, perhaps the lack of the scored phenotype upon specific subunit depletion may be due to their functional redundancy under the examined conditions, as has been observed in attempts to delete each *TbMic10* paralog individually. Nevertheless, we cannot completely rule out the likelihood that some of the identified TbMICOSs are auxiliary factors, although we believe this to be a remote possibility.

Novel Features of TbMICOS

Although lacking the C-terminal mitofilin domain, TbMic60 retains the domain architecture of the N-terminal half of the protein, comprising of a mitochondrial presequence, single TMD, and CC domain [1, 2], that justifies its designation as a Mic60 ortholog. The α-proteobacterial ortholog of Mic60 also contains these elements, minus the presequence. Interestingly, the β- and γ-proteobacterial HemX protein, whose gene is syntenic to α-proteobacterial *Mic60* [2], bears these elements. Yet HemX lacks a mitofilin domain, setting a naturally occurring precedent for its absence between distantly related but still structurally conserved homologs. However, although bacterial Mic60 has been shown to bend membranes *in vitro* [15], such an activity remains to be determined for HemX. Still, the mitofilin domain is unnecessary for membrane bending, an activity mediated instead by the CC-domain-trailing α helix interspersed with aromatic and charged amino acids [33], a feature found in TbMic60. Finally, TbMic60 ablation exhibits one of the strongest cristae morphology phenotypes, analogous to the severity of Δ*Mic10* and Δ*Mic60* on yeast cristae [8, 10].

It is plausible that another TbMICOS subunit may assume the missing mitofilin domain's role, with TbMic34 being a top candidate. HA-tagged TbMic60 and TbMic34 have similar expression levels, which is compatible with their stoichiometric relationship. Furthermore, they are the only two subunits with CC domains, which could allow them to form an ~60-kDa heterodimer. Finally, TbMic34 RNAi caused a perceptible cristae-elongation phenotype, albeit to a lesser extent than observed upon TbMic60 silencing.

Uniquely, most trypanosomatid genomes encode two TbMic10 paralogs. They are functionally redundant in cultured PS *T. brucei*, because an obvious phenotype occurs only when both paralogs are ablated simultaneously. We speculate that the two isoforms help to regulate cristae formation in trypanosomatids with complicated life cycles, exemplified by cristae emergence during differentiation of *T. brucei* from BS to PS [25]. Concordantly, a single Mic10 ortholog is found in *B. saltans*, a free-living kinetoplastid, and the monoxenous trypanosomatid *C. fasciculata*, both having simpler life cycles.

Although simultaneous ablation of TbMic10-1/2 causes CJ loss and some TbMICOS subunits were detected at CJs, we mostly observe TbMICOS distributed throughout the cristae membrane. This localization is in contrast to the CJ enrichment of yeast MICOS [8–10, 39]. This may be due to the difficulty of capturing *T. brucei* CJs in cryosections. However, we favor the interpretation that TbMICOS is distributed throughout discoidal cristae for two reasons. The first involves the yeast lamellar cristae biogenesis pathway, requiring fusion of MIMs from two mitochondria [49]. MICOS was proposed to participate in this process by halting complete fusion of the MIM at CJs, which would otherwise lead to the detached cristae seen in Δ*MICOS* mutants. As kinetoplastids have a single mitochondrion, this cristae formation pathway may be absent, thus explaining the broad distribution of TbMICOS. The second reason is related to the thioredoxin-like TbMic20.

TbMICOS Is Involved in Intermembrane Space Protein Import

Until this study, an analog of Mia40, the central MIA enzyme in opisthokonts [20, 21] that is widely distributed throughout eukaryotes [50], has remained unidentified in *T. brucei* [42, 43]. We have serendipitously found a putative functional analog, TbMic20, among the stably interacting TbMICOS subunits. Its CIPC motif could execute disulfide bridge formation in IMS precursors by a similar mechanism as the Mia40 CPC reaction center [22]. Although more evidence is needed to support TbMic20 as the genuine MIA catalyst arising from convergent evolution, the fact that its depletion results in a preferential decrease of IMS proteins points to this conclusion.

In yeast, the sulfhydryl oxidase Erv1 directly binds Mia40 during IMS import [51]. However, TbERV1 is absent in all TbMICOS

Figure 7. TbMic20 RNAi Affects IMS Proteins

(A) Summary of downregulated proteins (≥1.6-fold threshold) in TbMic20 depletome. CXC, predicted $CX_{3,9}C$ pair containing proteins; IMS, experimentally or by homology identified IMS proteins; Mito, experimentally or by homology identified mitochondrial proteins; OXPHOS, subunits of respiratory chain; Rest, proteins that do not fall into these categories; TbERV1, depletome proteins. See also Figure S6.

(B) Venn diagram comparing TbMic20 and TbERV1 depletomes using category definitions as in (A).

(C) Heatmaps of log_2-transformed relative abundancies in TbMic20 (20) and TbMic60 (60) depletomes organized into categories as in (A). Brackets indicate proteins achieving the ≥1.6-fold threshold. Roman numerals in parentheses indicate OXPHOS complex component and/or assembly factor. Scale of relative protein abundance is on bottom of TbERV1 column.

(D) Violin plot of the log_2-transformed relative abundancies of respiratory chain complexes I–V, cytochrome-*c*-related proteins, and core matrix metabolism proteins (core), such as TCA cycle enzymes. Median downregulation for each protein population is marked by white circle; thick lines indicate the interquartile range of downregulated proteins and thin lines extend 1.5 times from the quartiles. Red dotted line across graph demarks median value for relative abundance of core proteins. Above each plot is the statistical significance of the different categories relative to the core group as indicated (****$p < 0.0001$; ***$p < 0.001$; **$p < 0.01$; *$p < 0.05$; n.s., not significant). Related to Figure S7.

(E) Proposed role of TbMICOS in cristae biogenesis. Mechanistic details are described in Discussion. IMS proteins are shown with blue α helices and thiols. Respiratory chain complexes (C) I and III–V are in gray. Inset depicts the theoretical composition of TbMICOS with undefined subunit stoichiometry. Faint color of TbMic17 reflects its low abundance in PS *T. brucei.* Possible interaction with TbERV1 bearing KISS domain is also depicted. P, Sam50 POTRA domain. See also Data S2.

preparations and reciprocally TbERV1 IP did not immunocapture TbMICOS [43]. However, TbERV1 localizes within discoidal cristae [43], as does TbMic20. Furthermore, TbERV1 has a "kinetoplastid-specific second" (KISS) domain [52], which may be an adaptation for binding another oxidoreductase besides Mia40 and/or stabilize the TbERV1 dimer when it is not transiently interacting with TbMic20.

TbMic20 RNAi not only results in a decrease of IMS proteins but also causes cristae elongation. This observation encapsulates our current model that TbMICOS serves as a hub for cristae shaping and IMS protein import (Figure 7E). TbMICOS via TbMic20 facilitates the oxidative folding of $CX_{3,9}C$-containing OXPHOS components, including OXPHOS assembly factors. TbMICOS distribution throughout cristae membranes allows the concentration of mature assembly factors in proximity to this membrane. In turn, this mechanism aids the population of cristae membrane with OXPHOS complex subunits that require these IMS proteins. TbMICOS also maintains CJs, anchoring cristae to the MOM via TbSAM50 interaction, bringing the crista lumen closer to the ATOM protein import pores [53], through which IMS protein precursors are translocated.

TbMICOS subunit depletion impairs *T. brucei* growth even under conditions in which energy generation occurs independently of OXPHOS. Thus, we propose that this is ultimately a consequence of mitochondrial import disruption. Indeed, many MIA substrates are involved in mitochondrial biogenesis, such as the small Tim chaperones [54]. Furthermore, the ATOM complex, the entry gate for nearly all proteins into the organelle, is also essential for *T. brucei* grown in ample glucose [53].

The Evolutionary Cell Biology of MICOS

We have explored the composition and function of MICOS in *T. brucei* to obtain much needed data about how this complex works outside of opisthokonts. Ultimately, our goal has been to better understand the MICOS complex by gaining insight into the evolutionary constraints that shape it. We confirm the hypothesis that the core function of MICOS in diverged eukaryotes is the maintenance of CJs, cristae shaping, and mediating MOM and MIM contacts. However, we also uncovered many surprising novelties that demonstrate MICOS has the potential to follow diverse evolutionary paths to adapt to different cellular contexts. Among them are TbMic60's lacking the conserved mitofilin domain and TbMic10 duplication into two distinct proteins. Yet most surprising is the presence of a thioredoxin-like TbMICOS subunit, which may allow MICOS to participate in IMS protein import. This activity extends the currently accepted functional model of MICOS, helping OXPHOS complex insertion into cristae membranes. It remains to be seen whether these novel TbMICOS properties are restricted to trypanosomatids or have a wider distribution in eukaryotes, indicating that opisthokont MICOS may actually represent the outlier.

STAR★METHODS

Detailed methods are provided in the online version of this paper and include the following:

- KEY RESOURCES TABLE
- CONTACT FOR REAGENT AND RESOURCE SHARING
- EXPERIMENTAL MODEL AND SUBJECT DETAILS
- METHOD DETAILS
  - Generation of T. brucei transgenic cell lines
  - T. brucei growth measurements
  - Mitochondria isolation and sub-fractionation
  - Antibody crosslinking to protein G Dynabeads
  - Immunoprecipitations
  - Mass spectrometry
  - LC-MS^2 analysis of peptides
  - SILAC proteomics
  - Proteinase K protection assay
  - Transmission electron microscopy
  - Bioinformatic analysis
- QUANTIFICATION AND STATISTICAL ANALYSIS
  - Analysis of immunogold and RNAi transmission electron microscopy data
  - Analysis of TbMic20 and TbMic60 depletome data
- DATA AND SOFTWARE AVAILABILITY

SUPPLEMENTAL INFORMATION

Supplemental Information includes seven figures, three tables, two videos, and two data files and can be found with this article online at https://doi.org/10.1016/j.cub.2018.09.008.

ACKNOWLEDGMENTS

We thank Jan Mani and Julia Bruggisser (University of Bern) for help at early phases of the project, Andreas Reichert (University of Düsseldorf) for initial consultation, Bettina Knapp for technical assistance with SILAC LC-MS/MS, and Aleš Horák for advice on phylogenetics. Support from the Czech Grant Agency (16-18699S to J.L. and 17-24036S to H.H.), ERC CZ (LL1601) to J.L., and ERD Funds (project OPVVV 16_019/0000759) to H.H. and J.L. is acknowledged. A.S. was supported by Swiss National Science Foundation grant 175563 and NCCR "RNA & Disease." B.W. was supported by ERC Consolidator Grant 648235, the Deutsche Forschungsgemeinschaft (Research Training Group RTG 2202), and Excellence Initiative of the German Federal and State Governments (EXC 294 BIOSS). Support from MEYS CR is acknowledged by M.V. and T.B. for the Czech BioImaging grant (LM2015062) and D.P. and Z.Z. for the CIISB research infrastructure project (LM2015043) and CEITEC 2020 (LQ1601) for supporting LC-MS/MS measurements at the Proteomics Core Facility, CEITEC, Masaryk University.

AUTHOR CONTRIBUTIONS

M.V., B.S., and H.H. designed the study. I.K., M.V., B.S., L.R.C., J.H., T.B., D.P., C.E., H.B., S.O., and H.H. performed the experiments. I.K., M.V., B.S., T.B., D.P., S.O., A.S., and H.H. analyzed the data. B.S., M.V., D.P., B.W., Z.Z., A.S., J.L., and H.H. wrote the paper.

DECLARATION OF INTERESTS

The authors declare no competing interests.

Received: June 25, 2018
Revised: August 2, 2018
Accepted: September 4, 2018
Published: October 25, 2018

REFERENCES

1. Muñoz-Gómez, S.A., Slamovits, C.H., Dacks, J.B., Baier, K.A., Spencer, K.D., and Wideman, J.G. (2015). Ancient homology of the mitochondrial contact site and cristae organizing system points to an endosymbiotic origin of mitochondrial cristae. Curr. Biol. *25*, 1489–1495.

2. Huynen, M.A., Mühlmeister, M., Gotthardt, K., Guerrero-Castillo, S., and Brandt, U. (2016). Evolution and structural organization of the mitochondrial contact site (MICOS) complex and the mitochondrial intermembrane space bridging (MIB) complex. Biochim. Biophys. Acta *1863*, 91–101.
3. Vogel, F., Bornhövd, C., Neupert, W., and Reichert, A.S. (2006). Dynamic subcompartmentalization of the mitochondrial inner membrane. J. Cell Biol. *175*, 237–247.
4. Davies, K.M., Anselmi, C., Wittig, I., Faraldo-Gómez, J.D., and Kühlbrandt, W. (2012). Structure of the yeast F1Fo-ATP synthase dimer and its role in shaping the mitochondrial cristae. Proc. Natl. Acad. Sci. USA *109*, 13602–13607.
5. Davies, K.M., Strauss, M., Daum, B., Kief, J.H., Osiewacz, H.D., Rycovska, A., Zickermann, V., and Kühlbrandt, W. (2011). Macromolecular organization of ATP synthase and complex I in whole mitochondria. Proc. Natl. Acad. Sci. USA *108*, 14121–14126.
6. Cogliati, S., Enriquez, J.A., and Scorrano, L. (2016). Mitochondrial cristae: where beauty meets functionality. Trends Biochem. Sci. *41*, 261–273.
7. Kühlbrandt, W. (2015). Structure and function of mitochondrial membrane protein complexes. BMC Biol. *13*, 89.
8. Harner, M., Körner, C., Walther, D., Mokranjac, D., Kaesmacher, J., Welsch, U., Griffith, J., Mann, M., Reggiori, F., and Neupert, W. (2011). The mitochondrial contact site complex, a determinant of mitochondrial architecture. EMBO J. *30*, 4356–4370.
9. Hoppins, S., Collins, S.R., Cassidy-Stone, A., Hummel, E., Devay, R.M., Lackner, L.L., Westermann, B., Schuldiner, M., Weissman, J.S., and Nunnari, J. (2011). A mitochondrial-focused genetic interaction map reveals a scaffold-like complex required for inner membrane organization in mitochondria. J. Cell Biol. *195*, 323–340.
10. von der Malsburg, K., Müller, J.M., Bohnert, M., Oeljeklaus, S., Kwiatkowska, P., Becker, T., Loniewska-Lwowska, A., Wiese, S., Rao, S., Milenkovic, D., et al. (2011). Dual role of mitofilin in mitochondrial membrane organization and protein biogenesis. Dev. Cell *21*, 694–707.
11. Kozjak-Pavlovic, V. (2017). The MICOS complex of human mitochondria. Cell Tissue Res. *367*, 83–93.
12. Wollweber, F., von der Malsburg, K., and van der Laan, M. (2017). Mitochondrial contact site and cristae organizing system: A central player in membrane shaping and crosstalk. Biochim. Biophys. Acta *1864*, 1481–1489.
13. Rampelt, H., Zerbes, R.M., van der Laan, M., and Pfanner, N. (2017). Role of the mitochondrial contact site and cristae organizing system in membrane architecture and dynamics. Biochim. Biophys. Acta *1864*, 737–746.
14. Barbot, M., Jans, D.C., Schulz, C., Denkert, N., Kroppen, B., Hoppert, M., Jakobs, S., and Meinecke, M. (2015). Mic10 oligomerizes to bend mitochondrial inner membranes at cristae junctions. Cell Metab. *21*, 756–763.
15. Tarasenko, D., Barbot, M., Jans, D.C., Kroppen, B., Sadowski, B., Heim, G., Möbius, W., Jakobs, S., and Meinecke, M. (2017). The MICOS component Mic60 displays a conserved membrane-bending activity that is necessary for normal cristae morphology. J. Cell Biol. *216*, 889–899.
16. Bohnert, M., Zerbes, R.M., Davies, K.M., Mühleip, A.W., Rampelt, H., Horvath, S.E., Boenke, T., Kram, A., Perschil, I., Veenhuis, M., et al. (2015). Central role of Mic10 in the mitochondrial contact site and cristae organizing system. Cell Metab. *21*, 747–755.
17. Bohnert, M., Wenz, L.S., Zerbes, R.M., Horvath, S.E., Stroud, D.A., von der Malsburg, K., Müller, J.M., Oeljeklaus, S., Perschil, I., Warscheid, B., et al. (2012). Role of mitochondrial inner membrane organizing system in protein biogenesis of the mitochondrial outer membrane. Mol. Biol. Cell *23*, 3948–3956.
18. Körner, C., Barrera, M., Dukanovic, J., Eydt, K., Harner, M., Rabl, R., Vogel, F., Rapaport, D., Neupert, W., and Reichert, A.S. (2012). The C-terminal domain of Fcj1 is required for formation of crista junctions and interacts with the TOB/SAM complex in mitochondria. Mol. Biol. Cell *23*, 2143–2155.
19. Zerbes, R.M., Bohnert, M., Stroud, D.A., von der Malsburg, K., Kram, A., Oeljeklaus, S., Warscheid, B., Becker, T., Wiedemann, N., Veenhuis, M., et al. (2012). Role of MINOS in mitochondrial membrane architecture: cristae morphology and outer membrane interactions differentially depend on mitofilin domains. J. Mol. Biol. *422*, 183–191.
20. Stojanovski, D., Bragoszewski, P., and Chacinska, A. (2012). The MIA pathway: a tight bond between protein transport and oxidative folding in mitochondria. Biochim. Biophys. Acta *1823*, 1142–1150.
21. Mordas, A., and Tokatlidis, K. (2015). The MIA pathway: a key regulator of mitochondrial oxidative protein folding and biogenesis. Acc. Chem. Res. *48*, 2191–2199.
22. Banci, L., Bertini, I., Cefaro, C., Ciofi-Baffoni, S., Gallo, A., Martinelli, M., Sideris, D.P., Katrakili, N., and Tokatlidis, K. (2009). MIA40 is an oxidoreductase that catalyzes oxidative protein folding in mitochondria. Nat. Struct. Mol. Biol. *16*, 198–206.
23. Lynch, M., Field, M.C., Goodson, H.V., Malik, H.S., Pereira-Leal, J.B., Roos, D.S., Turkewitz, A.P., and Sazer, S. (2014). Evolutionary cell biology: two origins, one objective. Proc. Natl. Acad. Sci. USA *111*, 16990–16994.
24. Hampl, V., Hug, L., Leigh, J.W., Dacks, J.B., Lang, B.F., Simpson, A.G., and Roger, A.J. (2009). Phylogenomic analyses support the monophyly of Excavata and resolve relationships among eukaryotic "supergroups". Proc. Natl. Acad. Sci. USA *106*, 3859–3864.
25. Zíková, A., Verner, Z., Nenarokova, A., Michels, P.A.M., and Lukeš, J. (2017). A paradigm shift: The mitoproteomes of procyclic and bloodstream *Trypanosoma brucei* are comparably complex. PLoS Pathog. *13*, e1006679.
26. Ebenezer, T.E., Carrington, M., Lebert, M., Kelly, S., and Field, M.C. (2017). *Euglena gracilis* genome and transcriptome: organelles, nuclear genome assembly strategies and initial features. In Euglena: Biochemistry, Cell and Molecular Biology, S. Schwartzbach, and S. Shigeoka, eds. (Cham: Springer), pp. 125–140.
27. Jackson, A.P., Quail, M.A., and Berriman, M. (2008). Insights into the genome sequence of a free-living Kinetoplastid: *Bodo saltans* (Kinetoplastida: Euglenozoa). BMC Genomics *9*, 594.
28. Pfanner, N., van der Laan, M., Amati, P., Capaldi, R.A., Caudy, A.A., Chacinska, A., Darshi, M., Deckers, M., Hoppins, S., Icho, T., et al. (2014). Uniform nomenclature for the mitochondrial contact site and cristae organizing system. J. Cell Biol. *204*, 1083–1086.
29. Urbaniak, M.D., Guther, M.L., and Ferguson, M.A. (2012). Comparative SILAC proteomic analysis of *Trypanosoma brucei* bloodstream and procyclic lifecycle stages. PLoS ONE *7*, e36619.
30. Butter, F., Bucerius, F., Michel, M., Čičová, Z., Mann, M., and Janzen, C.J. (2013). Comparative proteomics of two life cycle stages of stable isotope-labeled *Trypanosoma brucei* reveals novel components of the parasite's host adaptation machinery. Mol. Cell. Proteomics *12*, 172–179.
31. Peikert, C.D., Mani, J., Morgenstern, M., Käser, S., Knapp, B., Wenger, C., Harsman, A., Oeljeklaus, S., Schneider, A., and Warscheid, B. (2017). Charting organellar importomes by quantitative mass spectrometry. Nat. Commun. *8*, 15272.
32. Mach, J., Poliak, P., Matusková, A., Zárský, V., Janata, J., Lukeš, J., and Tachezy, J. (2013). An advanced system of the mitochondrial processing peptidase and core protein family in *Trypanosoma brucei* and multiple origins of the core I subunit in eukaryotes. Genome Biol. Evol. *5*, 860–875.
33. Hessenberger, M., Zerbes, R.M., Rampelt, H., Kunz, S., Xavier, A.H., Purfürst, B., Lilie, H., Pfanner, N., van der Laan, M., and Daumke, O. (2017). Regulated membrane remodeling by Mic60 controls formation of mitochondrial crista junctions. Nat. Commun. *8*, 15258.
34. Söding, J., Biegert, A., and Lupas, A.N. (2005). The HHpred interactive server for protein homology detection and structure prediction. Nucleic Acids Res. *33*, W244–W248.
35. Pusnik, M., Small, I., Read, L.K., Fabbro, T., and Schneider, A. (2007). Pentatricopeptide repeat proteins in *Trypanosoma brucei* function in mitochondrial ribosomes. Mol. Cell. Biol. *27*, 6876–6888.
36. Panigrahi, A.K., Zíková, A., Dalley, R.A., Acestor, N., Ogata, Y., Anupama, A., Myler, P.J., and Stuart, K.D. (2008). Mitochondrial complexes in

Trypanosoma brucei: a novel complex and a unique oxidoreductase complex. Mol. Cell. Proteomics *7*, 534–545.

37. Týc, J., Faktorová, D., Kriegová, E., Jirků, M., Vávrová, Z., Maslov, D.A., and Lukeš, J. (2010). Probing for primary functions of prohibitin in *Trypanosoma brucei*. Int. J. Parasitol. *40*, 73–83.
38. Mayhew, T.M., Lucocq, J.M., and Griffiths, G. (2002). Relative labelling index: a novel stereological approach to test for non-random immunogold labelling of organelles and membranes on transmission electron microscopy thin sections. J. Microsc. *205*, 153–164.
39. Friedman, J.R., Mourier, A., Yamada, J., McCaffery, J.M., and Nunnari, J. (2015). MICOS coordinates with respiratory complexes and lipids to establish mitochondrial inner membrane architecture. eLife *4*, e07739.
40. Coustou, V., Biran, M., Breton, M., Guegan, F., Rivière, L., Plazolles, N., Nolan, D., Barrett, M.P., Franconi, J.M., and Bringaud, F. (2008). Glucose-induced remodeling of intermediary and energy metabolism in procyclic *Trypanosoma brucei*. J. Biol. Chem. *283*, 16342–16354.
41. Pusnik, M., Charrière, F., Mäser, P., Waller, R.F., Dagley, M.J., Lithgow, T., and Schneider, A. (2009). The single mitochondrial porin of Trypanosoma brucei is the main metabolite transporter in the outer mitochondrial membrane. Mol. Biol. Evol. *26*, 671–680.
42. Basu, S., Leonard, J.C., Desai, N., Mavridou, D.A., Tang, K.H., Goddard, A.D., Ginger, M.L., Lukeš, J., and Allen, J.W. (2013). Divergence of Erv1-associated mitochondrial import and export pathways in trypanosomes and anaerobic protists. Eukaryot. Cell *12*, 343–355.
43. Haindrich, A.C., Boudová, M., Vancová, M., Diaz, P.P., Horáková, E., and Lukeš, J. (2017). The intermembrane space protein Erv1 of *Trypanosoma brucei* is essential for mitochondrial Fe-S cluster assembly and operates alone. Mol. Biochem. Parasitol. *214*, 47–51.
44. Guarani, V., McNeill, E.M., Paulo, J.A., Huttlin, E.L., Fröhlich, F., Gygi, S.P., Van Vactor, D., and Harper, J.W. (2015). QIL1 is a novel mitochondrial protein required for MICOS complex stability and cristae morphology. eLife *4*, e06265.
45. Zerbes, R.M., Höß, P., Pfanner, N., van der Laan, M., and Bohnert, M. (2016). Distinct roles of Mic12 and Mic27 in the mitochondrial contact site and cristae organizing system. J. Mol. Biol. *428*, 1485–1492.
46. Ott, C., Dorsch, E., Fraunholz, M., Straub, S., and Kozjak-Pavlovic, V. (2015). Detailed analysis of the human mitochondrial contact site complex indicate a hierarchy of subunits. PLoS ONE *10*, e0120213.
47. Chojnacka, M., Gornicka, A., Oeljeklaus, S., Warscheid, B., and Chacinska, A. (2015). Cox17 protein is an auxiliary factor involved in the control of the mitochondrial contact site and cristae organizing system. J. Biol. Chem. *290*, 15304–15312.
48. Harner, M.E., Unger, A.K., Izawa, T., Walther, D.M., Ozbalci, C., Geimer, S., Reggiori, F., Brügger, B., Mann, M., Westermann, B., and Neupert, W. (2014). Aim24 and MICOS modulate respiratory function, tafazzin-related cardiolipin modification and mitochondrial architecture. eLife *3*, e01684.
49. Harner, M.E., Unger, A.K., Geerts, W.J., Mari, M., Izawa, T., Stenger, M., Geimer, S., Reggiori, F., Westermann, B., and Neupert, W. (2016). An evidence based hypothesis on the existence of two pathways of mitochondrial crista formation. eLife *5*, e18853.
50. Muñoz-Gómez, S.A., Slamovits, C.H., Dacks, J.B., and Wideman, J.G. (2015). The evolution of MICOS: Ancestral and derived functions and interactions. Commun. Integr. Biol. *8*, e1094593.
51. Mesecke, N., Terziyska, N., Kozany, C., Baumann, F., Neupert, W., Hell, K., and Herrmann, J.M. (2005). A disulfide relay system in the intermembrane space of mitochondria that mediates protein import. Cell *121*, 1059–1069.
52. Eckers, E., Petrungaro, C., Gross, D., Riemer, J., Hell, K., and Deponte, M. (2013). Divergent molecular evolution of the mitochondrial sulfhydryl:cytochrome C oxidoreductase Erv in opisthokonts and parasitic protists. J. Biol. Chem. *288*, 2676–2688.
53. Mani, J., Desy, S., Niemann, M., Chanfon, A., Oeljeklaus, S., Pusnik, M., Schmidt, O., Gerbeth, C., Meisinger, C., Warscheid, B., and Schneider, A. (2015). Mitochondrial protein import receptors in Kinetoplastids reveal convergent evolution over large phylogenetic distances. Nat. Commun. *6*, 6646.
54. Wenger, C., Oeljeklaus, S., Warscheid, B., Schneider, A., and Harsman, A. (2017). A trypanosomal orthologue of an intermembrane space chaperone has a non-canonical function in biogenesis of the single mitochondrial inner membrane protein translocase. PLoS Pathog. *13*, e1006550.
55. Poon, S.K., Peacock, L., Gibson, W., Gull, K., and Kelly, S. (2012). A modular and optimized single marker system for generating *Trypanosoma brucei* cell lines expressing T7 RNA polymerase and the tetracycline repressor. Open Biol. *2*, 110037.
56. Dean, S., Sunter, J., Wheeler, R.J., Hodkinson, I., Gluenz, E., and Gull, K. (2015). A toolkit enabling efficient, scalable and reproducible gene tagging in trypanosomatids. Open Biol. *5*, 140197.
57. McAllaster, M.R., Sinclair-Davis, A.N., Hilton, N.A., and de Graffenried, C.L. (2016). A unified approach towards *Trypanosoma brucei* functional genomics using Gibson assembly. Mol. Biochem. Parasitol. *210*, 13–21.
58. Merritt, C., and Stuart, K. (2013). Identification of essential and non-essential protein kinases by a fusion PCR method for efficient production of transgenic *Trypanosoma brucei*. Mol. Biochem. Parasitol. *190*, 44–49.
59. Schimanski, B., Nguyen, T.N., and Günzl, A. (2005). Characterization of a multisubunit transcription factor complex essential for spliced-leader RNA gene transcription in *Trypanosoma brucei*. Mol. Cell. Biol. *25*, 7303–7313.
60. Wiśniewski, J.R., Ostasiewicz, P., and Mann, M. (2011). High recovery FASP applied to the proteomic analysis of microdissected formalin fixed paraffin embedded cancer tissues retrieves known colon cancer markers. J. Proteome Res. *10*, 3040–3049.
61. Stejskal, K., Potěšil, D., and Zdráhal, Z. (2013). Suppression of peptide sample losses in autosampler vials. J. Proteome Res. *12*, 3057–3062.
62. Käser, S., Willemin, M., Schnarwiler, F., Schimanski, B., Poveda-Huertes, D., Oeljeklaus, S., Haenni, B., Zuber, B., Warscheid, B., Meisinger, C., and Schneider, A. (2017). Biogenesis of the mitochondrial DNA inheritance machinery in the mitochondrial outer membrane of *Trypanosoma brucei*. PLoS Pathog. *13*, e1006808.
63. Katoh, K., Misawa, K., Kuma, K., and Miyata, T. (2002). MAFFT: a novel method for rapid multiple sequence alignment based on fast Fourier transform. Nucleic Acids Res. *30*, 3059–3066.
64. Stamatakis, A. (2014). RAxML version 8: a tool for phylogenetic analysis and post-analysis of large phylogenies. Bioinformatics *30*, 1312–1313.
65. Ronquist, F., Teslenko, M., van der Mark, P., Ayres, D.L., Darling, A., Höhna, S., Larget, B., Liu, L., Suchard, M.A., and Huelsenbeck, J.P. (2012). MrBayes 3.2: efficient Bayesian phylogenetic inference and model choice across a large model space. Syst. Biol. *61*, 539–542.
66. Biasini, M., Bienert, S., Waterhouse, A., Arnold, K., Studer, G., Schmidt, T., Kiefer, F., Gallo Cassarino, T., Bertoni, M., Bordoli, L., and Schwede, T. (2014). SWISS-MODEL: modelling protein tertiary and quaternary structure using evolutionary information. Nucleic Acids Res. *42*, W252–W258.
67. Krogh, A., Larsson, B., von Heijne, G., and Sonnhammer, E.L. (2001). Predicting transmembrane protein topology with a hidden Markov model: application to complete genomes. J. Mol. Biol. *305*, 567–580.
68. Lupas, A., Van Dyke, M., and Stock, J. (1991). Predicting coiled coils from protein sequences. Science *252*, 1162–1164.

STAR★METHODS

KEY RESOURCES TABLE

REAGENT or RESOURCE	SOURCE	IDENTIFIER
Antibodies		
Mouse anti-V5	ThermoScientific (Life Technologies)	Catalog #: 377500; RRID: AB_2533339
Mouse anti-HA	ThermoScientific (Life Technologies)	Catalog #: 26183; RRID: AB_10978021
Rabbit anti-V5	Sigma Aldrich	Catalog #: V8137; RRID: AB_261889
Rabbit anti-HA	Sigma Aldrich	Catalog #: H6908; RRID: AB_260070
Rabbit anti-TbMic10-1	This study	N/A
Mouse anti-HSP70	[36]	N/A
Rabbit anti-TbERV1	[42]	N/A
Rabbit anti-VDAC	[41]	N/A
Rabbit anti-prohibitin	[37]	N/A
Chemicals, Peptides, and Recombinant Proteins		
Proteinase K, recombinant, PCR Grade	Sigma Aldrich (Roche)	Catalog #: 000000003115879001
Digitonin	Sigma Aldrich	Catalog #: D141
Protein G Dynabeads	ThermoScientific (Life Technologies)	Catalog #: 10004D
Dimethyl pimelimidate dihydrochloride	Sigma Aldrich	Catalog #: D8388
Q5 High-Fidelity DNA Polymerase	New England Biolabs	Catalog #: M0491
Critical Commercial Assays		
Direct-zol RNA MiniPrep w/ Zymo-Spin IIC Columns	Zymo Research (Amplicon)	Catalog #: R2050
Human T Cell Nucleofector Kit, 100 reactions	Lonza	Catalog #: VVPA-1002
Bolt TM 4-12% Bis-Tris Plus Gels	ThermoScientific (LifeTechnologies)	Catalog #: NW04120BOX
Deposited Data		
Trypanosomatid ortholog sequences	See Table S1	N/A
927 immunoprecipitation plus TbMic20 and TbMic60 depletome MS^2 data	PRIDE	ID#: PXD009601
Experimental Models: Cell Lines		
TbMic10-1-V5	This study	N/A
TbMic10-2-V5	This study	N/A
ΔTbMic10-1:TbMic10-2↓	This study	N/A
TbMic10-1-HA	This study	N/A
TbMic10-2-HA:TbMic10-1-V5	This study	N/A
TbMic60-HA:TbMic10-1-V5:TbMic60↓	This study	N/A
TbMic16-HA:TbMic10-1-V5:TbMic16↓	This study	N/A
TbMic17-HA:TbMic10-1-V5:TbMic17↓	This study	N/A
TbMic34-HA:TbMic10-1-V5:TbMic34↓	This study	N/A
TbMic32-HA:TbMic10-1-V5:TbMic32↓	This study	N/A
TbMic20-HA:TbMic10-1-V5:TbMic20↓	This study	N/A
TbMic40-HA:TbMic10-1-V5:TbMic40↓	This study	N/A
TbSAM50-HA:TbMic10-1-V5:TbSAM50↓	This study	N/A
Experimental Models: Organisms/Strains		
SMOXP *T. brucei* cell line	[54]	RRID: SCR_004786
Oligonucleotides		
For oligonucleotides used in this study, see Table S3	N/A	N/A

(*Continued on next page*)

Continued

REAGENT or RESOURCE	SOURCE	IDENTIFIER
Recombinant DNA		
pTrypSon	[55]	N/A
pPOTv4	[38]	N/A
pPOT-V5-HygR	This study	N/A
pPOT-HA-NeoR	This study	N/A
Software and Algorithms		
GraphPad Prism 7	GraphPad	https://www.graphpad.com/
Image Lab	Bio-Rad	http://www.bio-rad.com/en-de/product/image-lab-software?ID=KRE6P5E8Z
Geneious 9.1.7	Biomatters	https://www.geneious.com/

CONTACT FOR REAGENT AND RESOURCE SHARING

Further information and requests for resources and reagents should be directed to and will be fulfilled by the Lead Contact, Hassan Hashimi (hassan@paru.cas.cz)

EXPERIMENTAL MODEL AND SUBJECT DETAILS

The procyclic *T. brucei* (RRID: SCR_004786) 927 strain SmOxP cell line [55] served as the parental cell line for all experiments except those depicted in Figures 3D–3H, which utilized 427 strain 29-13 cell line. *T. brucei* were grown at 27°C and ambient atmosphere in SDM79 medium, which was supplemented with 6 mM glucose, or SDM80, a glucose poor medium [40]. Both media contained heat-inactivated 10% (v/v) fetal bovine serum and 7.5 mg/L hemin. Cells were maintained at exponential growth phase as exemplified by the growth curves in Figures 6B, S2C, and S5A plus described in Method Details.

METHOD DETAILS

Generation of T. brucei transgenic cell lines

The SmOxP cell lines were transformed with gene tagging constructs derived from the pPOTv4 vector [56] modified to contain the V5 (with original hygromycin resistance cassette) and HA epitope tags, the latter also with a neomycin resistance marker. Transformants were selected using the appropriate antibiotic. For generation of long hairpin RNAi cell lines, PCR amplicons derived from a given TbMICOS subunit gene were cloned into the pTrypSon vector by the already described Gibson assembly protocol [57]. Constructs for gene knockout were generated by an established fusion PCR approach [58]. Oligonucleotides used for PCR amplification and destination plasmids are given in Table S3.

For SILAC-IP transgenic cell lines based on *T. brucei* 29-13 were generated. The coding sequences of TbMic10-1, TbMic10-2 and TbMic34 were amplified from genomic DNA and cloned into a derivative of pLEW100 modified to enable tetracycline-inducible expression of C-terminal triple, c-Myc tagged proteins after selection with puromycin. In the case of TbMic20, one allele was tagged *in situ* at the N terminus with a single HA epitope via site directed integration of a PCR product amplified from pPURO-HA-TFIIA-1 [59]. Long primers containing homologous regions of the 5′ UTR (positions - 89 to −1 relative to the start codon) and the ORF (positions +4 to + 94) were designed to provide sequences for homologous recombination. Puromycin was used to select for stable transfectants.

T. brucei growth measurements

Cultures were grown in triplicate in the presence and absence of the tetracycline-class antibiotic doxycycline for RNAi-induction. Cell density was counted using the Beckman Coulter Z2 Cell and Particle Counter every 24 H and subsequently diluted to 2×10^6 cells/ml, maintaining cells in exponential phase of growth.

Mitochondria isolation and sub-fractionation

Subfractionation of mitochondria was performed using an established protocol [35]. A suspension of hypotonically isolated mitochondria in 10 mM $MgCl_2$ were initially sub-fractionated into matrix and membrane parts by 10 cycles of snap freezing in liquid N_2 and thawing at RT. The suspension was then centrifuged for 5 min at 10,000 x g at 4°C. The supernatant was collected as the matrix fraction. Part of the pellet was collected as the membrane fraction while the rest was further processed by resuspension in 0.1 M Na_2CO_3. After a 10 minute incubation on ice, the suspension was centrifuged for 20 min at 100,000 x g at 4°C. The supernatant was removed as the peripheral fraction. Fresh 0.1 M Na_2CO_3 was applied to the pellet for another centrifugation as mentioned before.

The pellet was removed as the integral protein fraction. Proteins were precipitated from all fractions with trichloroacetic acid prior to their resolution by SDS-PAGE.

Digitonin preparation of crude mitochondria and quantitative LC-MS^2 and mitoplasts for proteinase K protection assays were done according to an established protocol [54]. Briefly, to obtain crude mitochondrial fractions, 10^8 *T. brucei* cells were treated with 0.015% digitonin (w/v) on ice for 5 min. Mitochondria were concentrated by centrifugation at 6,800 x g for 3 min at 4°C. This pellet was further treated with 0.2% digitonin for 15 min on ice and centrifuged as before to obtain mitoplasts.

Antibody crosslinking to protein G Dynabeads

Fifteen μg of Dynabeads (Thermo Scientific) were washed twice in PBS with 0.02% (v/v) Tween 20 (PBS-T20) and rotated overnight at 4°C with 100μg of mouse anti-V5 or anti-HA antibodies (Thermo Scientific) in 1 mL PBS-T20. Afterward, the beads were washed twice in 0.1 M Triethanolamine in PBS (PBS TEA). The antibodies were conjugated to beads by rotation in PBS TEA supplemented with 6 mg/ml Dimethyl pimelimidate for 30 min at RT twice. The beads were washed again twice in PBS TEA. The beads were then treated with quenching buffer (25 mM ethanolamine in PBS) at RT for 5 min, washed once in PBS, and incubated twice with 1 M glycine pH 3.0 at RT to remove unbound antibody. The beads were washed three times with PBS-T20 and stored at 4°C in 0.09% NaN_3 until needed. Antibodies used in the study are listed in Key Resources Table.

Immunoprecipitations

Hypotonically isolated frozen mitoplast pellets (0.5 mg) were solubilized in IPP50 (50 mM KCl, 20 mM Tris-HCl pH 7.7, 3 mM $MgCl_2$, 10% glycerol, 0.5 mM DTT, 1 mM phenylmethanesulfonyl fluoride (PMSF), complete EDTA free protease inhibitor cocktail (Rosche)) supplemented with 1% Igepal (v/v) for 20 min on ice. After centrifugation (18 000 X g, 15 min, 4°C) the supernatant was added to 1.5 mg of anti-V5 or anti-HA magnetic beads, previously washed three times in 200μl of IPP50 + 1% Igepal for 5 min at RT. The solubilized mitochondria were rotated with beads for 90 min at 4°C. After removal of the flow through, the beads were washed three times in IPP50 + 1% Igepal. Before elution the beads were transferred into a fresh tube. Elution was done in 0.1 M glycine pH 2.0 for 10 min at 70°C and shaking at 1000 rpm. The eluate was neutralized with 1 M Tris pH 8.0. The eluates were further processed for LC-MS^2 analysis or resolved by SDS-PAGE. IPs were performed in triplicate.

Mass spectrometry

Triplicate eluates of co-IP proteins from the 927 strain and duplicate TbMic20 and TbMic60 depletomes were processed by filter-aided sample preparation (FASP) method [60] with some modifications. The samples were mixed with 8 M UA buffer (8 M urea in 100 mM Tris-HCl, pH 8.5), loaded onto a Microcon device with a molecular weight cut-off of 30 kDa (Merck Millipore) and centrifuged at 7,000 × *g* (subsequent centrifugation steps done at 14,000 × *g*) for 30 min at 20°C. The retained proteins were washed with 200 μL UA buffer. The final protein concentrates trapped in the Microcon device were mixed with 100 μL of UA buffer containing 50 mM iodoacetamide and incubated in the dark for 20 min. After the next centrifugation step, the samples were washed three times with 100 μL UA buffer and three times with 100 μL of 50 mM $NaHCO_3$. Sequencing grade trypsin (Promega) was added onto the filter and the mixture was incubated for 18 h at 37°C (enzyme:protein ratio 1:100). The tryptic peptides were finally eluted by centrifugation followed by two additional elutions with 50 μL of 50mM $NaHCO_3$. After FASP, peptides of co-IP proteins were directly extracted into LC-MS vials by 2.5% formic acid (FA) in 50% acetonitrile (ACN) and 100% ACN with addition of polyethylene glycol (20,000; final concentration 0.001%) [61] and concentrated by SpeedVac (Thermo Fisher Scientific) prior to LC-MS analyses.

Triethylammonium bicarbonate was used instead of $NaHCO_3$ during all FASP steps in case of depletome samples. Duplicate TbMic20 or TbMic60 samples were separately labeled using Tandem Mass Tags (TMT6plex; Thermo Fisher Scientific) using the manufacturer's instructions. Labeling efficiency was checked by LC-MS analyses and database searches using variable TMT-related modifications and was found to be > 96% (portion of the correctly labeled peptide spectrum matches (PSMs) out of all PSMs). Individual samples were mixed in the ratio of 1:1:1:1.

Both pooled samples were offline fractionated using basic pH reverse phase liquid chromatography (mobile phase A: 20 mM Ammonium Hydroxide in water; mobile phase B: 20 mM Ammonium Hydroxide in 80% acetonitrile (ACN); stationary phase: XBridge C18 3.5μm, 150 × 3mm; Waters) using the Ultimate3000 UHPLC+ system (SR-3000, LPG-3400 XRS, WPS-3000 TXRS, TCC-3000 RS, VWD-3400 RS). A 30 minute nonlinear gradient (0 min: 0.5% B, 5 min: 10% B, 30 min: 60% B; 35 min: 80% B – system wash; flow rate 0.5 ml/min) was used to fractionate peptides into 33 fractions (1 fraction/min), which were pooled into 11 fractions (1+11+21, 2+12+22, etc.) that were analyzed on the LC-MS system.

LC-MS^2 analysis of peptides

LC-MS^2 analyses of all peptide mixtures were done using RSLCnano system (SRD-3400, NCS-3500RS CAP, WPS-3000 TPL RS) connected to the Orbitrap Elite hybrid spectrometer (Thermo Fisher Scientific). Prior to LC separation, tryptic digests were online concentrated and desalted using a trapping column (100 μm × 30 mm) filled with 3.5-μm X-Bridge BEH 130 C18 sorbent (Waters). After washing of the trapping column with 0.1% FA, the peptides were eluted (flow 300 nl/min) from the trapping column onto an analytical column (Acclaim Pepmap100 C18, 3 μm particles, 75 μm × 500 mm; Thermo Fisher Scientific) by 100 min nonlinear gradient program (1%–56% of mobile phase B; mobile phase A: 0.1% FA in water; mobile phase B: 0.1% FA in 80% ACN). Equilibration of the trapping column and the column was done prior to sample injection to sample loop. The analytical column outlet was

directly connected to the Digital PicoView 550 (New Objective) ion source sheath gas option a PicoTip emitter SilicaTip (New Objective; FS360-20-15-N-20-C12). ABIRD (Active Background Ion Reduction Device, ESI Source Solutions) was installed.

MS data were acquired in a data-dependent strategy selecting up to top 10 precursors based on precursor abundance in the survey scan (350-2000 m/z). The resolution of the survey scan was 60 000 (400 m/z) with a target value of 1×10^6 ions, one microscan and maximum injection time of 200 ms. HCD MS/MS (32 or 36% relative fragmentation energy used for co-immunoprecipitated or depleted samples, respectively) spectra were acquired with a target value of 50 000 and resolution of 15 000 (400 m/z). The maximum injection time for MS/MS was 500 ms. Dynamic exclusion was enabled for 45 s after one MS/MS spectra acquisition and early expiration was disabled. The isolation window for MS/MS fragmentation was set to 2 or 1.4 m/z (co-IP or depletome samples, respectively).

The analysis of the mass spectrometric RAW data files was carried out using the Proteome Discoverer software (Thermo Fisher Scientific; version 1.4) with in-house Mascot (Matrixscience, London, UK; version 2.6) and Sequest search engine utilization. MS/MS ion searches were done at first against modified cRAP database (based on http://www.thegpm.org/crap/; 111 sequences in total) containing protein contaminants like keratin, trypsin etc. MS/MS spectra assigned by Mascot search engine to any cRAP protein peptide with Mascot ion score > 30 were excluded from the next database searches. Final database searches were done against TriTrypDB protein database (http://tritrypdb.org/common/downloads/release-9.0/TbruceiTREU927/fasta/data/TriTrypDB-9.0_TbruceiTREU927_AnnotatedProteins.fasta; number of proteins 11,567). Mass tolerance for peptides and MS/MS fragments were 10 ppm and 0.05 Da, respectively. Oxidation of methionine, deamidation (N, Q) and acetylation (protein N terminus) as optional modification, carbamidomethylation (C) (plus TMT6plex (K, N-term) modifications in case of TMT6plex labeled samples) as fixed modification and one enzyme miss cleavage were set for all searches. A percolator was used for post-processing of the search results. Raw files from all 11 high pH fractions were searched together. Peptides with q-value < 0.01, rank 1 and with at least 6 amino acids were considered only. Proteins matching the same set of peptides were reported as protein groups. Protein groups/proteins were reported only if they had at least one unique peptide.

Co-IP protein abundance was assessed using protein area calculation in Proteome Discoverer. Protein group reports from all individual samples were combined into a single supergroup (SG) report where each SG is list of proteins reported within a single protein group in at least single sample report.

TMT6plex reporter ion intensities of unique peptides were normalized to get equal reporter intensity sum for each channel.

SILAC proteomics

Protein labeling with light and heavy amino acids in cells either expressing or not expressing the tagged bait proteins and subsequent IPs from lysates of 1:1 mixtures of differentially labeled cells were essentially done as described [62]. TbMic10-1 protein complexes were eluted by boiling the resin for 5 min in 60 mM Tris-HCl, pH 6.8 containing 0.1% SDS. The eluate was flash frozen and stored at −80°C until proteins were reduced, alkylated and digested with trypsin in solution and analyze by LC-MS^2 as described [31]. In contrast, IP proteins using tagged TbMic10-2, TbMic34 and TbMic20 as bait were eluted with SDS-PAGE gel loading buffer without β-mercaptoethanol, separated electrophoretically and finally identified after treatment of gel slices and LC-MS^2 analysis exactly as previously described [62]. IPs were performed in triplicate.

Proteinase K protection assay

Mitoplasts resusupended in SoTE buffer (20 mM Tris-HCl pH 7.5, 0.6 M Sorbitol, 2 mM EDTA) from 5 X 10^8 cells were split into 3 tubes. One hundred μg of proteinase K was added to 2 tubes, with one supplemented with 1% Triton-X (v/v). The third tube was left untreated as a mock control. All samples were incubated on ice for 30 min. Five mM PMSF was then added to each tube to stop the reaction.

Transmission electron microscopy

For ultrastructural studies, cells were centrifuged at 620 X g for 10 min at RT and immediately high-pressure frozen using a Leica EM Pact2 high pressure freezing (HPF) machine in the presence of 20% BSA. Freeze substitution was performed in 2% OsO4 diluted in 100% acetone at −90°C for 96 h. Samples were then warmed to −20°C at a rate 5°C/h. After 24 h, the temperature was increased (3°C/h) to 4°C. At RT, cells were rinsed 3 times for 15 min each in 100% acetone, infiltrated in 25%, 50%, 75% SPI-pon resin (SPI) solutions for 1 h at each step. After overnight incubation at 100°C, the samples were polymerized at 60°C for 48 h. Ultrathin sections were stained with ethanolic uranyl acetate (30 min) and lead citrate (20 min). For electron tomography (ET), both sides of sections were covered by gold nanoparticles (NPs) of 10 nm in diameter (BBI) and carbon coated.

For immunogold labeling, cells were fixed with 4% formaldehyde with 0.1% glutaraldehyde in 0.1 M HEPES for 1 h at RT. After washing, pellets of cells embedded in 10% gelatin were immersed in 2.3 M sucrose for 24 h at 4°C and frozen by plunging into liquid nitrogen. Cryosections were cut using a EM UC6 ultramicrotome equipped with a EM FC6 cryochamber (Leica). Cryosections were picked up with a drop of 1.15 M sucrose /1% methylcellulose. Sections were incubated in blocking solution (2% (w/v) nonfat milk in HEPES with 20 mM glycine) for 1 hr at RT and incubated with rabbit anti-HA antibody (Sigma) diluted 1:40. Sections were washed (6 times, 2 min each) with blocking solution and incubated with protein A conjugated to 5 nm gold NPs (UMC, Utrecht) diluted 1:50 for 1h. Samples were washed in HEPES (6 times, 2 min each) and dH2O, contrasted and embedded in 1.8% methylcellulose/0.3% uranyl acetate.

Samples were observed with a JEOL 1010 transmission electron microscope (TEM) operating at an accelerating voltage 80 kV and equipped with a MegaView III CCD camera (SIS). Electron tomograms were collected at tilt steps of 0.6-0.8° using the JEOL 2100F TEM working at 200 kV, equipped with a high-tilt stage plus a Gatan camera (Orius SC 1000) and controlled with SerialEM automated acquisition software. Tomograms were reconstructed using the IMOD software package or Amira. A 3D median filter was applied on reconstructed stacks. Manual masking of the area of interest was employed to generate 3D surface models.

Bioinformatic analysis

Mic10 sequences from various genomes were aligned using MAFFT using the local pair algorithm [63]. Parts of this initial alignment that were represented by $\geq$ 60% gaps were removed via the GAPTREEZ server (https://www.hiv.lanl.gov/content/sequence/GAPSTREEZE/gap.html). This processed alignment was then used to construct a maximum likelihood tree using RAxML [64] with the LG+G model. The fast-bootstrap algorithm from 1000 replicates was used to estimate the best scoring tree and bootstrap support. Additional branching support was then determined by computing Bayesian posterior probabilities using Mr. Bayes 3.2 [65]. Four independent MCMC chains were run for 3×10^6 generations under the LG+G model and default chain parameters. Topology and posterior probabilities were reconstructed after omitting the first 5×10^5 generations.

Homology models generated in SWISSPROT [66]. Transmembrane domain and coiled coil prediction performed using TMHMM v2.0 [67] and COILS [68] servers, respectively.

QUANTIFICATION AND STATISTICAL ANALYSIS

Analysis of immunogold and RNAi transmission electron microscopy data

Immunogold-labeling data were statistically evaluated as follows: NPs were counted in two compartments from randomly acquired areas of sections: mitochondria (subdivided into the following sub-compartments: inner boundary membrane, cristae and a undefined area) and background. Labeling density (LD) was calculated as the number of gold NPs per area. Random images were analyzed until at least 100 NPs were counted in the HA-epitope containing samples. Chi-square analysis, with the null hypothesis of no difference from random distribution, and RLI index were counted according to Mayhew and colleagues [38]. The null hypothesis was rejected in all examined immunodecorated HA-epitope samples. LD data are summarized in Table S2.

Cristae lengths were measured using ImageJ on images of randomly acquired mitochondrial sections. Between 39 and 74 mitochondrial sections were counted to measure the length of at least 200 cristae. Statistical significance of cristae lengths in comparison to the parental cell line controls were determined by unpaired Student's t test using GraphPad Prism 7 software.

Analysis of TbMic20 and TbMic60 depletome data

TbMic20 and TbMic60 RNAi 4 dpi for depletome analysis, which includes their respective non-induced controls, was performed in duplicate. Proteins with $\log_2$ transformed relative values $\geq$ 1.6-fold in each RNAi relative to non-induced controls were considered to be part of the TbMic20 depletome. For determination of a secondary effect of TbMic20 RNAi on OXPHOS proteins compared to matrix controls, all $\log_2$ relative values of proteins fitting into the catagories as defined by Ziková and colleagues [25] from each duplicate was incorporated into a violin plot. Statistical significance of subunits of each respiratory chain complex compared to core matrix proteins was determined by unpaired Student's t test using GraphPad Prism 7 software.

DATA AND SOFTWARE AVAILABILITY

The mass spectrometry proteomics data pertaining to *T. brucei* 927 IPs plus TbMic20 and TbMic60 depletomes have been deposited to the ProteomeXchange Consortium via the PRIDE partner repository with the dataset identifier PRIDE: PXD009601.

Current Biology, Volume *28*

Supplemental Information

The Diverged Trypanosome MICOS Complex as a Hub for Mitochondrial Cristae Shaping and Protein Import

Iosif Kaurov, Marie Vancová, Bernd Schimanski, Lawrence Rudy Cadena, Jiří Heller, Tomáš Bílý, David Potěšil, Claudia Eichenberger, Hannah Bruce, Silke Oeljeklaus, Bettina Warscheid, Zbyněk Zdráhal, André Schneider, Julius Lukeš, and Hassan Hashimi

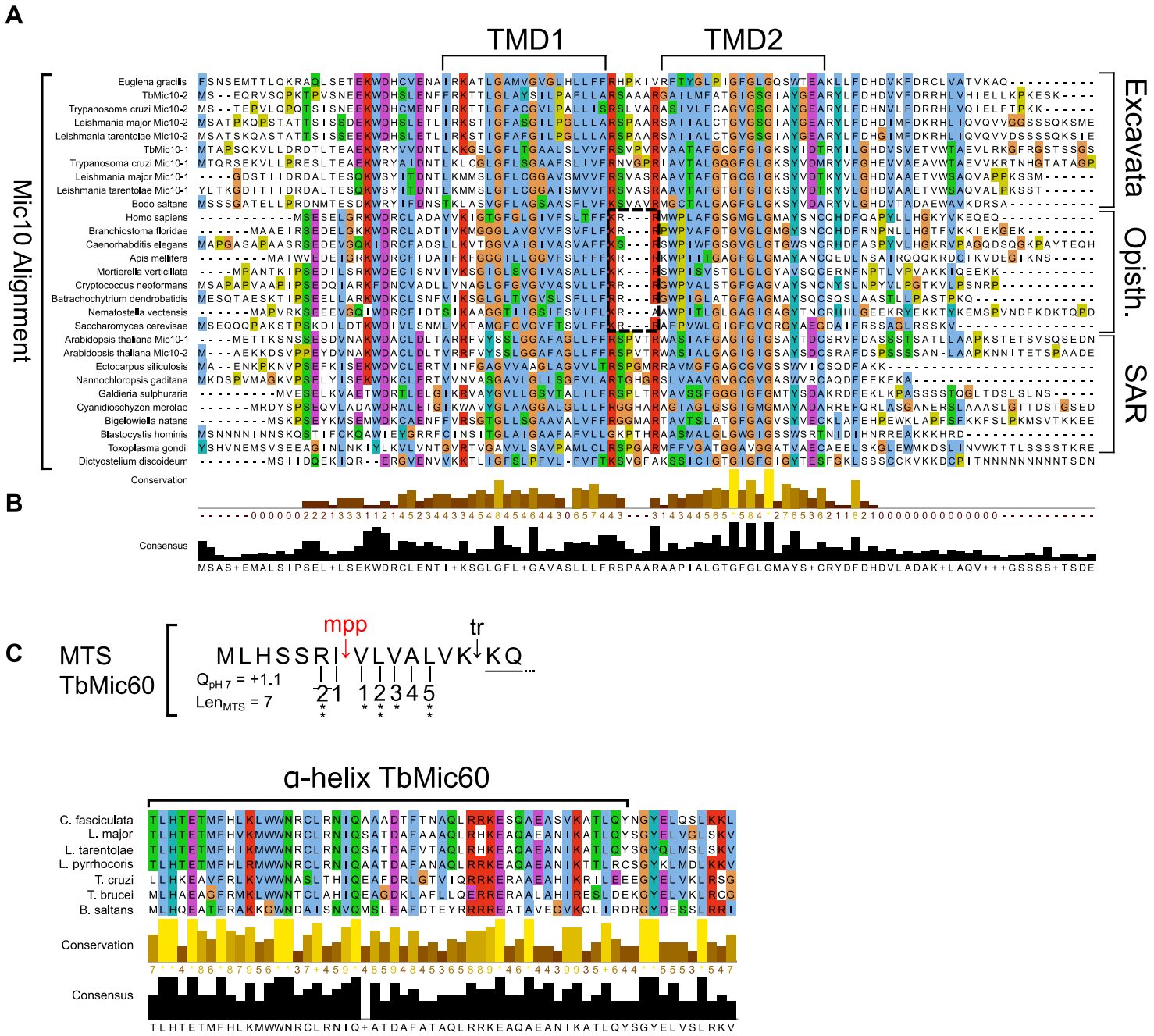

Figure S1. Bioinformatic analysis of TbMICOS. Related to Figures 1A and 4B.
(A) Alignment of Mic10 orthologs of selected representatives from the Excavata, Opisthikonta and SAR supergroups, plus the slime mold *Dictyostelium discoideum*. Supergroup designation of sequences in brackets on right; opisth., Opisthikonta. TMD1 and 2 indicated by top brackets. KRR loop of Opisthokonta indicated with a dashed box. Analysis of multiple aligned sequences (AMAS) conservation score and consensus sequence given on the bottom. **Related to Figure 1A.**
(B) Predicted mitochondrial presequence of TbMic60. Most likely cleavage site by mitochondrial processing peptidase (mpp) in red, first trypsin (tr) cleavage site in black and first mapping peptide detected by LC-MS2 underlined. Conserved sequence around the mpp site according to Mach and colleagues [S1] indicated below the sequence (**, highly conserved, *, moderately conserved). $Q_{pH\,7}$, presequence charge at physiological pH; Len_{MTS}, presequence length. **Related to Figure 4B.**
(C) Alignment of predicted α-helix sequences (in brackets) of TbMic60 and its homologs from indicated kinetoplastids. Alignment labelled as in A. **Related to Figure 4B.**

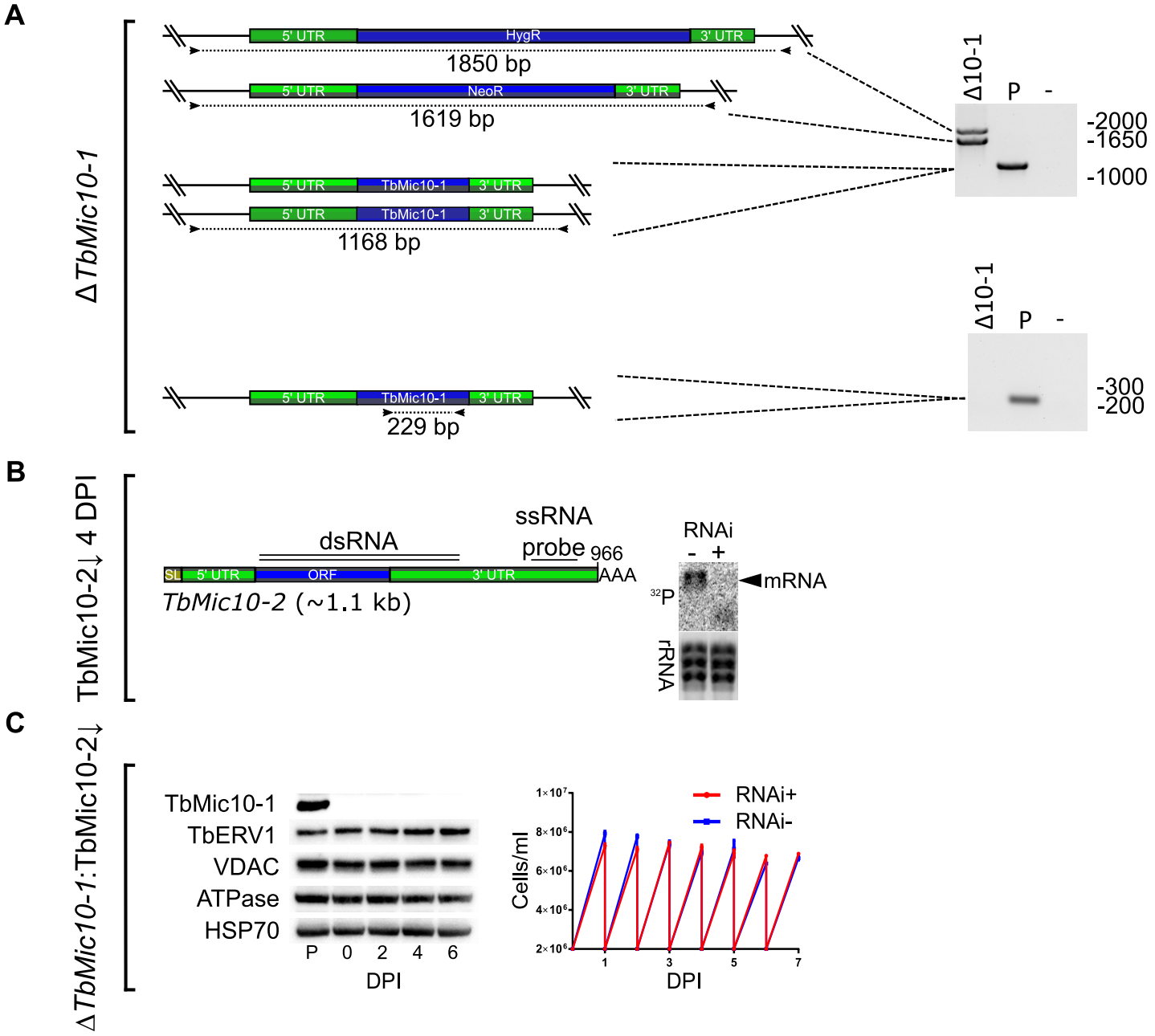

Figure S2. Characterization of ΔTbMic10-1/TbMic10-2↓ cell line. Related to Figure 2.
(A) Verification of Δ*TbMic10-1* by PCR amplification of *TbMic10-1* gene locus. Top, PCR amplification using primers flanking the resistance marker cassette integration site. Bottom, PCR primers annealing within the *TbMic10-1* ORF to demonstrate its deletion from the genome. DNA ladder sizes indicated on right. P, parental cell line of Δ*TbMic10-1*. Schemas on the left: arrowheads show PCR primer annealing sites, dotted lines indicate PCR amplicons with their sizes below.
(B) Northern blot of *TbMic10-2* mRNA 4 days post RNAi induction (DPI). Arrowhead indicates target mRNA. Scheme on the left shows both mRNA sequences targeted by tetracycline-induced double stranded RNA (dsRNA, double line) and complementary to single stranded DNA probe (ssDNA, single line). SL, spliced leader RNA.
(C) Immunoblot of RNAi cell lines (left of brackets) with antibody indicated on the left. DPI shown below panel. P, parental cell line from which Δ*TbMic10-1*/TbMic10-2↓ was derived. Right, measurement of TbMic10-2 RNAi cell growth in glucose-poor medium (n=3). Y-axis, cell density; x-axis, DPI.

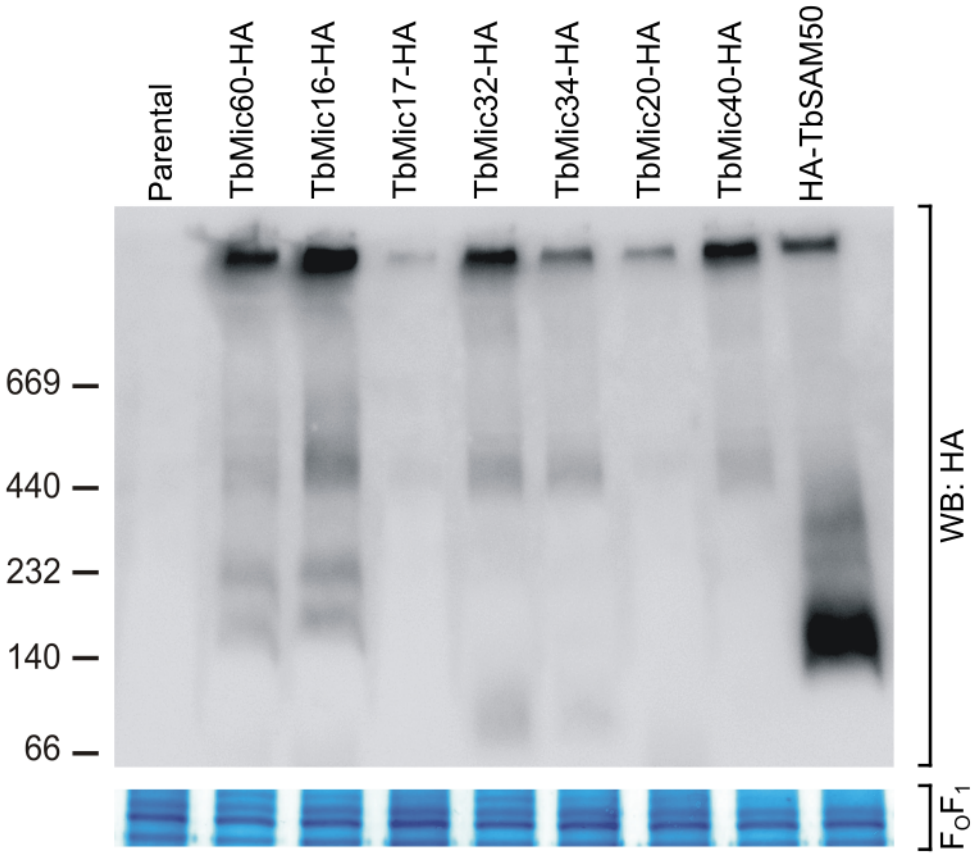

Figure S3. TbMICOS subunits are part of a >1 MDa complex. Related to Figure 3.
BN-PAGE resolution of HA-tagged TbMICOS subunits plus TbSAM50 (indicated on top) probed with α-HA antibody. Size markers indicated on the left. Bottom panel, Coomassie Blue staining of FOF1-ATP synthase from BN-PAGE used as a loading control.

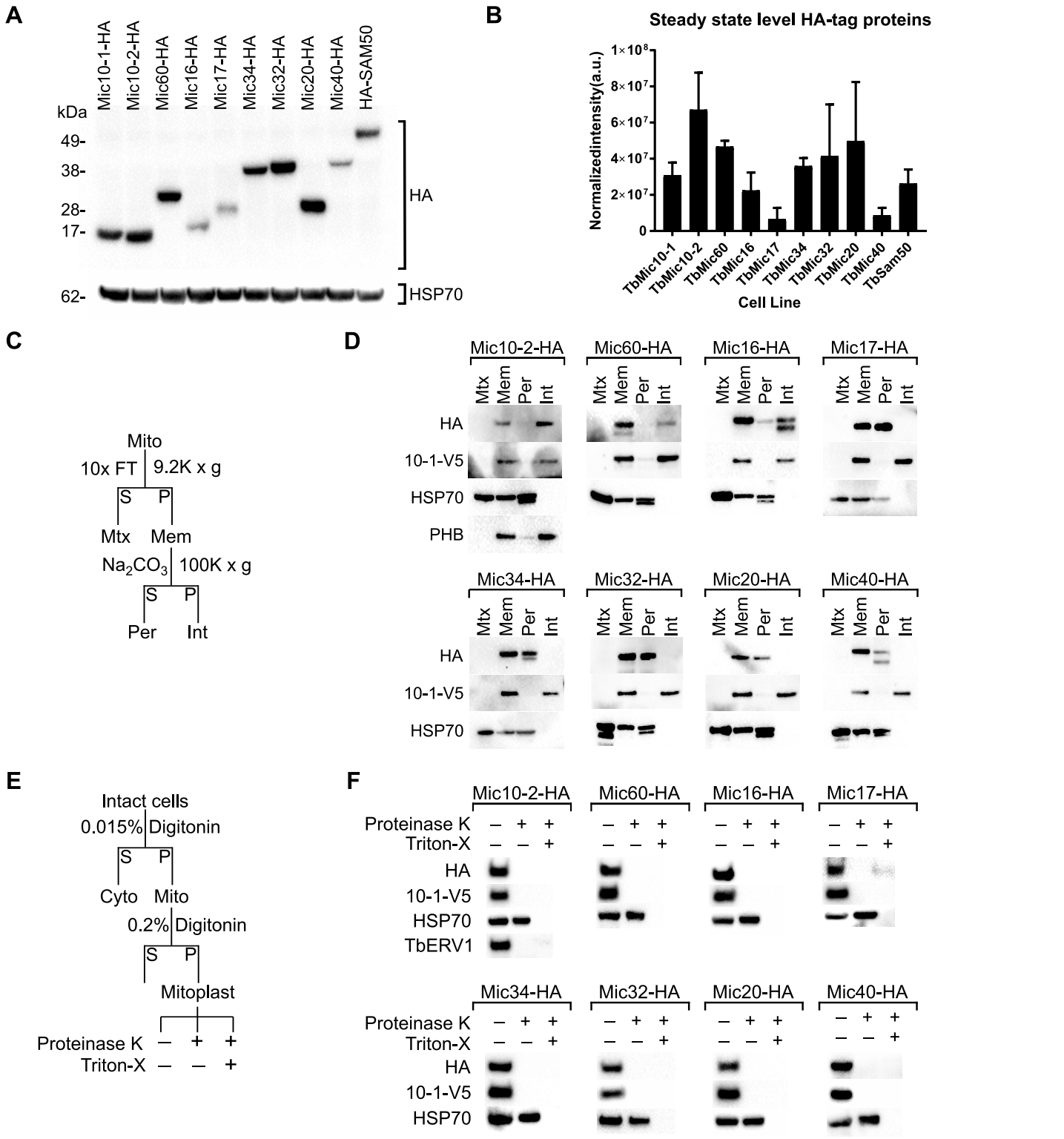

Figure S4. Biochemical properties of TbMICOS subunits. Related to Figure 5.

(A) Representative Western blot probed with α-HA (top) or α-HSP70 (bottom) antibodies, the latter used as a loading control. Size markers indicated on left. Sample and size markers indicated on the top and left, respectively.

(B) Densitometry of HA tagged TbMICOS subunit signals normalized to that of HSP70 in arbitrary units (a.u.). Bar whiskers, standard deviation (n=3).

(C) Schema of fractionation into matrix (Mtx) and membrane (Mem) fractions by freeze/thaw (FT) cycles. The latter fraction was further separated into peripheral (Per) and integral (Int) parts by carbonate extraction. Centrifugation speeds used to separate supernatant (S) and pellet (P) fractions shown on the left.

(D) Western blots of fractions from the indicated cell lines (Top) with antibodies indicated on the left. PHB, prohibitin.
(E) Schema of mitoplast production for proteinase K protection assay.
(F) Western blots of proteinase K protection assay samples labelled as in D.

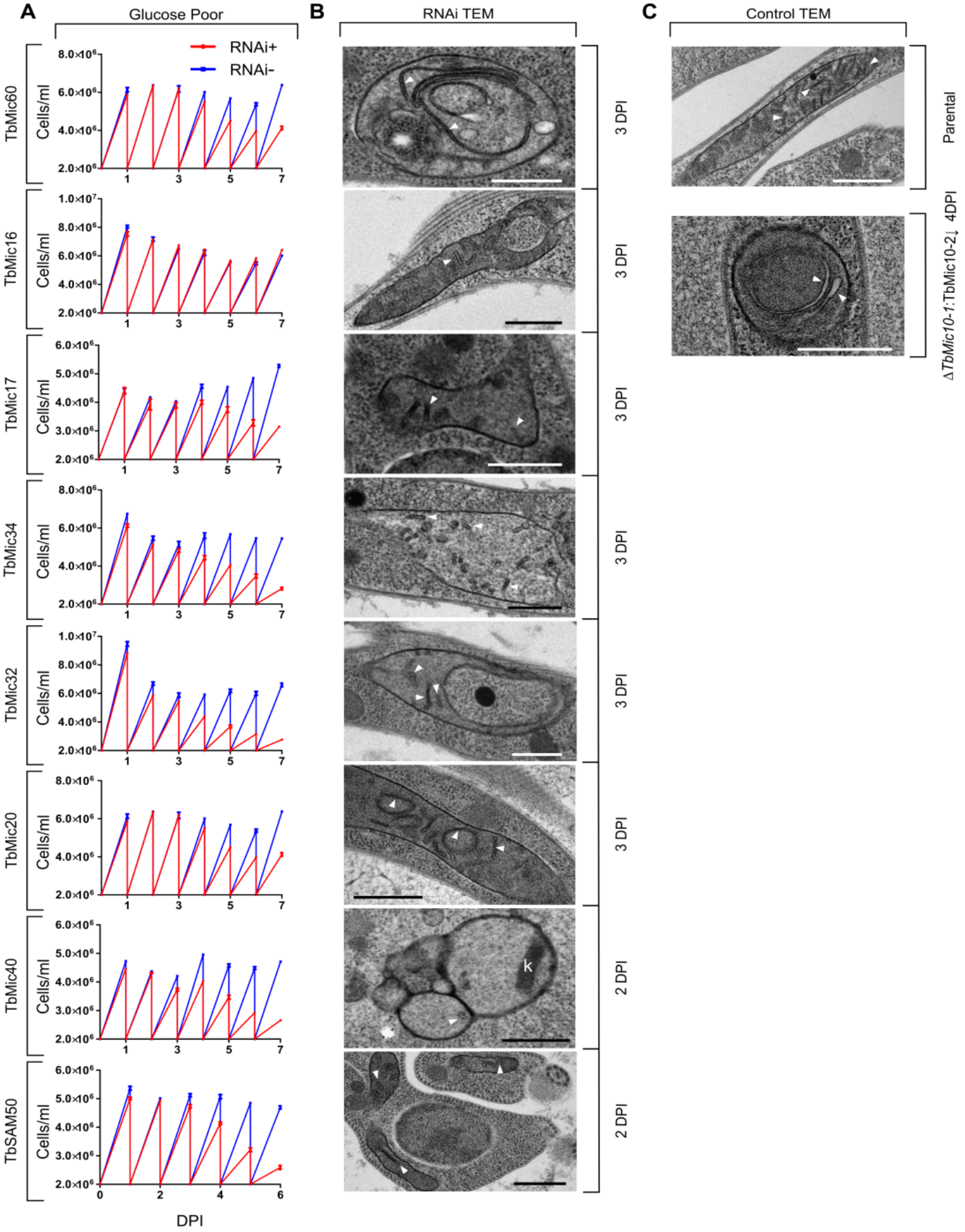
A
Glucose Poor
RNAi+
RNAi-
TbMic60
TbMic16
TbMic17
TbMic34
TbMic32
TbMic20
TbMic40
TbSAM50
Cells/ml
DPI
B
RNAi TEM
3 DPI
3 DPI
3 DPI
3 DPI
3 DPI
3 DPI
2 DPI
2 DPI
k
C
Control TEM
Parental
Δ*TbMic10-1*:TbMic10-2↓ 4DPI

Figure S5. TbMICOS RNAi phenotypes. Related to Figure 6.
(A) Measurement of TbMICOS RNAi growth in glucose-poor medium (n=3). Y-axis, cell density; x-axis, days post induction (DPI). Cell lines indicated to the left of brackets.
(B) Representative transmission electron micrographs (TEM) of TbMICOS RNAi cell lines at DPI to the right of brackets. Arrowheads point to cristae. Bars, 500 nm.
(C) TEM of control cell lines indicated to left and marked as in B.

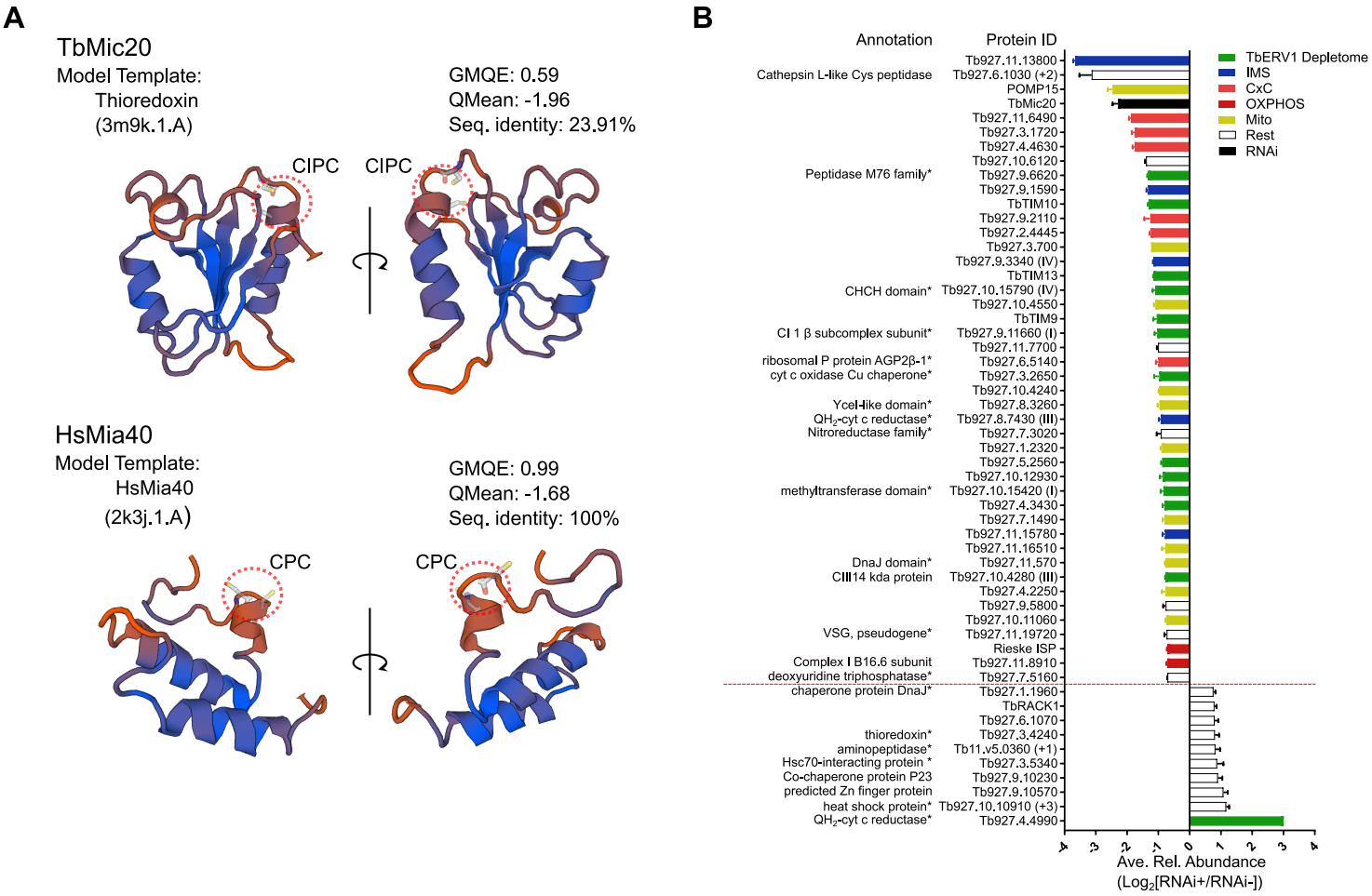

Figure S6. TbMic20 is a thioredoxin-like protein that affects IMS proteins. protein. Related to Figure 7.

(A) SWISSPROT homology model of TbMic20 (Top) and human Mia40 (Bottom). Model template indicated below title and other model parameters to the right. CIPC and CPC reaction centers (C residues visible) are in red dashed circles.

(B) Bar graph summarizing proteins down-regulated (above red line) and up-regulated (below red line) ≥1.6-fold threshold in the TbMic20 depletome. Color key on the top right (same as pie chart in Figure 7A). Roman numerals in parenthesis indicate oxidative phosphorylation (OXPHOS) complex component/ assembly factor while Arabic numerals indicate protein-encoding gene copy number. Bar whiskers, standard deviation (n=2);*, putative annotations; QH2, ubiquinol; cyt c, cytochrome c; IMS, intermembrane space proteins identified by homology or experimentally; CxC, proteins with predicted twin CX3,9C; Mito, mitochondrial.

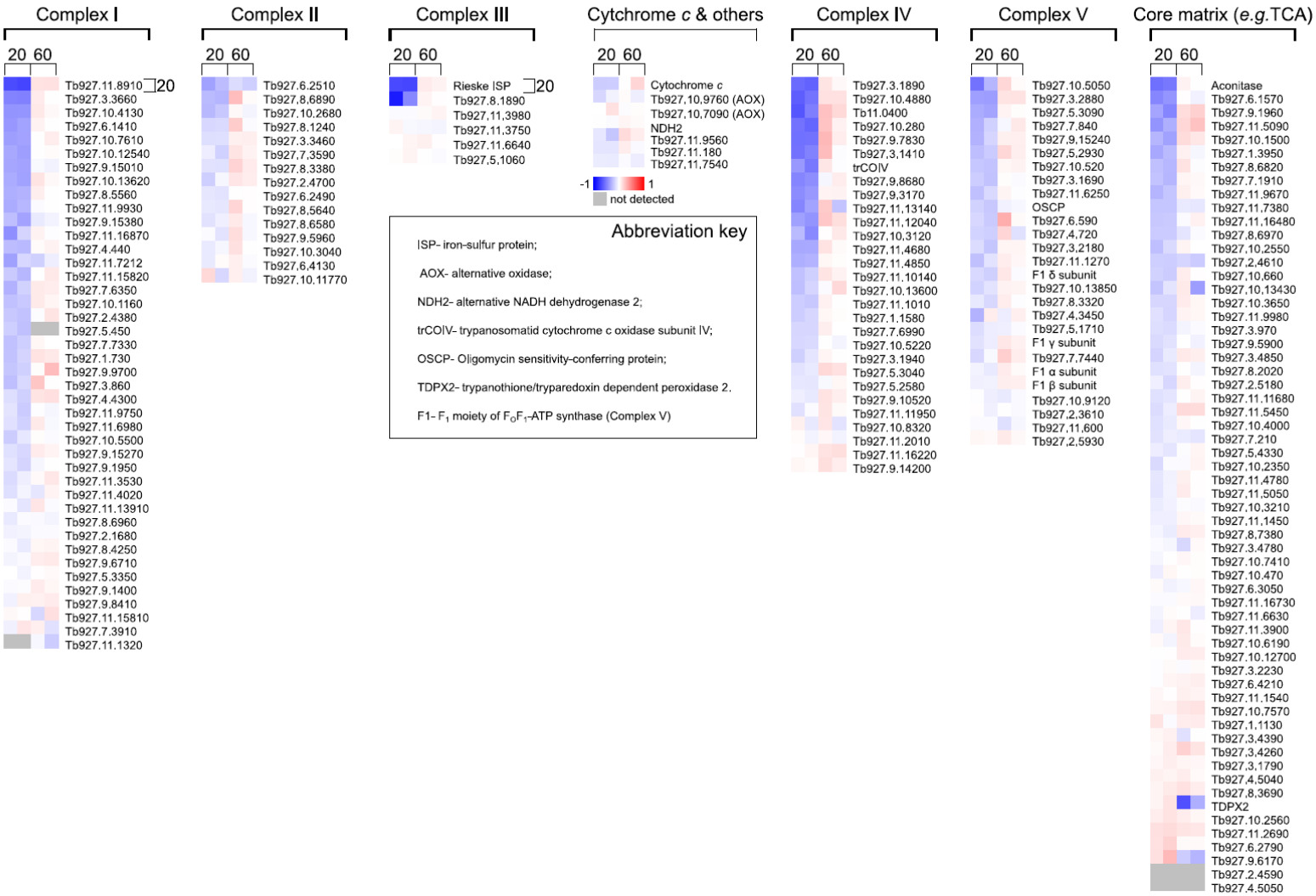

Figure S7. Oxidative phophorylation proteins are preferentially affected compared to matrix proteins in the TbMic20 depletome. Related to Figure 7D.

Heat maps of indicated subunits of oxidative phosphorylation (OXPHOS) complexes (indicated on top of brackets). The "core matrix" category is made of proteins involved in core mitochondrial matrix metabolism, such as the TCA cycle. Scale of relative protein abundancies and abbreviation key on the bottom of the “cytochrome c & others” column. Labelled as in Figure 7C.

	Kinetoplastid species and strain							
TbMICOS subunit	**T.brucei**	**T.cruzi CL Brener Non-Esmeraldo-like**	**T.cruzi CL Brener Esmeraldo-like**	**Leishmania major strain Friedlin**	**Leishmania tarentolae Parrot-TarII**	**Leptomonas pyrrhocoris H10**	**Crithidia fasciculata strain Cf-Cl**	**Bodo saltans**
TbMic10-1	Tb927.10.1580	TcCLB.506977.60	--	LmjF.21.0735	LtaP21.0750	LpyrH10_14_0830	--	BS59735
TbMic10-2	Tb927.11.2190	TcCLB.508355.114	TcCLB.507467.104	LmjF.27.1530	LtaP27.1610	LpyrH10_07_1840	CFAC1_230034600	--
TbMic60	Tb927.9.10160	TcCLB.507007.40	TcCLB.509551.100	LmjF.35.4510	LtaP35.4530	LpyrH10_01_6920	CFAC1_300096600	BS38685
TbMic16	Tb927.11.6470	TcCLB.507765.100	TcCLB.510101.390	LmjF.11.0800	LtaP11.0780	LpyrH10_18_1020	CFAC1_070013900	BS39520
TbMic17	Tb927.5.690	TcCLB.511459.60	TcCLB.508539.20	LmjF.35.0890	LtaP35.1010	LpyrH10_01_2590	CFAC1_240034600	BS39755
TbMic34	Tb927.4.630	TcCLB.507053.140		LmjF.34.4100	LtaP34.4070	LpyrH10_05_4420	CFAC1_290072200	BS48655
TbMic32	Tb927.2.2940	TcCLB.508737.170	TcCLB.509127.80	LmjF.02.0650	LtaP02.0570	LpyrH10_27_1050, LpyrH10_33_0970	CFAC1_210027800	BS18045
TbMic20	Tb927.10.11900	TcCLB.507049.70	TcCLB.506567.90	LmjF.33.1280	LtaP33.1480, LtaP26.1460	LpyrH10_19_0340	CFAC1_280023000	BS08895
TbMic40	Tb927.8.580	TcCLB.509611.150	TcCLB.510857.4	LmjF.07.1110	LtaP07.1200	LpyrH10_30_0060	CFAC1_080022500	--
TbSam50	Tb927.3.4380	TcCLB.506701.20	TcCLB.509379.20	LmjF.29.1820	LtaP29.1930	LpyrH10_08_2170	CFAC1_200025600	BS40310

Table S1: Accession numbers of kinetoplastid orthologs of TbMICOS subunits. Related to Figure 4A.

TbMCIOS Subunit	LD Mt^2	LD Bg^2	ΣAu Mt observed (expected)	ΣAu Bg observed (expected)	Σarea (μm^2) Mt/Bg	χ^2 Mt/Bg	RLI Mt/Bg
TbMic10-1	16.3	0.8	161 (38.1)	25 (113.7)	9.9/29.5	396.8/69.2	4.2/0.2
TbMic10-1	17.3	0.8	122 (27.2)	27 (128)	7.1/33.2	328.8/79.7	4.5/0.2
TbMic60	17.1	1.2	110 (24.8)	33 (138.9)	6.4/36	291.9/80.8	4.4/0.2
TbMic16	14	1.8	117 (32.1)	56 (120.1)	8.3/31.2	224/34.5	3.6/0.5
TbMic17	10	0.9	104 (39.9)	34(138.9)	10.4/36	102.7/79.3	2.6/0.2
TbMic34	15.8	1.4	141 (34.4)	42(118.8)	8.9/30.8	329.8/49.7	4.1/0.4
TbMic32	14.9	0.8	155 (40.1)	32 (156.5)	10.4/40.6	328.7/99.1	3.9/0.2
TbMic20	18.1	1.7	118 (25)	36 (83.3)	6.5/21.6	344.1/26.9	4.4/0.2
TbMic40	11.7	0.6	110 (36.3)	22 (149)	9.4/38.6	149.3/108.2	3/0.1
Parental	4.1	1.2	21 (20)	-	5.2/-	0.05	1.05
Total						2973.4	

Table S2: Immunogold distribution and labelling density of HA tagged TbMICOS subunits by Relative Labelling Index (RLI)[1]. Related to Figure 5U.

[1] LD and RLI were calculated using data from images of immunogold-labelled cryosections that were taken from randomly chosen areas of a minimal 2 grids. This was done on samples that were processed in parallel to mitigate potential variability. Done as described in Method Details of Star Methods.

[2] LD (Labelling Density), NPs/μm^2; Mt, mitochondria; Bg, background; χ^2, chi squared.

SUPPLEMENTAL REFERENCES

S1. Mach, J., Poliak, P., Matušková, A., Žárský, V., Janata, J., Lukeš, J., and Tachezy, J. (2013). An advanced system of the mitochondrial processing peptidase and core protein family in *Trypanosoma brucei* and multiple origins of the core I subunit in eukaryotes. Genome Biol. Evol. *5*, 860-875.

3.

Chapter 2. The highly diverged trypanosomal MICOS complex is organized in a non-essential integral membrane and an essential peripheral module

Molecular Microbiology (2019) 0(0), 1–13 doi:10.1111/mmi.14389

The highly diverged trypanosomal MICOS complex is organized in a nonessential integral membrane and an essential peripheral module

Claudia Eichenberger,[1] Silke Oeljeklaus,[2,3] Julia Bruggisser,[1,†] Jan Mani,[1] Beat Haenni,[4] Iosif Kaurov,[5,6] Moritz Niemann,[1] Benoît Zuber,[4] Julius Lukeš,[5,6] Hassan Hashimi,[5,6] Bettina Warscheid,[2,3] Bernd Schimanski[1]* and André Schneider [1]*

[1] *Department of Chemistry and Biochemistry, University of Bern, Freiestrasse 3, Bern, CH-3012, Switzerland.*
[2] *Department of Biochemistry and Functional Proteomics, Faculty of Biology, University of Freiburg, Freiburg, 79104, Germany.*
[3] *Signalling Research Centres BIOSS and CIBSS, University of Freiburg, Freiburg, 79104, Germany.*
[4] *Institute of Anatomy, University of Bern, Baltzerstrasse 2, Bern, 3012, Switzerland.*
[5] *Institute of Parasitology, Biology Center, Czech Academy of Sciences, České Budějovice (Budweis), Czech Republic.*
[6] *Faculty of Science, University of South Bohemia, 370 05, České Budějovice (Budweis), Czech Republic.*

Summary

The mitochondrial contact site and cristae organization system (MICOS) mediates the formation of cristae, invaginations in the mitochondrial inner membrane. The highly diverged MICOS complex of the parasitic protist *Trypanosoma brucei* consists of nine subunits. Except for two Mic10-like and a Mic60-like protein, all subunits are specific for kinetoplastids. Here, we determined on a proteome-wide scale how ablation of individual MICOS subunits affects the levels of the other subunits. The results reveal co-regulation of TbMic10-1, TbMic10-2, TbMic16 and TbMic60, suggesting that these nonessential, integral inner membrane proteins form an interdependent network. Moreover, the ablation of TbMic34 and TbMic32 reveals another network consisting of the essential, intermembrane space-localized TbMic20, TbMic32, TbMic34 and TbMic40, all of which are peripherally associated with the inner membrane. The downregulation of TbMic20, TbMic32 and TbMic34 also interferes with mitochondrial protein import and reduces the size of the TbMic10-containing complexes. Thus, the diverged MICOS of trypanosomes contains two subcomplexes: a nonessential membrane-integrated one, organized around the conserved Mic10 and Mic60, that mediates cristae formation, and an essential membrane-peripheral one consisting of four kinetoplastid-specific subunits, that is required for import of intermembrane space proteins.

Accepted 14 September, 2019. *For correspondence. E-mail bernd.schimanski@dcb.unibe.ch (BS); Tel. +41 31 631 42 25, andre.schneider@dcb.unibe.ch (AS); Tel. +41 31 631 42 53. †Present address: Department of Infectious Diseases and Pathobiology, Institute of Animal Pathology, Vetsuisse Faculty, University of Bern, Bern, 3012, Switzerland.

Introduction

All mitochondria capable of oxidative phosphorylation contain cristae, invaginations which enlarge the area of the inner membrane (IM). Cristae divide the mitochondrial IM into two domains: the inner boundary membrane, which is adjacent to the outer membrane (OM) and that is enriched for protein import complexes, and the cristae membranes, where the electron transport chain complexes and the ATP synthase are localized. The two membrane domains are separated by the cristae junctions (CJs), narrow neck-like structures in which the IM is sharply bent. CJs are formed by the mitochondrial contact site and cristae organizing system (MICOS), a hetero-oligomeric protein complex consisting of at least 6–7 subunits in yeast and mammals, respectively (Harner *et al*., 2011; Hoppins *et al*., 2011; von der Malsburg *et al*., 2011; Alkhaja *et al*., 2012; Kozjak-Pavlovic, 2017). Except for the one or two peripheral membrane proteins that face the intermembrane space (IMS) all are integral IM proteins. MICOS is essential for the building of CJs and contact sites to the OM and thus for the formation of submitochondrial microcompartments optimized for oxidative phosphorylation (van der Laan *et al*., 2016; Rampelt

et al., 2017; Kozjak-Pavlovic, 2017; Schorr and van der Laan, 2018; Quintana-Cabrera *et al.*, 2018). Moreover, the contact sites were shown to promote mitochondrial protein import (von der Malsburg *et al.*, 2011; Bohnert *et al.*, 2012; Wrobel *et al.*, 2015) and facilitate lipid transport (Harner *et al.*, 2014; Aaltonen *et al.*, 2016; Michaud *et al.*, 2016). In a wider context, MICOS can be viewed as a mitochondrial IM organizing structure that directly or indirectly influences many mitochondrial features including calcium uptake (Schorr and van der Laan, 2018) and mitochondrial DNA organization (Itoh *et al.*, 2013; Li *et al.*, 2016). It is therefore no surprise that MICOS dysfunction has been linked to a number of human diseases (van der Laan *et al.*, 2016; Rampelt *et al.*, 2017; Kozjak-Pavlovic, 2017; Wollweber *et al.*, 2017).

Studies in yeast and humans identified two distinct MICOS subcomplexes organized around each of its two core subunits Mic10 and Mic60 respectively (Bohnert *et al.*, 2015; Ding *et al.*, 2015; Friedman *et al.*, 2015; Guarani *et al.*, 2015; Ott *et al.*, 2015; Li *et al.*, 2016). The yeast Mic60 subcomplex contains Mic60 and Mic19 and mediates contact site formation by interaction with various OM proteins and protein complexes including the sorting and assembly machinery (SAM), the protein translocase of the OM (TOM) as well as the voltage dependent anion channel (VDAC) (Korner *et al.*, 2012; Zerbes *et al.*, 2012; Schorr and van der Laan, 2018). The Mic10 subcomplex on the other hand consists of Mic10, Mic12, Mic26 and Mic27 and appears to be mainly devoted to the formation and maintenance of CJs (Zerbes *et al.*, 2012).

The MICOS complex has experimentally been studied mainly in yeast and humans, both of which belong to the same eukaryotic supergroup Opisthokonta (Burki, 2014; Huynen *et al.*, 2016). However, two MICOS subunits, Mic10 and Mic60, are evolutionarily conserved in all eukaryotes that have cristae-containing mitochondria (Munoz-Gomez *et al.*, 2015; 2017). Moreover, Mic60 orthologues are found in α-proteobacteria, suggesting that a Mic60-like protein was present in the bacterial ancestor that was converted into the mitochondrion (Munoz-Gomez *et al.*, 2015; 2017; Tarasenko *et al.*, 2017).

The only experimentally studied MICOS complex outside the Opisthokonta is the one of the parasitic protist *Trypanosoma brucei*, a member of the eukaryotic supergroup Excavata (Burki, 2014; Munoz-Gomez *et al.*, 2015). Identification of the Mic10 orthologues in the *T. brucei* genome opened the way for the characterization of its MICOS complex (Kaurov *et al.*, 2018). Pulldown experiments using epitope tagged Mic10 orthologues recovered 9 proteins. Moreover, the same set of proteins was consistently detected by several reciprocal immunoprecipitations (IPs) using the newly identified MICOS subunits. Three of them are conserved: the two Mic10 paralogues, termed TbMic10-1 and TbMic10-2, and a putative Mic60 orthologue, termed TbMic60, which shows a similar domain structure as the yeast protein but lacks the mitofilin domain. It has been suggested that the absence of this domain might be compensated for by association of TbMic60 with the peripheral membrane protein TbMic34 which has two coiled–coiled domains (Kaurov *et al.*, 2018). The remaining trypanosomal MICOS subunits TbMic16, TbMic17, TbMic20, TbMic32, TbMic34 and TbMic40 are unique to the kinetoplastid flagellates. The *T. brucei* MICOS was shown to be required for the maintenance of the typical discoidal cristae found in the kinetoplastids and euglenids. Moreover, ablation of the thioredoxin-like protein TbMic20 inhibited import of IMS-localized proteins suggesting it may be the long sought functional analogue of Mia40 (Kaurov *et al.*, 2018), that seems to be absent from kinetoplastids (Basu *et al.*, 2013; Haindrich *et al.*, 2017). Mia40 is the central catalyst of mitochondrial intermembrane space assembly (MIA) pathway that mediates the oxidative-folding IMS proteins to sequester them in the IMS (Stojanovski *et al.*, 2012; Mordas and Tokatlidis, 2015).

All trypanosomal MICOS subunits are present in a complex bigger than 1 MDa that was difficult to resolve by blue native polyacrylamide electrophoresis (BN-PAGE) (Kaurov *et al.*, 2018). However, using IPs and BN-PAGE it was not possible to deduce whether the trypanosomal MICOS complex is organized into two subcomplexes as is the case in yeast and mammals. Thus, we decided to combine knockout/knockdown of individual MICOS components with proteome-wide analyses to investigate which subunits of the trypanosomal MICOS subunits might form networks whose members depend on each other.

Results

ΔTbMic10 strains define a network of integral membrane MICOS subunits

Using serial transfections two knockout cell lines, ΔTbMic10-1 and ΔTbMic10-2, were produced in which both alleles of either TbMic10-1 or TbMic10-2 were replaced by antibiotic resistance cassettes. Growth of the ΔTbMic10-2 cell line was not altered and that of the ΔTbMic10-1 cell line was only slightly affected in media containing or lacking glucose (Fig. 1). In the latter case, cells depend on oxidative phosphorylation for energy conversion (Lamour *et al.*, 2005). Thus, as reported before (Kaurov *et al.*, 2018), neither TbMic10-1 nor TbMic10-2 is essential for growth of procyclic *T. brucei* in culture.

Next, we compared the proteomes of mitochondria-enriched fractions of the ΔTbMic10-1 cell line with its parental cell line having two intact alleles of TbMic10-1. Proteins in the fractions of the two cell lines were quantified by mass spectrometry (MS) using peptide

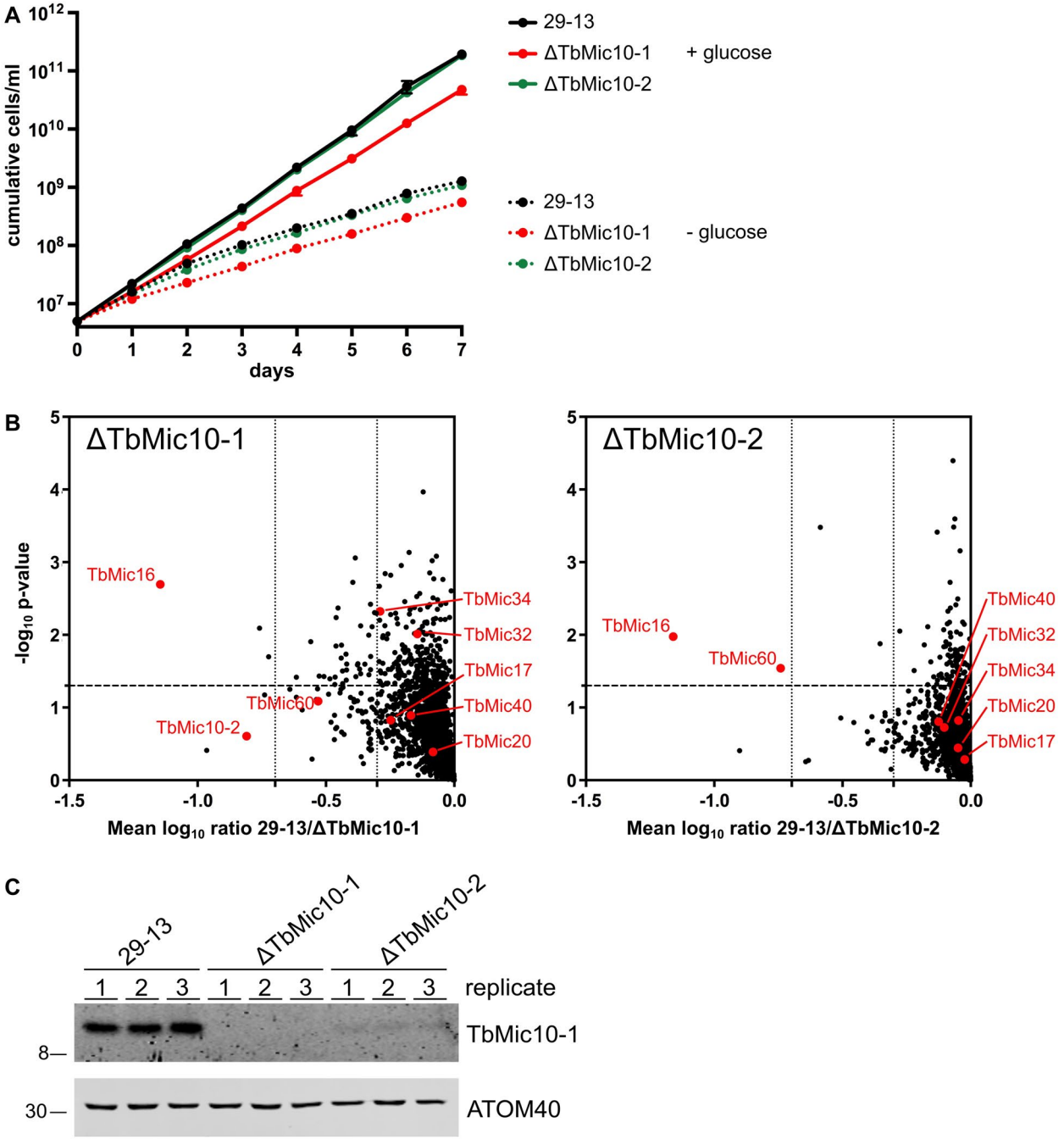

Fig. 1. Growth and proteomic characterization of the ΔMic10-1 and ΔMic10-2 cell lines.
A. Growth curves of the ΔMic10-1, ΔMic10-2 and the corresponding parent cell line *T. brucei* 29-13 in SDM80 medium containing or lacking glucose.
B. Graph on the left indicates proteins reduced in abundance in mitochondria-enriched fractions of the ΔMic10-1 cell line. MS-based quantification of proteins from the ΔMic10-1 cell line versus *T. brucei* 29-13 cells was based on peptide stable isotope dimethyl labeling ($n = 3$). Vertical dashed lines indicate a two- and fivefold reduction respectively. Horizontal dashed line indicates a p-value of 0.05. MICOS subunits are indicated with red dots. Graph on the right shows the same analysis for the ΔMic10-2 cell line. For a complete list of protein see Table S1.
C. Immunoblots of crude mitochondrial extracts from *T. brucei* 29-13, ΔMic10-1 and ΔMic10-2 grown in standard medium were probed for TbMic10-1 and ATOM40 as a loading control.

stable isotope dimethyl labeling (Peikert *et al.*, 2017). Lack of TbMic10-1 resulted in a significant, approximately 16-fold, reduction of TbMic16 (Fig. 1B, left panel). TbMic10-2 and TbMic60 are also downregulated although to a lesser extent and with quite high variability between sample replicates. All other MICOS subunits

remained unaltered or were only marginally downregulated (Fig. 1B, left panel).

The corresponding experiment for the ΔTbMic10-2 cell line gave comparable results (Fig. 1B, right panel). Again, an approximately 16-fold decrease of TbMic16 was observed. Moreover, the level of TbMic60 was significantly reduced even to a higher extent as in ΔTbMic10-1. Like in the ΔTbMic10-1 cell line, the levels of all other detected MICOS subunits were not affected. Interestingly, TbMic10-1 could not be detected by MS. Immunoblot analysis (Fig. 1C) showed that knockout of TbMic10-2 causes a dramatic reduction in TbMic10-1 steady-state levels. In summary, these results demonstrate that TbMic10-1, TbMic10-2, TbMic60 and TbMic16, all of which are integral membrane proteins, form an interdependent network. Ablation of either of the two paralogous MICOS core subunits, TbMic10-1 and TbMic10-2, impairs the stability of all other members of this network.

To investigate whether the TbMic10-containing network is required for cristae formation or maintenance, we analyzed ΔTbMic10-1 and its parental cell line by transmission electron microscopy (EM). The ratio between the lengths of the cristae membranes and the OM (a proxy for the adjacent inner boundary membranes) was blindly quantified from a randomized selection of pictures from both cell lines. A significant reduction of cristae membranes in the ΔTbMic10-1 cell line was evident, suggesting that the TbMic10-containing network is required for CJ formation (Fig. 2). Moreover, it can be concluded that cristae membranes can be dramatically reduced without affecting growth of procyclic *T. brucei* in culture. This is further supported by the observation that in the *T. brucei* strain 29-13, investigated in the present study, ablation of TbMic60 does not interfere with growth (Fig. S1).

Knockdown of TbMic34 defines a soluble second MICOS subunits network

TbMic34 is a trypanosomal MICOS subunit that is not part of the TbMic10-containing network defined above. The protein is of special interest since it was suggested to compensate for the lacking mitofilin domain of TbMic60 (Kaurov *et al.*, 2018). Carbonate extraction at high pH shows that C-terminally tagged TbMic34 fractionates with soluble proteins (Kaurov *et al.*, 2018) indicating that tagged TbMic34 is a peripheral membrane protein that is tightly associated with the MICOS complex.

Knockdown of TbMic34 causes a growth arrest (Fig. 3A). However, the levels of TbMic10-1, the atypical protein translocase of the OM 40 (ATOM40) (Schneider, 2018) and VDAC remain constant (Fig. 3B). Interestingly,

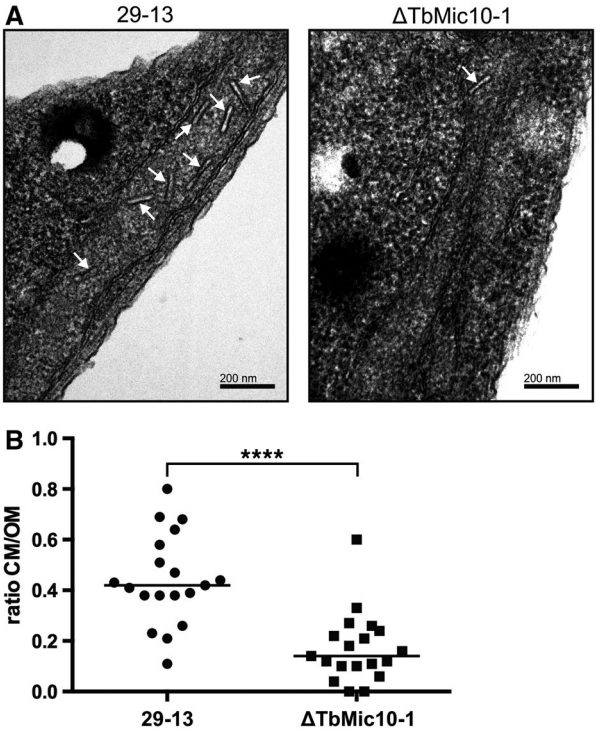

Fig. 2. TbMic10-1 is required for cristae formation.
A. Transmission EM images from *T. brucei* 29-13 (left) and the ΔTbMic10-1 cell line (right). The white arrows mark the cristae.
B. Quantitation of the ratio between the lengths of all discernable cristae membranes and discernable outer membranes in individual transmission EM images of the *T. brucei* 29-13 ($n = 19$) and the ΔTbMic10-1 cell lines ($n = 19$). **** indicates $P < 0.0001$.

we observe an accumulation of cytochrome oxidase subunit 4 (CoxIV) uncleaved precursor and in parallel a reduction of its mature form, which indicates an inhibition of mitochondrial protein import (Wenger *et al.*, 2017) (Fig. 3B, lowest panel). A protein import phenotype related to CoxIV was also evident after knockdown of TbMic20 (Fig. S2), the putative catalyst for import of IMS proteins (Kaurov *et al.*, 2018) such as the small Tim proteins (Wenger *et al.*, 2017). Inhibition of protein import after knock down of TbMic20 was also directly analyzed using in vitro assays. Fig. S2C shows that when in vitro translated CoxIV precursor is incubated with mitochondria that were isolated from the uninduced TbMic20-RNAi cell line the substrate is processed to its mature form and becomes resistant to externally added proteases. Moreover, import as expected for an IM protein, requires an intact membrane potential. However, when the same experiment was done with mitochondria isolated from the induced TbMic20 RNAi cell line essentially no import was observed, irrespectively whether they had an intact membrane potential or not.

To get a global view of the effect upon TbMic34 knockdown, we analyzed the proteome of mitochondria-enriched fractions using SILAC at two time points after

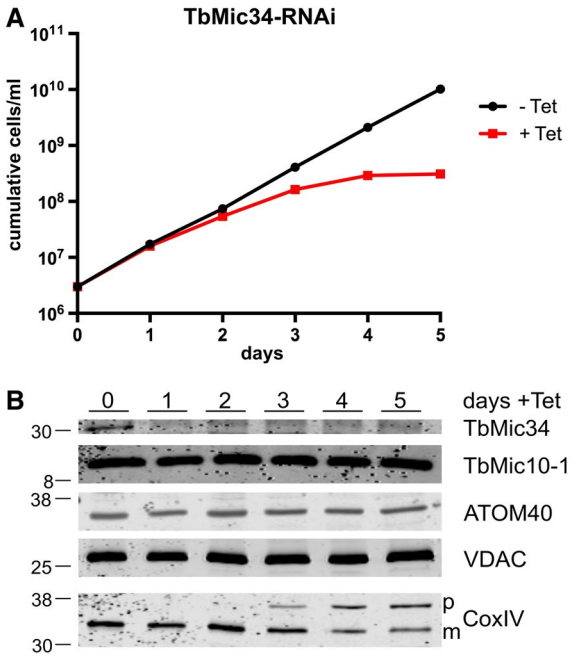

Fig. 3. Ablation of TbMic34 does not affect TbMic10-1 levels but inhibits protein import.
A. Growth curves of uninduced (-Tet) and induced (+Tet) TbMic34 RNAi cell lines.
B. Immunoblots of total cellular extracts from the TbMic34 RNAi cell lines induced for the indicated days were probed for TbMic34, TbMic10-1, ATOM40, VDAC and CoxIV using polyclonal antisera. The positions of precursor and mature form of CoxIV are indicated.

RNAi induction. 2.5 days after RNAi induction a downregulation of a subset of MICOS subunits was observed (Fig. 4A). Besides the RNAi target TbMic34, the levels of the essential MICOS components TbMic20, TbMic32 and TbMic40 were significantly reduced, whereas the TbMic10-containing network was not affected. This finding defines a second network of MICOS subunits whose stability depends on TbMic34. All of its members are membrane-associated soluble proteins that reside in the IMS.

At the later RNAi induction time point (3.5 days) indirect effects could be observed (Fig. 4B). Besides the downregulation of the TbMic34-containing network, a reduction in the levels of many proteins that are known or predicted to be localized, in the IMS (Peikert *et al.*, 2017) was measured. Thus, the observed results phenocopy what has previously been observed for the TbMic20 knockdown cell line (Kaurov *et al.*, 2018) and therefore support the notion that TbMic20 might be a functional analogue of Mia40 which has not been identified in trypanosomatid genomes so far (Basu *et al.*, 2013).

Moreover, many of the other proteins that are downregulated at the later time point are subunits of respiratory complexes (Table S2). A likely cause for this could be the reduced abundance of the IMS-localized small Tim chaperones (Wenger *et al.*, 2017) which are required for the import of TbTim17, the core subunit of the trypanosomal TIM complex (Singha *et al.*, 2008; Harsman *et al.*, 2016).

Characterization of TbMic32 confirms a second MICOS network

To further address the possible existence of a second MICOS network comprised of soluble IM proteins, we characterized another of its subunits, TbMic32. Fig. 5A shows that a C-terminally tagged version of TbMic32 is recovered in a crude mitochondrial fraction. Moreover, after carbonate extraction at high pH the tagged TbMic32 is found in the supernatant indicating that it is a soluble protein (Fig. 5A). TbMic32 contains two CX_9C motifs near its C-terminus, a signature found in many IMS-localized proteins (Stojanovski *et al.*, 2012; Mordas and Tokatlidis, 2015). In line with this, the protein gets depleted after RNAi-mediated ablation of TbErv1, an essential import factor for IMS proteins (Fig. 5B) (Peikert *et al.*, 2017).

RNAi-mediated downregulation of TbMic32 results in a growth arrest as previously reported (Fig. 6A) (Kaurov *et al.*, 2018). Moreover, concomitant with its ablation, a reduction of TbMic34 is observed, whereas the levels of TbMic10-1 and two mitochondrial OM membrane proteins (VDAC and ATOM40) are not affected (Fig. 6B). Interestingly, a reduction of mature CoxIV and an accumulation of its precursor was observed, mirroring the mitochondrial protein import defect seen upon TbMic34 knockdown. The levels of ATOM40 (Schneider, 2018) and VDAC were unaffected under these conditions (Fig. 6B; lower panels). Thus, TbMic32 affects the abundance of TbMic34 but not of TbMic10-1, leading to the conclusion that these two proteins are members of the second network of interdependent MICOS subunits.

MICOS subunit networks reflect MICOS subcomplexes

Using proteome-wide analyses of knockdown/knockout cell lines for selected MICOS subunits, we have defined two nonoverlapping networks of MICOS subunits. The first one consists of integral membrane proteins, while the other one is composed of soluble IMS-localized proteins. It is difficult to prove that the two networks correspond to physical subcomplexes because IPs of individual subunits always recover all 9 trypanosomal MICOS subunits. Moreover, BN-PAGE analyses show that all tagged MICOS subunits are present in a difficult-to-resolve, very large complex of more than 1 MDa with little evidence for subcomplexes (Kaurov *et al.*, 2018). A caveat is that most of the available data have been obtained with tagged proteins, which may not be as efficiently integrated into the MICOS complex or subcomplexes as the endogenous untagged proteins. Using antibodies specific for TbMic10-1 allowed, the analysis of TbMic10-1-containing

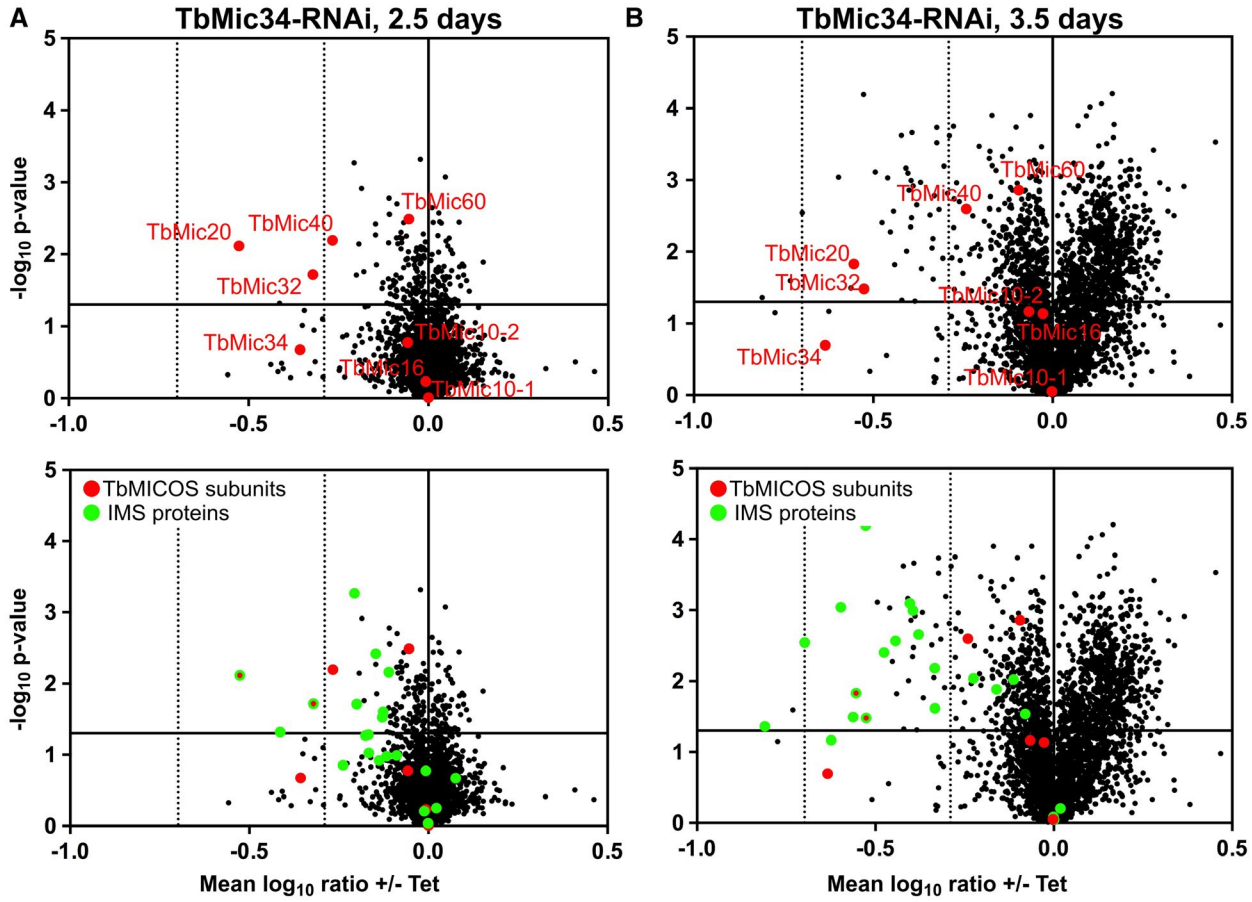

Fig. 4. Proteomic characterization of the TbMic34 RNAi cell line. The TbTim34-RNAi cell line was subjected to SILAC-based quantitative MS comparing protein abundances in 2.5 (A) and 3.5 days (B) induced versus uninduced mitochondria-enriched fractions. Vertical dashed lines indicate a two- and fivefold reduction respectively. Horizontal dashed line indicates a *P* value of 0.05. MICOS subunits are indicated by their names in red in the top panels. In the bottom panels MICOS subunits and proteins that localize or are predicted to be localized in the IMS are indicated by red and green dots respectively. For a complete list of proteins see Table S2.

complexes after the ablation of other MICOS subunits (Fig. 7). In untreated cells, most TbMic10-1 is found in the high-molecular weight MICOS complex that was shown to contain all tagged MICOS subunits. In addition, two low abundance TbMic10-1-containing subcomplexes of approximately 80 and 120 kDa could be detected. Knockdown of TbMic32, TbMic34 or TbMic20, all members of the second, soluble network, resulted in essentially the same phenotype: a partial shift of the high molecular weight MICOS complex to three low-molecular weight Mic10-1-containing subcomplexes of approximatey 80, 120 and 200 kDa. Their existence suggests that deficiency of the second MICOS network allows the TbMic10-1-containing network to be recovered as smaller physical subcomplexes. The molecular weight differences between these subcomplexes may be due to different amounts of TbMic10-1, and possibly TbMic10-2, as their orthologues in yeast and mammals are known to form oligomers (Barbot *et al.*, 2015; Bohnert *et al.*, 2015).

Discussion

BN-PAGE shows that each of the 9 tagged MICOS subunits comigrates in a very large complex of more than 1 MDa (Kaurov *et al.*, 2018). Using proteome-wide analysis of cell lines depleted for specific subunits we show that in trypanosomes this high-molecular weight MICOS complex consists of two largely independent functional networks of MICOS subunits that likely represent physical subcomplexes.

The first network consists of the integral membrane proteins TbMic10-1, TbMic10-2, TbMic16 and TbMic60, whereas the second network comprises the soluble IMS-localized proteins TbMic20, TbMic32, TbMic34 and TbMic40. TbMic17 was not downregulated in the proteomes of the ΔMic10-1 and ΔMic10-2 cell lines and is therefore not part of the first network. Whether it contributes to the second one is unclear since it was not detected in the SILAC RNAi analysis of TbMic34 RNAi.

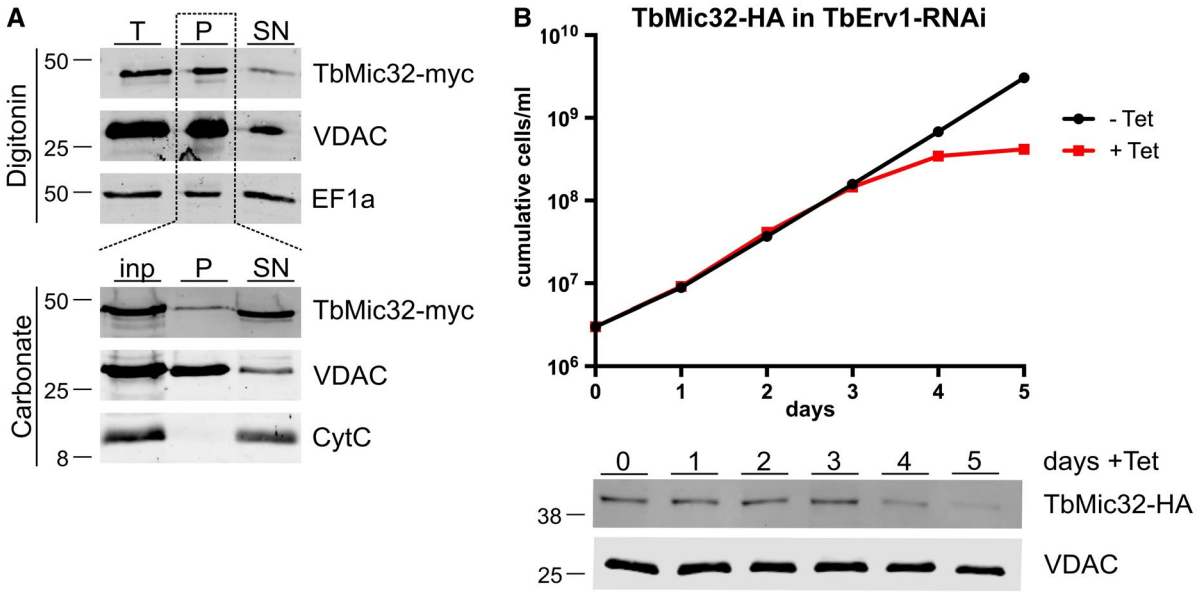

Fig. 5. TbMic32 is a soluble IMS-localized protein.
A. Top panels, digitonin extraction of total cells (T) to separate a mitochondria-enriched fraction (P) from the cytosol-containing supernatant (SN). The tagged TbMic32 co-fractionates with the mitochondrial marker VDAC while the cytosolic elongation factor 1A (EF1a) stays in the supernatant. Bottom panels, carbonate extraction at pH 11.5 of the mitochondria-enriched pellet fraction (inp) probed for TbMic32-myc. The pellet (P) and the supernatant (SN) fractions correspond to integral membrane and soluble proteins. VDAC and cytochrome C (Cyt C) serve as markers for integral and peripheral membrane proteins respectively.
B. Growth curve of an uninduced and induced TbErv1-RNAi cell line that constitutively expresses C-terminally HA-tagged TbMic32. Bottom panels, immunoblots of total cellular extracts of the same cell line probed for HA-tagged TbMic32. Time of induction is indicated. The OM protein VDAC serves as loading control.

The bipartite nature of the MICOS complex is conserved among trypanosomes, yeast and humans. However, the resulting subcomplexes are very different in opisthokonts as compared to trypanosomes. In yeast and humans they are each organized around one of the widely conserved core components, the integral membrane proteins Mic10 and Mic60 respectively. Mic10 is associated with the integral membrane proteins Mic26 and Mic27 forming the Mic10 subcomplex, whereas the Mic60 subcomplex includes the peripheral membrane proteins Mic19 in yeast or Mic25, the paralogue thereof in humans. The main function of the Mic10 subcomplex appears to be membrane sculpting and thus the building of the CJs, whereas the Mic60 subcomplex mainly forms the contact sites between the OM and the IM, although Mic60 also has a membrane-bending activity (Hessenberger *et al.*, 2017; Tarasenko *et al.*, 2017). Both subcomplexes are independently anchored in the cristae membranes, as most of their subunits are integral membrane proteins. Finally, it was shown that the integral IM protein Mic12 in yeast, or its orthologue in humans QIL12/MIC13 (Guarani *et al.*, 2015), mediate the lateral interaction of the two subcomplexes (Bohnert *et al.*, 2015; Ding *et al.*, 2015; Friedman *et al.*, 2015; Guarani *et al.*, 2015; Ott *et al.*, 2015; Li *et al.*, 2016).

While the trypanosomal MICOS contains orthologues of Mic10 and Mic60, the way the complex is organized in two networks is strikingly different from what is observed in yeast and mammals. One network of MICOS subunits is composed of the four integral membrane proteins TbMic10-1, TbMic10-2, TbMic16 and TbMic60. Thus, unlike in opisthokonts, both conserved MICOS subunits, the Mic-10 paralogues TbMic10-1 and TbMic10-2 together with TbMic60 belong to the same network, whereas all soluble IMS-localized proteins – TbMic34, TbMic32, TbMic20 and TbMic40 – comprise the second network. Therefore, rather than the lateral association of the two membrane-embedded MICOS subcomplexes that is described in opisthokonts, a vertical association of the trypanosomal subcomplexes between a module consisting exclusively of integral membrane proteins and a membrane peripheral network that includes only soluble proteins was observed (Fig. 8). The existence of two independent MICOS networks, composed of subunits whose stability depend on each other, suggests that the two subcomplexes are assembled independently. Regarding the functions of the two networks, it seems that the membrane-integrated subcomplex is mainly responsible for formation of CJs, whereas the most striking phenotype observed after the ablation of subunits of the peripheral subcomplex is an inhibition of mitochondrial protein import. Deletion or downregulation of individual subunits of the membrane-integrated MICOS network does not

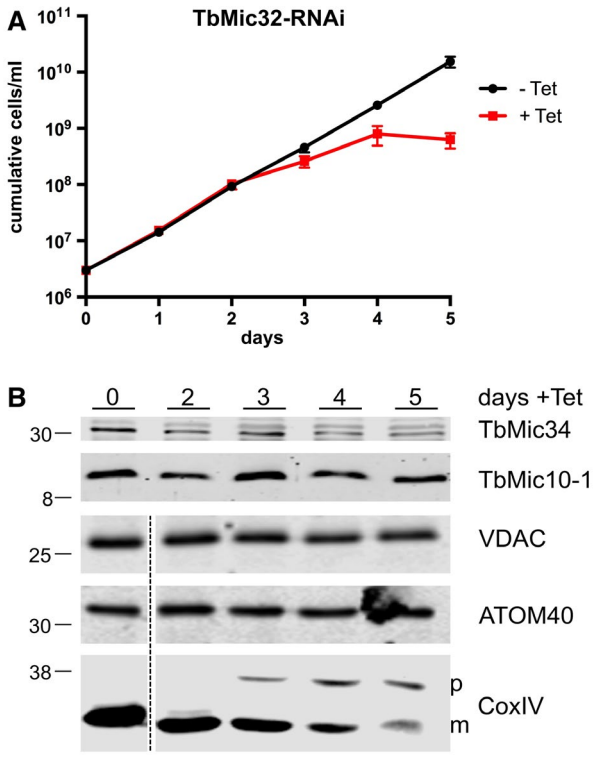

Fig. 6. Ablation of TbMic32 affects TbMic34 but not TbMic10 levels and inhibits protein import.
A. Growth curve of an uninduced and induced TbMic32-RNAi cell line.
B. Immunoblots of total cellular extracts from the TbMic34 RNAi cell lines induced for the indicated days were probed for TbMic34 and TbMic10-1 (top panel) or VDAC, ATOM40, and CoxIV (bottom panel) using polyclonal antisera. The positions of precursor and mature form of CoxIV are indicated.

affect growth, indicating the formation of CJs is not essential for procyclic *T. brucei* 29-13, not even when it is grown in the absence of glucose which forces the cell to rely on oxidative phosphorylation for energy conversion (Lamour *et al.*, 2005).

Ablation of individual subunits of the peripheral MICOS network in trypanosomes strongly interferes with mitochondrial protein import. Connections between protein import and MICOS have first been described in yeast, where it was shown that there are two different ways of how MICOS promotes protein import, both mediated by Mic60 (von der Malsburg *et al.*, 2011; Bohnert *et al.*, 2012; Wrobel *et al.*, 2015). Mic60 facilitates membrane insertion of β-barrel proteins by its binding to the TOM and the SAM complexes, although the exact mechanism is unclear. Moreover, Mic60 transiently interacts with Mia40 and thus promotes import of IMS proteins by recruiting Mia40 to the vicinity of the TOM complex (von der Malsburg *et al.*, 2011). Proteomics analyses of the TbMic34 RNAi cell line demonstrated that the earliest affected proteins are those localized in the IMS, including small Tim chaperones (Wenger *et al.*, 2017), whose downregulation explains the general import phenotype that is observed at later time points. β-Barrel proteins, however, were not affected. Trypanosomes do not have a Mia40 orthologue (Basu *et al.*, 2013) and their Mic60 orthologue is a member of the membrane integral subcomplex that is not essential for normal growth of the *T. brucei* 29-13 strain. The deficiency of IMS protein import that is seen after ablation of the essential membrane peripheral subcomplex can therefore not be connected to the lack of TbMic60. However, in *T. brucei* the function of Mic60 may be split between the Mic60 orthologue and TbMic34 (Kaurov *et al.*, 2018), the core component of the peripheral network that may functionally compensate for the lacking mitofilin domain of TbMic60. In this regard the peripheral MICOS network may still contain a Mic60 remnant corresponding to the C-terminal half of the protein.

Nevertheless, we find it unlikely that TbMic34 is directly linked to the protein import phenotype. We prefer the previously proposed scenario, that the thioredoxin-like protein TbMic20 – a member of the peripheral MICOS subcomplex – might be a functional analogue of Mia40 and together with Erv1 directly mediate IMS protein import (Kaurov *et al.*, 2018). Thus, protein import inhibition seen after the ablation of the peripheral MICOS network might ultimately be due to the concomitant depletion of TbMic20. However presently, indirect effects cannot be excluded and more evidence is required to show that TbMic20 indeed is a functional analogue of Mia40.

In summary, our study illustrates the value of a comparative analysis of the MICOS complex between opisthokonts and excavates. Together with future studies in other organisms this will provide us with an 'evolutionary cell biology' perspective (Brodsky *et al.*, 2012; Lynch *et al.*, 2014; Richardson *et al.*, 2015) of the MICOS complex. This in turn should help us to determine which structural and functional features of the MICOS complex are universally conserved, not necessarily because of common descent but because of chemical and physical constraints imposed by functional selection.

Experimental procedures

Transgenic cell lines

All experiments were performed with procyclic *T. brucei* 29-13 and derivatives thereof (Wirtz *et al.*, 1999). Double knockouts of TbMic10-1 and TbMic10-2 were generated by replacement of their ORFs of both alleles with the coding sequences of genes leading to resistance against phleomycin and puromycin. Growth of these cells was monitored in SDM-80 containing 10% (v/v) fetal calf serum supplemented with either 5.55 mM glucose (rich) or 50 mM N-acetylglucosamine (glucose-poor) (Lamour *et al.*, 2005; Ebikeme *et al.*, 2008). All

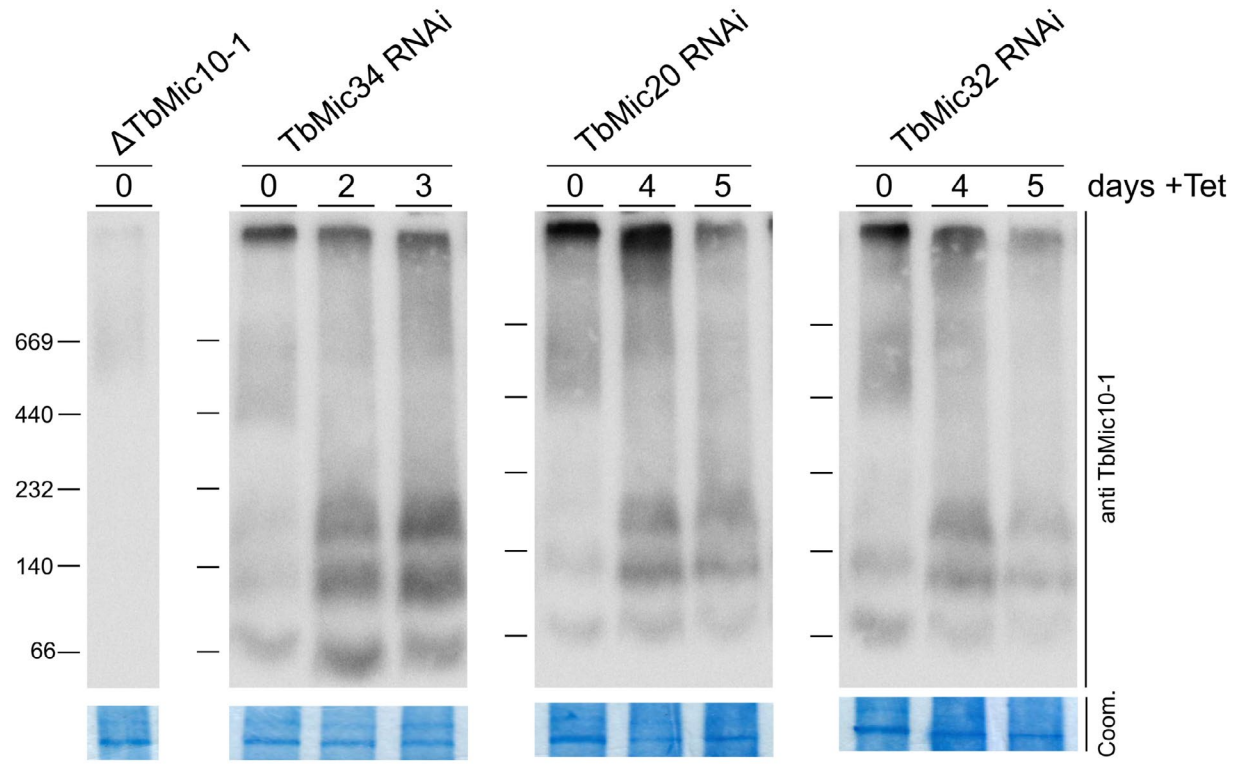

Fig. 7. TbMic20, TbMic32 and TbMic34 RNAi disrupts the high molecular weight TbMic10-containing complex. Mitochondria enriched fractions of the indicated uninduced and induced RNAi cell lines were resolved by BN-PAGE, blotted to PVDF membranes and probed for TbMic10-1. A section of the corresponding Coomassie-stained gel is shown as a loading control.

other experiments were performed with cells cultured at 27°C in standard SDM-79 containing 10% FCS.

Tetracycline inducible RNAi against the ORFs of TbMic34 (nt 167–628), TbMic32 (nt 229–806), TbMic60 (nt 386–669) and TbMic20 (nt 54–504) was achieved by stable integration of NotI-linearized plasmids containing stem–loop constructs targeting the indicated sequences.

TbMic32 was tagged in situ with 3xHA (Oberholzer *et al.*, 2005) in the background of RNAi against TbErv1 (Peikert *et al.*, 2017). An additional cell line was made for inducible overexpression of a triple c-myc tagged TbMic32 from an ectopic copy encoded on a derivative of pLEW100 (Bochud-Allemann and Schneider, 2002).

Protein analysis

Digitonin extraction was used to separate cytoplasmic proteins from a crude mitochondrial pellet. In brief, 5×10^7 cells were harvested, washed in PBS and incubated in 20 mM Tris HCl pH 7.5, 0.6 M sorbitol, 2 mM EDTA and 0.015% (w/v) digitonin for 10 min on ice. Subsequently, the suspension was centrifuged for 5 min at 6,800 × *g* at 4°C and samples containing equal cell equivalents of whole cells, the supernatant and the mitochondria-enriched pellet were subjected to SDS-PAGE and immunoblot analysis.

For alkaline extraction, a mitochondria-enriched fraction was prepared as described above, resuspended in 100 mM Na_2CO_3 pH11.5 and incubated for 10 min on ice. Centrifugation at 100,000 × *g* for 10 min at 4°C separated the supernatant containing soluble proteins from pelleted integral membrane proteins.

For BN-PAGE analysis, a crude mitochondrial pellet was prepared by digitonin extraction (see above) from 1×10^7 cells. The pellet was then resupended in 100 µl of 20 mM Tris-HCl pH 7.4, 50 mM NaCl, 10% glycerol, 0.1 mM EDTA and 1.5% (w/v) digitonin and proteins were solubilized by incubation on ice for 20 min. After a clearing spin (15 min, 4°C, 21,000 × *g*) a fraction of the supernatant corresponding to 4×10^7 cells was separated on a 4-13 % BN-PAGE gradient gel. After electrophoresis the gel was incubated briefly in SDS-PAGE running buffer (25 mM Tris, 1 mM EDTA, 190 mM glycine, 0.05 % SDS) and proteins were blotted onto a PVDF membrane via semi-dry transfer.

Antibodies

Polyclonal antibodies against TbMic10-1 (used in a 1:1,000 dilution) and TbMic34 (diluted 1:2,500 for immunoblots) were obtained upon immunization of rabbits with a synthetic peptide (LRKGFRGSTGVSDRESSGS) or recombinant full-length protein expressed in *E. coli* respectively. All other antibodies are described in detail (Käser *et al.*, 2017).

Transmission electron microscopy

Transmission electron microscopy on strain 29-13 and TbMic10-1 knockout cells was done as described

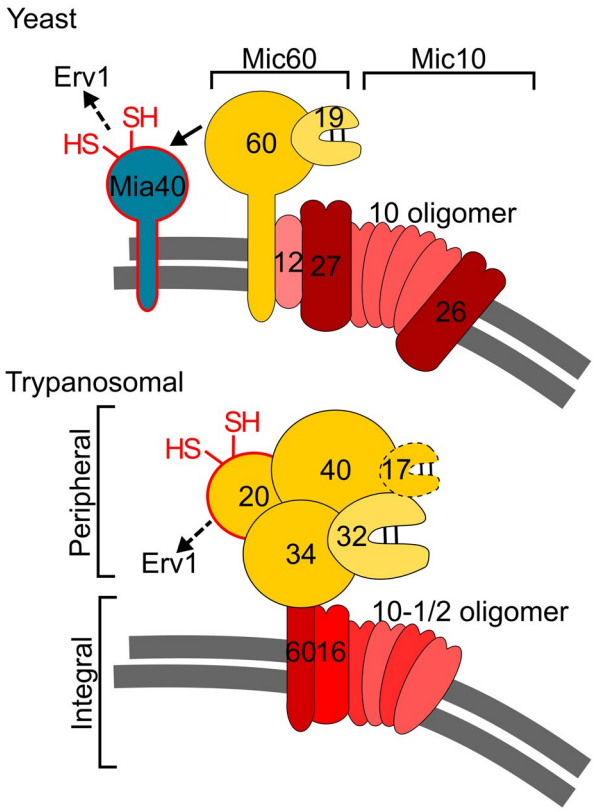

Fig. 8. The subcomplex architecture of yeast and trypanosomal MICOS complexes. A scheme comparing the laterally organized integral Mic10 and Mic60 subcomplexes of yeast with the vertically associated integral and membrane peripheral subcomplexes of *T. brucei*. Subunits are indicated by the last digits of their names. The twin CX_9C motif bearing Mic19 and TbMic32 are shown as hairpins with two intramolecular thiol bridges. TbMic17, shown with broken lines, is tentatively assigned to peripheral subcomplex. The transient interaction of the yeast Mic60 mitofilin domain with Mia40 is depicted by an arrow. The putative role of TbMic20 in MIA in an analogous way to Mia40 is shown by their red outlines and reduced thiol-groups. The path of electrons from Mia40/TbMic20 to Erv1 is indicated by a broken arrows. TbMic34 is positioned above TbMic60 to indicate it may represent the missing mitofilin domain present in yeast Mic60. IM is shown in gray.

(Schnarwiler *et al*., 2014) and pictures were analyzed with ImageJ. In short, uninduced and induced TAC40-RNAi cells of *T. brucei* were fixed in culture for at least 24 h, using 2.5% glutaraldehyde in 0.15 M Hepes buffer. Samples were postfixed with 1% (wt/vol) osmium tetroxide, dehydrated in ascending concentrations of ethanol, and embedded in Epon. Ultrathin sections were stained with uranyl acetate and lead citrate, using an ultrostainer (Leica), and observed in a Philips CM12 electron microscope at 80 kV equipped with a Morada camera system, using iTEM software.

Proteolytic digestion for MS analysis

Mitochondria-enriched fractions prepared from ΔTbMic10-1, ΔTbMic10-2 and control cells (110 µg of protein per sample) as well as from SILAC-labeled tetracycline-induced and uninduced TbMic34-RNAi cells (20 µg of protein per sample) were resuspended in 8 M urea/50 mM NH_4HCO_3. Cysteine residues were reduced using 5 mM Tris(2-carboxy-ethyl) phosphine/10 mM NH_4HCO_3 (incubation for 30 min at 37°C) and free thiol groups were subsequently alkylated with 50 mM iodoacetamide/10 mM NH_4HCO_3 (30 min at room temperature in the dark). Dithiothreitol was added to a final concentration of 20 mM to quench the alkylation reaction. Samples were diluted with 50 mM NH_4HCO_3 to a final urea concentration of 1.6 M and proteins were digested with trypsin (37°C, overnight). The reaction was stopped by adding acetic acid to a final concentration of 0.25% (v/v). Samples were desalted using StageTips and dried *in vacuo* (Rappsilber *et al*., 2007).

Peptide stable isotope dimethyl labeling and high-pH reversed-phase fractionation

Peptides derived from mitochondria-enriched fractions of ΔTbMic10-1, ΔTbMic10-2 and control cells were reconstituted in 100 mM tetraethylammonium bicarbonate (100 µl per 10 µg of protein). Peptides were labeled light, medium–heavy or heavy by stable isotope dimethyl labeling (Boersema *et al*., 2009) essentially as described previously (Peikert *et al*., 2017) including label switch. For light labeling, formaldehyde (CH_2O) and sodium cyanoborohydride ($NaBH_3CN$) were used, medium–heavy labeling was performed with deutered formaldehyde (CD_2O) instead of the light variant, and for heavy labeling, ^{13}C-containing deuterated formaldehyde ($^{13}CD_2O$) was used in combination with deuterated sodium cyanoborohydride ($NaBD_3CN$). Labeling was performed by mixing 100 µl of reconstituted peptides with the respective isotopologue of formaldehyde (4% [v/v], 4 µl) and sodium cyanoborohydride (0.6 M, 4 µl) and incubation for 1 h at 20°C and 800 rpm. Reactions were stopped by addition of 16 µl of 1% NH_3 and samples were subsequently acidified with 8 µl of 100% formic acid (FA). Differentially light, medium–heavy and heavy dimethyl-labeled peptides were mixed, purified using StageTips and dried *in vacuo*. Peptides were subsequently fractionated by high-pH reversed-phase chromatography on StageTips (Peikert *et al*., 2017). To this end, peptides were resuspended in 10 mM NH_4OH and loaded onto StageTips equilibrated with 10 mM NH_4OH. Peptides were fractionated by stepwise elution with 0%, 3%, 6%, 10%, 13%, 18%, 40% and 72% (v/v) ACN/10 mM NH_4OH. Solvents and peptides were applied by centrifugation for 1–2 min at 800 × *g*. Peptides were dried *in vacuo*, reconstituted in 15 µl of 0.1% (v/v) TFA per fraction, of which 10 µl were analyzed by liquid chromatography–mass spectrometry (LC-MS).

LC-MS and analysis and data processing

Peptides corresponding to approximately 2 µg of protein were analyzed by nano-HPLC-ESI-MS/MS on an Orbitrap Elite (TbMic34-RNAi experiments) or a Q Exactive (ΔTbMic10-1/2 experiments) instrument (Thermo Fisher Scientific) each directly connected to an UltiMate 3000 RSLCnano HPLC system (Thermo Fisher Scientific). The RSLC system coupled to the Orbitrap Elite was equipped with PepMap C18 precolumns (5 mm × 300 µm inner diameter; Thermo Scientific)

for preconcentration of peptides and C18 reversed-phase nano-LC columns (Acclaim PepMap RSLC columns; 50 cm × 75 µm inner diameter; particle size 2 µm, pore size 100 Å; Thermo Scientific) for peptide separation. The RSLC system coupled to the Q Exactive was operated with nanoEase M/Z Symmetry C18 precolumns (20 mm × 180 µm inner diameter; Waters) and a nanoEase M/Z HSS C18 T3 analytic column (25 cm × 75 µm inner diameter; particle size 1.8 µm, pore size 100 Å; Waters). Peptides of TbMic34-RNAi experiments were loaded onto the precolumns at a flow rate of 30 µl/min. The solvent system used for peptide separation consisted of 4% (v/v) DMSO/0.1% (v/v) FA (solvent A) and 48% (v/v) methanol/30% (v/v) ACN/4% (v/v) DMSO/0.1% (v/v) FA (solvent B). Peptides were eluted applying a gradient of 3%–60% solvent B in 315 min, 60%–95% B in 15 min at 5 min at 95%B at a flow rate of 250 nl/min and a column temperature of 40°C. Peptides of ΔTbMic10-1/2 experiments were loaded at a flow rate of 5 µl/min. Solvent system and gradient for peptide separation were as follows: 0.1% (v/v) FA (solvent A) and 86% (v/v) ACN (solvent B); 4%–40% B in 50 min, 40%–95% B in 5 min and 5 min at 95% B; flow rate and column temperature were 300 nl/min and 40°C respectively. MS data were acquired in data-dependent mode essentially as described before (Peikert *et al.*, 2017).

Mass spectrometric raw data were processed using MaxQuant/Andromeda (version 1.5.5.1; (Cox and Mann, 2008; Cox *et al.*, 2011)) and the fasta file for *T. brucei* TREU927 downloaded from the TriTryp database (version 8.1). MaxQuant default settings were used except that only one unique peptide and one ratio count were required for protein identification and relative quantification. For analysis of data from TbMic34-RNAi SILAC experiments, Lys0/Arg0 were set as light and Lys8/Arg10 as heavy labels; for data from peptide stable isotope dimethyl-labeling experiments (ΔTbMic10-1/2 experiments), dimethLys0/dimethNter0 was set as light, dimethLys4/dimethNter4 as medium–heavy and dimethLys8/dimethNter8 as heavy label. Data were visualized by plotting the mean of $\log_{10}$-tranformed normalized protein abundance ratios against the negative $\log_{10}$ of the corresponding p-value determined in a two-sided Student's *t*-test. Information about proteins identified and quantified in ΔTbMic10-1/2 experiments and TbMic34-RNAi experiments are provided in Tables S1 and S2A and B, respectively.

Miscellaneous

Knockdown efficiency of RNAi against TbMic60 was analyzed by RT-PCR. Briefly, total RNA was isolated and reverse transcribed using oligo-dT primers. Resulting cDNA was amplified using a TbMic60-specific reverse primer and a forward primer hybridizing to the spliced leader sequence ensuring that PCR products can only derive from cDNA and not from traces of genomic DNA. In vitro import assays were done as described (Hauser *et al.*, 1996), using in vitro translated CoxIV precursor as a substrate.

Acknowledgements

This study was supported by the NCCR 'RNA & Disease' (to AS) and in part by grants 175563 (to AS) all funded by the Swiss National Science Foundation. Work in the lab of BW was supported by the German Research Foundation (DFG) under Germany's Excellence Strategy (CIBSS – EXC-2189 – Project ID 390939984). Support from the Czech Science Foundation grant 17-24036S (to HH) as well as ERC CZ LL1601 and the ERD Funds, project OPVVV 16_019/0000759 (to JL) is acknowledged. Electron microscopy sample preparation and imaging were performed with devices supported by the Microscopy Imaging Center (MIC) of the University of Bern.

Author contributions

CE, JB, JM, BS designed and performed experiments and analyzed data. SO and BW produced and analyzed the proteomic MS results. BH and BZ performed the EM analysis. JL and HH conceived experiments. All authors edited the paper. AS wrote the paper, supervised the work and obtained the main funding.

Conflict of interest

The authors declare that they have no conflict of interest.

References

Aaltonen, M.J., Friedman, J.R., Osman, C., Salin, B., di Rago, J.P., Nunnari, J., *et al.* (2016) MICOS and phospholipid transfer by Ups2-Mdm35 organize membrane lipid synthesis in mitochondria. *Journal of Cell Biology*, **213**, 525–534.

Alkhaja, A.K., Jans, D.C., Nikolov, M., Vukotic, M., Lytovchenko, O., Ludewig, F., *et al.* (2012) MINOS1 is a conserved component of mitofilin complexes and required for mitochondrial function and cristae organization. *Molecular Biology of the Cell*, **23**, 247–257.

Barbot, M., Jans, D.C., Schulz, C., Denkert, N., Kroppen, B., Hoppert, M., *et al.* (2015) Mic10 oligomerizes to bend mitochondrial inner membranes at cristae junctions. *Cell Metabolism*, **21**, 756–763.

Basu, S., Leonard, J.C., Desai, N., Mavridou, D.A., Tang, K.H., Goddard, A.D., *et al.* (2013) Divergence of Erv1-associated mitochondrial import and export pathways in trypanosomes and anaerobic protists. *Eukaryotic Cell*, **12**, 343–355.

Bochud-Allemann, N. and Schneider, A. (2002) Mitochondrial substrate level phosphorylation is essential for growth of procyclic *Trypanosoma brucei*. *Journal of Biological Chemistry*, **277**, 32849–32854.

Boersema, P.J., Raijmakers, R., Lemeer, S., Mohammed, S. and Heck, A.J. (2009) Multiplex peptide stable isotope dimethyl labeling for quantitative proteomics. *Nature Protocols*, **4**, 484–494.

Bohnert, M., Wenz, L.S., Zerbes, R.M., Horvath, S.E., Stroud, D.A., von der Malsburg, K., *et al.* (2012) Role of mitochondrial inner membrane organizing system in protein biogenesis of the mitochondrial outer membrane. *Molecular Biology of the Cell*, **23**, 3948–3956.

Bohnert, M., Zerbes, R.M., Davies, K.M., Muhleip, A.W., Rampelt, H., Horvath, S.E., *et al.* (2015) Central role of Mic10 in the mitochondrial contact site and cristae organizing system. *Cell Metabolism*, **21**, 747–755.

Brodsky, F.M., Thattai, M. and Mayor, S. (2012) Evolutionary cell biology: lessons from diversity. *Nature Cell Biology*, **14**, 651.

Burki, F. (2014) The eukaryotic tree of life from a global phylogenomic perspective. *Cold Spring Harbor Perspectives in Biology*, **6**, a016147.

Cox, J. and Mann, M. (2008) MaxQuant enables high peptide identification rates, individualized p.p.b.-range mass accuracies and proteome-wide protein quantification. *Nature Biotechnology*, **26**, 1367–1372.

Cox, J., Neuhauser, N., Michalski, A., Scheltema, R.A., Olsen, J.V. and Mann, M. (2011) Andromeda: a peptide search engine integrated into the MaxQuant environment. *Journal of Proteome Research*, **10**, 1794–1805.

Ding, C., Wu, Z., Huang, L., Wang, Y., Xue, J., Chen, S., *et al.* (2015) Mitofilin and CHCHD6 physically interact with Sam50 to sustain cristae structure. *Scientific Reports*, **5**, 16064.

Ebikeme, C.E., Peacock, L., Coustou, V., Riviere, L., Bringaud, F., Gibson, W.C., *et al.* (2008) N-acetyl D-glucosamine stimulates growth in procyclic forms of *Trypanosoma brucei* by inducing a metabolic shift. *Parasitology*, **135**, 585–594.

Friedman, J.R., Mourier, A., Yamada, J., McCaffery, J.M. and Nunnari, J. (2015) MICOS coordinates with respiratory complexes and lipids to establish mitochondrial inner membrane architecture. *eLife*, **4**, e07739.

Guarani, V., McNeill, E.M., Paulo, J.A., Huttlin, E.L., Frohlich, F., Gygi, S.P., *et al.* (2015) QIL1 is a novel mitochondrial protein required for MICOS complex stability and cristae morphology. *eLife*, **4**, e06265.

Haindrich, A.C., Boudova, M., Vancova, M., Diaz, P.P., Horakova, E. and Lukes, J. (2017) The intermembrane space protein Erv1 of Trypanosoma brucei is essential for mitochondrial Fe–S cluster assembly and operates alone. *Molecular and Biochemical Parasitology*, **214**, 47–51.

Harner, M., Korner, C., Walther, D., Mokranjac, D., Kaesmacher, J., Welsch, U., *et al.* (2011) The mitochondrial contact site complex, a determinant of mitochondrial architecture. *EMBO Journal*, **30**, 4356–4370.

Harner, M.E., Unger, A.K., Izawa, T., Walther, D.M., Ozbalci, C., Geimer, S., *et al.* (2014) Aim24 and MICOS modulate respiratory function, tafazzin-related cardiolipin modification and mitochondrial architecture. *elife*, **3**, e01684.

Harsman, A., Oeljeklaus, S., Wenger, C., Huot, J.L., Warscheid, B. and Schneider, A. (2016) The non-canonical mitochondrial inner membrane presequence translocase of trypanosomatids contains two essential rhomboid-like proteins. *Nature Communications*, **19**, 13707.

Hauser, R., Pypaert, M., Häusler, T., Horn, E.K. and Schneider, A. (1996) In vitro import of proteins into mitochondria of *Trypanosoma brucei* and *Leishmania tarentolae*. *Journal of Cell Science*, **109**, 517–523.

Hessenberger, M., Zerbes, R.M., Rampelt, H., Kunz, S., Xavier, A.H., Purfurst, B., *et al.* (2017) Regulated membrane remodeling by Mic60 controls formation of mitochondrial crista junctions. *Nature Communications*, **8**, 15258.

Hoppins, S., Collins, S.R., Cassidy-Stone, A., Hummel, E., Devay, R.M., Lackner, L.L., *et al.* (2011) A mitochondrial-focused genetic interaction map reveals a scaffold-like complex required for inner membrane organization in mitochondria. *Journal of Cell Biology*, **195**, 323–340.

Huynen, M.A., Muhlmeister, M., Gotthardt, K., Guerrero-Castillo, S. and Brandt, U. (2016) Evolution and structural organization of the mitochondrial contact site (MICOS) complex and the mitochondrial intermembrane space bridging (MIB) complex. *Biochimica Biophysica Acta*, **1863**, 91–101.

Itoh, K., Tamura, Y., Iijima, M. and Sesaki, H. (2013) Effects of Fcj1-Mos1 and mitochondrial division on aggregation of mitochondrial DNA nucleoids and organelle morphology. *Molecular Biology of the Cell*, **24**, 1842–1851.

Käser, S., Willemin, M., Schnarwiler, F., Schimanski, B., Poveda-Huertes, D., Oeljeklaus, S., *et al.* (2017) Biogenesis of the mitochondrial DNA inheritance machinery in the mitochondrial outer membrane of *Trypanosoma brucei*. *PLoS Pathogen*, **13**, e1006808.

Kaurov, I., Vancova, M., Schimanski, B., Cadena, L.R., Heller, J., Bily, T., *et al.* (2018) The diverged trypanosome MICOS complex as a hub for mitochondrial cristae shaping and protein import. *Current Biology*, **28**(3393–3407), e3395.

Korner, C., Barrera, M., Dukanovic, J., Eydt, K., Harner, M., Rabl, R., *et al.* (2012) The C-terminal domain of Fcj1 is required for formation of crista junctions and interacts with the TOB/SAM complex in mitochondria. *Molecular Biology of the Cell*, **23**, 2143–2155.

Kozjak-Pavlovic, V. (2017) The MICOS complex of human mitochondria. *Cell Tissue Research*, **367**, 83–93.

van der Laan, M., Horvath, S.E. and Pfanner, N. (2016) Mitochondrial contact site and cristae organizing system. *Current Opinion in Cell Biology*, **41**, 33–42.

Lamour, N., Riviere, L., Coustou, V., Coombs, G.H., Barrett, M.P. and Bringaud, F. (2005) Proline metabolism in procyclic *Trypanosoma brucei* is down-regulated in the presence of glucose. *Journal of Biological Chemistry*, **280**, 11902–11910.

Li, H., Ruan, Y., Zhang, K., Jian, F., Hu, C., Miao, L., *et al.* (2016) Mic60/Mitofilin determines MICOS assembly essential for mitochondrial dynamics and mtDNA nucleoid organization. *Cell Death Differentiation*, **23**, 380–392.

Lynch, M., Field, M.C., Goodson, H.V., Malik, H.S., Pereira-Leal, J.B., Roos, D.S., *et al.* (2014) Evolutionary cell biology: two origins, one objective. *Proceedings of the National Academy of Science USA*, **111**, 16990–16994.

von der Malsburg, K., Muller, J.M., Bohnert, M., Oeljeklaus, S., Kwiatkowska, P., Becker, T., *et al.* (2011) Dual role of mitofilin in mitochondrial membrane organization and protein biogenesis. *Developmental Cell*, **21**, 694–707.

Michaud, M., Gros, V., Tardif, M., Brugiere, S., Ferro, M., Prinz, W.A., *et al.* (2016) AtMic60 Is involved in plant mitochondria lipid trafficking and is part of a large complex. *Current Biology*, **26**, 627–639.

Mordas, A. and Tokatlidis, K. (2015) The MIA pathway: a key regulator of mitochondrial oxidative protein folding and biogenesis. *Accounts of Chemical Research*, **48**, 2191–2199.

Munoz-Gomez, S.A., Slamovits, C.H., Dacks, J.B., Baier, K.A., Spencer, K.D. and Wideman, J.G. (2015) Ancient homology of the mitochondrial contact site and cristae

organizing system points to an endosymbiotic origin of mitochondrial cristae. *Current Biology*, **25**, 1489–1495.
Munoz-Gomez, S.A., Wideman, J.G., Roger, A.J. and Slamovits, C.H. (2017) The origin of mitochondrial cristae from alphaproteobacteria. *Molecular Biology and Evolution*, **34**, 943–956.
Oberholzer, M., Morand, S., Kunz, S. and Seebeck, T. (2005) A vector series for rapid PCR-mediated C-terminal in situ tagging of *Trypanosoma brucei* genes. *Molecular and Biochemical Parasitology*, **145**, 117–120.
Ott, C., Dorsch, E., Fraunholz, M., Straub, S. and Kozjak-Pavlovic, V. (2015) Detailed analysis of the human mitochondrial contact site complex indicate a hierarchy of subunits. *PLoS ONE*, **10**, e0120213.
Peikert, C.D., Mani, J., Morgenstern, M., Käser, S., Knapp, B., Wenger, C., *et al.* (2017) Charting organellar importomes by quantitative mass spectrometry. *Nature Communications*, **8**, 15272.
Quintana-Cabrera, R., Mehrotra, A., Rigoni, G. and Soriano, M.E. (2018) Who and how in the regulation of mitochondrial cristae shape and function. *Biochemical and Biophysical Research Communications*, **500**, 94–101.
Rampelt, H., Zerbes, R.M., van der Laan, M. and Pfanner, N. (2017) Role of the mitochondrial contact site and cristae organizing system in membrane architecture and dynamics. *Biochimica Biophysica Acta Mol Cell Res*, **1864**, 737–746.
Rappsilber, J., Mann, M. and Ishihama, Y. (2007) Protocol for micro-purification, enrichment, pre-fractionation and storage of peptides for proteomics using StageTips. *Nature Protocols*, **2**, 1896–1906.
Richardson, E., Zerr, K., Tsaousis, A., Dorrell, R.G. and Dacks, J.B. (2015) Evolutionary cell biology: functional insight from 'endless forms most beautiful'. *Molecular Biology of the Cell*, **26**, 4532–4538.
Schnarwiler, F., Niemann, M., Doiron, N., Harsman, A., Kaser, S., Mani, J., *et al.* (2014) Trypanosomal TAC40 constitutes a novel subclass of mitochondrial beta-barrel proteins specialized in mitochondrial genome inheritance. *Proceedings of the National Academy of Science USA*, **111**, 7624–7629.
Schneider, A. (2018) Mitochondrial protein import in trypanosomatids: variations on a theme or fundamentally different? *PLoS Pathogen*, **14**, e1007351.
Schorr, S. and van der Laan, M. (2018) Integrative functions of the mitochondrial contact site and cristae organizing system. *Seminars in Cell and Developmental Biology*, **76**, 191–200.
Singha, U.K., Peprah, E., Williams, S., Walker, R., Saha, L. and Chaudhuri, M. (2008) Characterization of the mitochondrial inner membrane protein translocator Tim17 from *Trypanosoma brucei*. *Molecular and Biochemical Parasitology*, **159**, 30–43.
Stojanovski, D., Bragoszewski, P. and Chacinska, A. (2012) The MIA pathway: a tight bond between protein transport and oxidative folding in mitochondria. *Biochimica Biophysica Acta*, **1823**, 1142–1150.
Tarasenko, D., Barbot, M., Jans, D.C., Kroppen, B., Sadowski, B., Heim, G., *et al.* (2017) The MICOS component Mic60 displays a conserved membrane-bending activity that is necessary for normal cristae morphology. *Journal of Cell Biology*, **216**, 889–899.
Wenger, C., Oeljeklaus, S., Warscheid, B., Schneider, A. and Harsman, A. (2017) A trypanosomal orthologue of an intermembrane space chaperone has a non-canonical function in biogenesis of the single mitochondrial inner membrane protein translocase. *PLoS Pathogen*, **13**, e1006550.
Wirtz, E., Leal, S., Ochatt, C. and Cross, G.A. (1999) A tightly regulated inducible expression system for conditional gene knock-outs and dominant-negative genetics in *Trypanosoma brucei*. *Molecular and Biochemical Parasitology*, **99**, 89–101.
Wollweber, F., von der Malsburg, K. and van der Laan, M. (2017) Mitochondrial contact site and cristae organizing system: a central player in membrane shaping and crosstalk. *Biochimica Biophysica Acta*, **1864**, 1481–1489.
Wrobel, L., Topf, U., Bragoszewski, P., Wiese, S., Sztolsztener, M.E., Oeljeklaus, S., *et al.* (2015) Mistargeted mitochondrial proteins activate a proteostatic response in the cytosol. *Nature*, **524**, 485–488.
Zerbes, R.M., Bohnert, M., Stroud, D.A., von der Malsburg, K., Kram, A., Oeljeklaus, S., *et al.* (2012) Role of MINOS in mitochondrial membrane architecture: cristae morphology and outer membrane interactions differentially depend on mitofilin domains. *Journal of Molecular Biology*, **422**, 183–191.

Supporting Information

Additional supporting information may be found online in the Supporting Information section at the end of the article.

Supplementary Material:

The highly diverged trypanosomal MICOS complex is organized in a non-essential integral membrane and an essential peripheral module

Claudia Eichenberger[1], Silke Oeljeklaus[2, 3], Julia Bruggisser[1a], Jan Mani[1], Beat Haenni[4], Iosif Kaurov[5], Moritz Niemann[1], Benoît Zuber[4], Julius Lukeš[5], Hassan Hashimi[5], Bettina Warscheid[2, 3], Bernd Schimanski[1]* and André Schneider[1]*

[1] Department of Chemistry and Biochemistry, University of Bern, Freiestrasse 3, Bern CH-3012, Switzerland

[2] Department of Biochemistry and Functional Proteomics, Faculty of Biology, University of Freiburg, Freiburg 79104, Germany

[3] Signalling Research Centres BIOSS and CIBSS, University of Freiburg, Freiburg 79104, Germany

[4] Institute of Anatomy, University of Bern, Baltzerstrasse 2, Bern 3012, Switzerland

[5] Institute of Parasitology, Biology Center, Czech Academy of Sciences and Faculty of Science, University of South Bohemia, 370 05 České Budějovice (Budweis), Czech Republic

Supplementary Figures

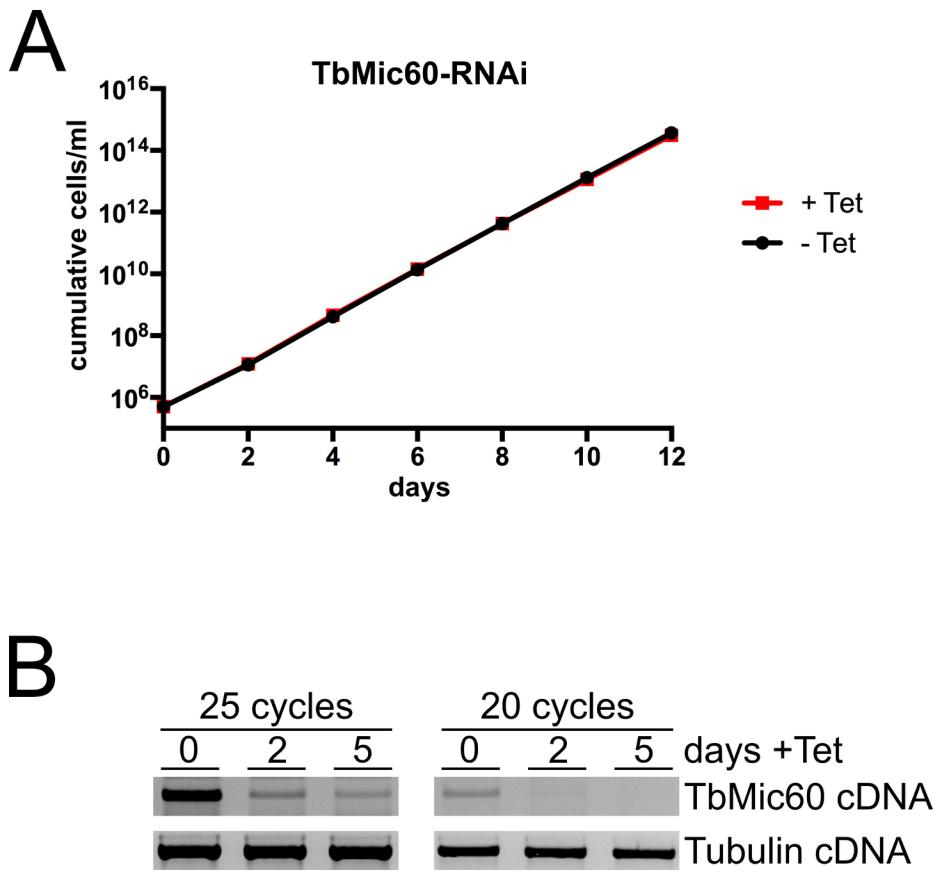

S1 Fig. RNAi-induced ablation of TbMic60 does not affect growth.
A) Growth curve of an inducible TbMic60 RNAi cell line in the presence and absence of tetracycline. B) RT-PCR anaysis analysis of TbMic60 and tubulin mRNAs at the indicated days of tetracycline induction. Number of amplification cycles are indicated at the top.

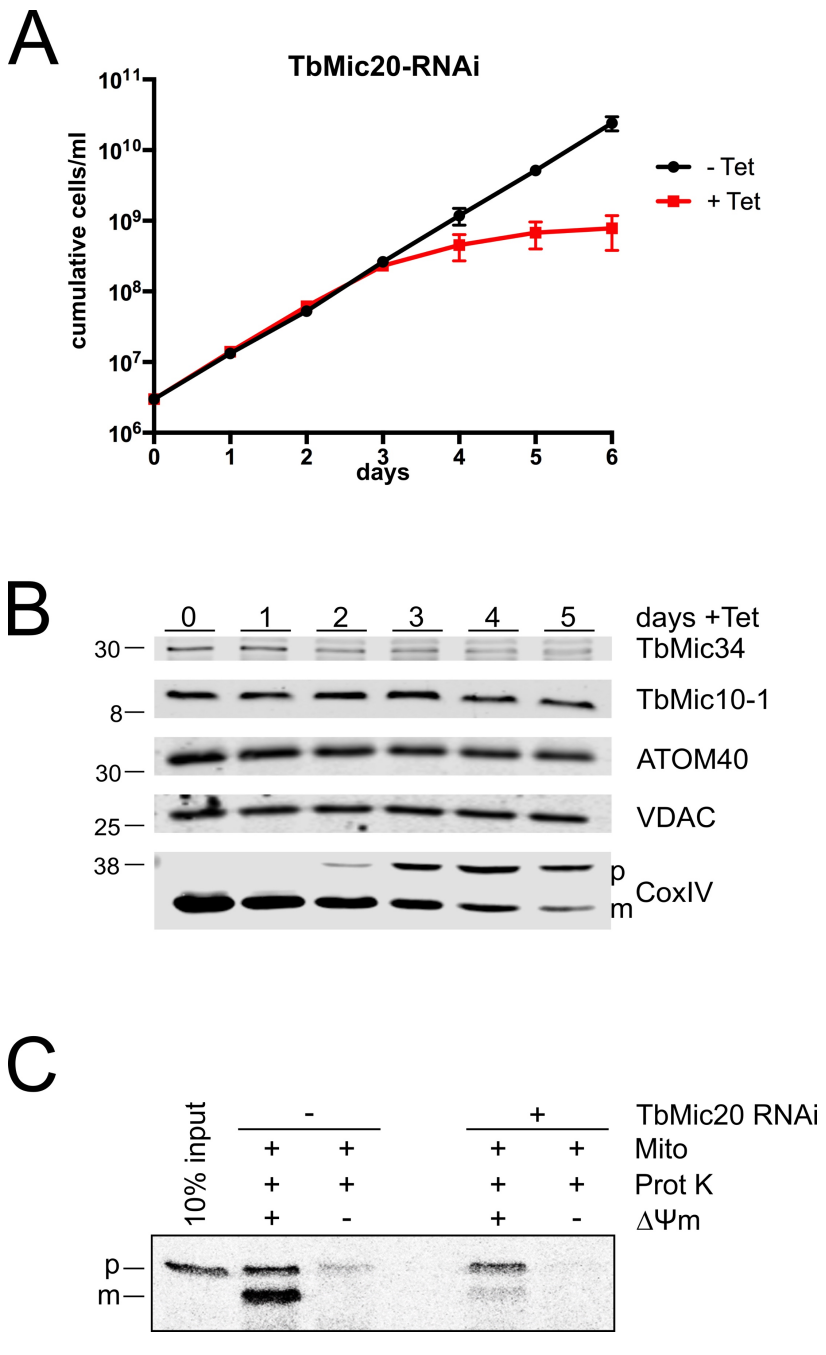

S2 Fig. Ablation of TbMic20 affects TbMic34 but not TbMic10 levels and inhibits protein import. A) Growth curve of an uninduced and induced TbMic20-RNAi cell line. B) Immunoblots of total cellular extracts from the TbMic20 RNAi cell lines induced for the indicated days were probed for TbMic34, TbMic10-1, ATOM40, VDAC and CoxIV using polyclonal antisera. The positions of precursor and mature form of CoxIV are indicated. C) In vitro import assays: ^{35}S-Met-labelled CoxIV precursor was imported into mitochondria isolated from the uninduced (-) and induced (+) TbMic20 RNAi cell lines. All import reactions were treated with 25 μg of proteinase K (Prot K) and analysed by SDS–PAGE followed by autoradiography. ΔΨm, membrane potential. The position of precursor (p) and mature forms (m) are indicated.

4.

Chapter 3. Thioredoxin-like MICOS subunit Mic20 promotes intermembrane space protein import

Thioredoxin-like MICOS subunit TbMic20 promotes intermembrane space protein import

Introduction

Mitochondria are protein-rich organelles. In distantly related organisms from different supergroups such as opisthokonts (specifically *Saccharomyces cerevisiae* and *Mus musculus*) and excavates (*Trypanosoma brucei*), the total number of mitochondrial proteins is roughly the same, approximately 1000 (Morgenstern et al., 2017; Pagliarini et al., 2008; Panigrahi et al., 2009). These proteins are involved such processes as mitochondrial biogenesis, oxidative phosphorylation(Kühlbrandt, 2015), Fe-S cluster synthesis (Stehling and Lill, 2013), lipid and amino acid metabolism, programmed cell death (Kasahara and Scorrano, 2014). Only a small portion of mitochondrial proteins are synthesized within the organelle because only a handful of genes are encoded in highly reduced mitochondrial genomes. The majority are translated in the cytosol and imported into the mitochondrion (Wiedemann et al., 2004). Thus, protein import into mitochondria is essential.

The classical signal targeting a newly synthetized protein into the mitochondria is a cleavable N-terminal presequence of 15-50 amino acids that form a positively charged amphipathic α-helix (Chacinska et al., 2009). Translocase of the outer membrane (TOM) complex, which is the most common entrance pathway for mitochondrial proteins, recognizes hydrophobic and hydrophilic faces of the presequence and performs the translocation (Chacinska et al., 2009). In addition to the classical presequence, protein precursors may contain other targeting signals. A combination of targeting sequences defines the final destination of the protein: outer membrane (OM) or inner membrane (IM) for integral proteins; matrix or intermembrane space (IMS) for soluble proteins. The distribution is performed by several sorting and import machineries.

The majority of IMS proteins go through the mitochondrial intermembrane space import and assembly (MIA) pathway (Becker et al., 2012). Unlike other mitochondrial import pathways, MIA couples oxidative folding and protein import. MIA substrates are usually small proteins less than 20 kDa, without detectable mitochondrial targeting presequence. They all contain cysteine residues, typically organized in twin $C(X_3)C$ or $C(X_9)C$ motifs. $C(X_3)C$ motifs are present in small TIM proteins (Baker et al., 2012). These chaperones guide hydrophobic precursors of the OM β-barrel proteins as well as IM carrier proteins across the IMS (Neupert and Herrmann, 2007; Stojanovski et al., 2008). Representatives of the proteins containing $C(X_9)C$ motifs are

Mia40 itself, Cox17 (Cavallaro, 2010) and Cox19 (Fraga et al., 2014). Additionally, Mia40 facilitates the import of some other proteins aside from typical IMS substrates (Wrobel et al., 2013). Interaction with Mia40 results in oxidative folding of the substrate (Fischer and Riemer, 2013), and the protein becomes trapped in the IMS because of the folded shape.

Apart of cysteine motifs, an internal targeting signal was found in the IMS substrates and named mitochondrial IMS sorting signal/IMS targeting signal (MISS/ITS). The motif is sufficient for targeting protein precursor to the mitochondrion (Sideris et al., 2009). It includes one of the cysteines of the $C(X_{3,9})C$ motif and 8 residues up-or downstream (Milenkovic et al., 2009). One aromatic and two hydrophobic residues are present in the consensus MISS/ITS sequence (Sideris et al., 2009). The interaction of the substrate and Mia40 starts with a non-covalent interaction between MISS/ITS signal and the concave hydrophobic domain of Mia40. This hydrophobic interaction facilitates precise positioning of the substrate cysteine in proximity with the docking cysteine of Mia40 (Kawano et al., 2009; Sideris et al., 2009). The first covalent intermolecular bond is formed. The following reshuffle of the disulfide bonds (DSBs) results in the formation of intramolecular bridge that covalently connects two cysteines of the substrate with each other (Banci et al., 2010). After the substrate is released, reduced Mia40 is reoxidized by the sulfhydryl oxidase ERV1 (Mesecke et al., 2005). Electrons are further transferred from ERV1 to cytochrome *c* (Bien et al., 2010). This system introducing disulfide bonds and shuttling electrons is named disulfide relay, and Mia40 with ERV1 are the core proteins.

Respiring mitochondria produce different reactive oxygen species (ROS), predominantly superoxide radical O_2^- (Murphy, 2009). ROS have signaling function in the cell, but in the first place they are toxic metabolites capable of carbonylation of proteins and peroxidation of lipids thus threatening the viability of the cell. To reduce the oxidative stress, protective systems exist, primarily glutathione redox buffer (Schafer and Buettner, 2001). Redox state is defined as a relation of reduced glutathione (GSH) and glutathione disulfide (GSSG). GSSG is reduced by glutathione reductase. Different cell compartments maintain redox potential independently. It was demonstrated that IMS is more oxidizing than cytosol and mitochondrial matrix (Hu et al., 2008). ROS can oxidize cysteine residues in proteins. On the other hand, glutathione protects cysteine-containing proteins from over-oxidation. The proofreading activity of glutathione in the

disulfide relay was shown (Bien et al., 2010). Thus, disulfide relay and the maintenance of the redox homeostasis in the IMS are tightly connected (Herrmann and Köhl, 2007).

Mia40 and ERV1 are functionally conserved in mammals, fungi and plants. In trypanosomatids, distantly related to these organisms, the ERV1 orthologue was characterized (Basu et al., 2013; Eckers et al., 2013) and was proved to be functionally conserved: mutated ERV1 of *Leishmania tarentolae* (LtERV1) can complement yeast ERV1 (Specht et al., 2018). *Trypanosoma brucei* ERV1 (TbERV1) is involved in the import of classical MIA pathway substrates like small TIMs (Peikert et al., 2017). No Mia40 orthologue was found in trypanosomatids so far (Allen et al., 2008; Deponte and Hell, 2009; Haindrich et al., 2017). In our recent study, we demonstrated that TbMic20, thioredoxin-like protein responsible for cristae formation, has CIPC reaction center, similar to the CPC motif of human Mia40 (Kaurov et al., 2018). Depletion of TbMic20 resulted in reduced abundance of IMS proteins including small TIMs and phenocopied depletion of TbERV1. TbMic20 was hypothesized to be as putative functional analog of Mia40 (Kaurov et al., 2018). In this chapter, I address the role of TbMic20 and the structure of *T. brucei* disulfide relay. We performed experiments to investigate the role of CIPC motif in the function of TbMic20. The ability of TbMic20 to substitute proteins that perform oxidative folding in other systems, is addressed. Our ultimate goal to purify TbMic20-substrate intermediates *in vivo* would provide strong support for our hypothesis. We performed preliminary experiments to demonstrate the ability to detect TbMic20-substrate complexes.

the following pages 85-94 contain classified information which is available only in the archived original of the graduation thesis deposited at the relevant USB Faculty

References

Alibu, V.P., Storm, L., Haile, S., Clayton, C., Horn, D., 2005. A doubly inducible system for RNA interference and rapid RNAi plasmid construction in Trypanosoma brucei. Molecular and Biochemical Parasitology 139, 75–82. https://doi.org/10.1016/j.molbiopara.2004.10.002

Allen, J.W.A., Ferguson, S.J., Ginger, M.L., 2008. Distinctive biochemistry in the trypanosome mitochondrial intermembrane space suggests a model for stepwise evolution of the MIA pathway for import of cysteine-rich proteins. FEBS Letters 582, 2817–2825. https://doi.org/10.1016/j.febslet.2008.07.015

Arts, I.S., Ball, G., Leverrier, P., Garvis, S., Nicolaes, V., Vertommen, D., Ize, B., Tamu Dufe, V., Messens, J., Voulhoux, R., Collet, J.-F., 2013. Dissecting the Machinery That Introduces Disulfide Bonds in Pseudomonas aeruginosa. mBio 4, e00912-13. https://doi.org/10.1128/mBio.00912-13

Baker, M.J., Mooga, V.P., Guiard, B., Langer, T., Ryan, M.T., Stojanovski, D., 2012. Impaired Folding of the Mitochondrial Small TIM Chaperones Induces Clearance by the i-AAA Protease. Journal of Molecular Biology 424, 227–239. https://doi.org/10.1016/j.jmb.2012.09.019

Banci, L., Bertini, I., Cefaro, C., Cenacchi, L., Ciofi-Baffoni, S., Felli, I.C., Gallo, A., Gonnelli, L., Luchinat, E., Sideris, D., Tokatlidis, K., 2010. Molecular chaperone function of Mia40 triggers consecutive induced folding steps of the substrate in mitochondrial protein import. Proceedings of the National Academy of Sciences 107, 20190–20195. https://doi.org/10.1073/pnas.1010095107

Banci, L., Bertini, I., Cefaro, C., Ciofi-Baffoni, S., Gallo, A., Martinelli, M., Sideris, D.P., Katrakili, N., Tokatlidis, K., 2009. MIA40 is an oxidoreductase that catalyzes oxidative protein folding in mitochondria. Nat Struct Mol Biol 16, 198–206. https://doi.org/10.1038/nsmb.1553

Basu, S., Leonard, J.C., Desai, N., Mavridou, D.A.I., Tang, K.H., Goddard, A.D., Ginger, M.L., Lukeš, J., Allen, J.W.A., 2013. Divergence of Erv1-Associated Mitochondrial Import and Export Pathways in Trypanosomes and Anaerobic Protists. Eukaryotic Cell 12, 343–355. https://doi.org/10.1128/EC.00304-12

Becker, T., Böttinger, L., Pfanner, N., 2012. Mitochondrial protein import: from transport pathways to an integrated network. Trends in Biochemical Sciences 37, 85–91. https://doi.org/10.1016/j.tibs.2011.11.004

Bien, M., Longen, S., Wagener, N., Chwalla, I., Herrmann, J.M., Riemer, J., 2010. Mitochondrial Disulfide Bond Formation Is Driven by Intersubunit Electron Transfer in

Erv1 and Proofread by Glutathione. Molecular Cell 37, 516–528. https://doi.org/10.1016/j.molcel.2010.01.017
Cavallaro, G., 2010. Genome-wide analysis of eukaryotic twin CX9C proteins. Mol. BioSyst. 6, 2459. https://doi.org/10.1039/c0mb00058b
Chacinska, A., Koehler, C.M., Milenkovic, D., Lithgow, T., Pfanner, N., 2009. Importing Mitochondrial Proteins: Machineries and Mechanisms. Cell 138, 628–644. https://doi.org/10.1016/j.cell.2009.08.005
Chacinska, A., Pfannschmidt, S., Wiedemann, N., Kozjak, V., Sanjuán Szklarz, L.K., Schulze-Specking, A., Truscott, K.N., Guiard, B., Meisinger, C., Pfanner, N., 2004. Essential role of Mia40 in import and assembly of mitochondrial intermembrane space proteins. EMBO J 23, 3735–3746. https://doi.org/10.1038/sj.emboj.7600389
Dailey, F.E., Berg, H.C., 1993. Mutants in disulfide bond formation that disrupt flagellar assembly in Escherichia coli. Proceedings of the National Academy of Sciences 90, 1043–1047. https://doi.org/10.1073/pnas.90.3.1043
Deponte, M., Hell, K., 2009. Disulphide Bond Formation in the Intermembrane Space of Mitochondria. Journal of Biochemistry 146, 599–608. https://doi.org/10.1093/jb/mvp133
Eckers, E., Petrungaro, C., Gross, D., Riemer, J., Hell, K., Deponte, M., 2013. Divergent Molecular Evolution of the Mitochondrial Sulfhydryl:Cytochrome *c* Oxidoreductase Erv in Opisthokonts and Parasitic Protists. J. Biol. Chem. 288, 2676–2688. https://doi.org/10.1074/jbc.M112.420745
Fischer, M., Riemer, J., 2013. The Mitochondrial Disulfide Relay System: Roles in Oxidative Protein Folding and Beyond. International Journal of Cell Biology 2013, 1–12. https://doi.org/10.1155/2013/742923
Fraga, H., Bech-Serra, J.-J., Canals, F., Ortega, G., Millet, O., Ventura, S., 2014. The Mitochondrial Intermembrane Space Oxireductase Mia40 Funnels the Oxidative Folding Pathway of the Cytochrome *c* Oxidase Assembly Protein Cox19. J. Biol. Chem. 289, 9852–9864. https://doi.org/10.1074/jbc.M114.553479
Gibson, D.G., Young, L., Chuang, R.-Y., Venter, J.C., Hutchison, C.A., Smith, H.O., 2009. Enzymatic assembly of DNA molecules up to several hundred kilobases. Nat Methods 6, 343–345. https://doi.org/10.1038/nmeth.1318
Haindrich, A.C., Boudová, M., Vancová, M., Diaz, P.P., Horáková, E., Lukeš, J., 2017. The intermembrane space protein Erv1 of Trypanosoma brucei is essential for mitochondrial Fe-S cluster assembly and operates alone. Molecular and Biochemical Parasitology 214, 47–51. https://doi.org/10.1016/j.molbiopara.2017.03.009
Herrmann, J.M., Köhl, R., 2007. Catch me if you can! Oxidative protein trapping in the intermembrane space of mitochondria. J Cell Biol 176, 559–563. https://doi.org/10.1083/jcb.200611060
Hofhaus, G., Lee, J.-E., Tews, I., Rosenberg, B., Lisowsky, T., 2003. The N-terminal cysteine pair of yeast sulfhydryl oxidase Erv1p is essential for in vivo activity and interacts with the primary redox centre. Eur J Biochem 270, 1528–1535. https://doi.org/10.1046/j.1432-1033.2003.03519.x
Hu, J., Dong, L., Outten, C.E., 2008. The Redox Environment in the Mitochondrial Intermembrane Space Is Maintained Separately from the Cytosol and Matrix. J. Biol. Chem. 283, 29126–29134. https://doi.org/10.1074/jbc.M803028200

Kasahara, A., Scorrano, L., 2014. Mitochondria: from cell death executioners to regulators of cell differentiation. Trends in Cell Biology 24, 761–770. https://doi.org/10.1016/j.tcb.2014.08.005

Kaurov, I., Vancová, M., Schimanski, B., Cadena, L.R., Heller, J., Bílý, T., Potěšil, D., Eichenberger, C., Bruce, H., Oeljeklaus, S., Warscheid, B., Zdráhal, Z., Schneider, A., Lukeš, J., Hashimi, H., 2018. The Diverged Trypanosome MICOS Complex as a Hub for Mitochondrial Cristae Shaping and Protein Import. Current Biology 28, 3393-3407.e5. https://doi.org/10.1016/j.cub.2018.09.008

Kawano, S., Yamano, K., Naoe, M., Momose, T., Terao, K., Nishikawa, S. -i., Watanabe, N., Endo, T., 2009. Structural basis of yeast Tim40/Mia40 as an oxidative translocator in the mitochondrial intermembrane space. Proceedings of the National Academy of Sciences 106, 14403–14407. https://doi.org/10.1073/pnas.0901793106

Kühlbrandt, W., 2015. Structure and function of mitochondrial membrane protein complexes. BMC Biol 13, 89. https://doi.org/10.1186/s12915-015-0201-x

Mesecke, N., Terziyska, N., Kozany, C., Baumann, F., Neupert, W., Hell, K., Herrmann, J.M., 2005. A Disulfide Relay System in the Intermembrane Space of Mitochondria that Mediates Protein Import. Cell 121, 1059–1069. https://doi.org/10.1016/j.cell.2005.04.011

Milenkovic, D., Ramming, T., Wenz, L.-S., Gebert, N., Schulze-Specking, A., Stojanovski, D., Rospert, S., Chacinska, A., 2009. Identification of the Signal Directing Tim9 and Tim10 into the Intermembrane Space of Mitochondria. Molecular Biology of the Cell 20, 10.

Mordas, A., Tokatlidis, K., 2015. The MIA Pathway: A Key Regulator of Mitochondrial Oxidative Protein Folding and Biogenesis. Acc. Chem. Res. 48, 2191–2199. https://doi.org/10.1021/acs.accounts.5b00150

Morgenstern, M., Stiller, S.B., Lübbert, P., Peikert, C.D., Dannenmaier, S., Drepper, F., Weill, U., Höß, P., Feuerstein, R., Gebert, M., Bohnert, M., van der Laan, M., Schuldiner, M., Schütze, C., Oeljeklaus, S., Pfanner, N., Wiedemann, N., Warscheid, B., 2017. Definition of a High-Confidence Mitochondrial Proteome at Quantitative Scale. Cell Reports 19, 2836–2852. https://doi.org/10.1016/j.celrep.2017.06.014

Murphy, M.P., 2009. How mitochondria produce reactive oxygen species. Biochem. J. 417, 1–13. https://doi.org/10.1042/BJ20081386

Neupert, W., Herrmann, J.M., 2007. Translocation of Proteins into Mitochondria. Annu. Rev. Biochem. 76, 723–749. https://doi.org/10.1146/annurev.biochem.76.052705.163409

Pagliarini, D.J., Calvo, S.E., Chang, B., Sheth, S.A., Vafai, S.B., Ong, S.-E., Walford, G.A., Sugiana, C., Boneh, A., Chen, W.K., Hill, D.E., Vidal, M., Evans, J.G., Thorburn, D.R., Carr, S.A., Mootha, V.K., 2008. A Mitochondrial Protein Compendium Elucidates Complex I Disease Biology. Cell 134, 112–123. https://doi.org/10.1016/j.cell.2008.06.016

Panigrahi, A.K., Ogata, Y., Zíková, A., Anupama, A., Dalley, R.A., Acestor, N., Myler, P.J., Stuart, K.D., 2009. A comprehensive analysis of Trypanosoma brucei mitochondrial proteome. Proteomics 9, 434–450. https://doi.org/10.1002/pmic.200800477

Peikert, C.D., Mani, J., Morgenstern, M., Käser, S., Knapp, B., Wenger, C., Harsman, A., Oeljeklaus, S., Schneider, A., Warscheid, B., 2017. Charting organellar importomes by quantitative mass spectrometry. Nat Commun 8, 15272. https://doi.org/10.1038/ncomms15272

Schafer, F.Q., Buettner, G.R., 2001. Redox environment of the cell as viewed through the redox state of the glutathione disulfide/glutathione couple. Free Radical Biology and Medicine 30, 1191–1212. https://doi.org/10.1016/S0891-5849(01)00480-4

Sideris, D.P., Petrakis, N., Katrakili, N., Mikropoulou, D., Gallo, A., Ciofi-Baffoni, S., Banci, L., Bertini, I., Tokatlidis, K., 2009. A novel intermembrane space–targeting signal docks cysteines onto Mia40 during mitochondrial oxidative folding. J Cell Biol 187, 1007–1022. https://doi.org/10.1083/jcb.200905134

Specht, S., Liedgens, L., Duarte, M., Stiegler, A., Wirth, U., Eberhardt, M., Tomás, A., Hell, K., Deponte, M., 2018. A single-cysteine mutant and chimeras of essential Leishmania Erv can complement the loss of Erv1 but not of Mia40 in yeast. Redox Biology 15, 363–374. https://doi.org/10.1016/j.redox.2017.12.010

Stehling, O., Lill, R., 2013. The Role of Mitochondria in Cellular Iron-Sulfur Protein Biogenesis: Mechanisms, Connected Processes, and Diseases. Cold Spring Harbor Perspectives in Biology 5, a011312–a011312. https://doi.org/10.1101/cshperspect.a011312

Stojanovski, D., Müller, J.M., Milenkovic, D., Guiard, B., Pfanner, N., Chacinska, A., 2008. The MIA system for protein import into the mitochondrial intermembrane space. Biochimica et Biophysica Acta (BBA) - Molecular Cell Research 1783, 610–617. https://doi.org/10.1016/j.bbamcr.2007.10.004

Wiedemann, N., Frazier, A.E., Pfanner, N., 2004. The Protein Import Machinery of Mitochondria. J. Biol. Chem. 279, 14473–14476. https://doi.org/10.1074/jbc.R400003200

Wrobel, L., Trojanowska, A., Sztolsztener, M.E., Chacinska, A., 2013. Mitochondrial protein import: Mia40 facilitates Tim22 translocation into the inner membrane of mitochondria. MBoC 24, 543–554. https://doi.org/10.1091/mbc.e12-09-0649

5. Conclusions and perspectives

This study represents the first characterization of the MICOS complex outside opisthokonts. Among nine TbMICOS subunits only two paralogs of Mic10 retain enough sequence similarity with opisthokont proteins to be recognized bioinformatically. Other TbMICOS subunits were immunoprecipitated using two TbMic10 paralogs as a bait and subsequently characterized. In such a distant relative of opisthokonts as *T. brucei*, MICOS retained its characteristic function, a role in cristae shaping, CJ biogenesis, and contact site formation. We demonstrated that upon depletion of several TbMICOS subunits cristae shape is significantly altered and the number of crista junctions is reduced. Despite its role in CJ biogenesis, TbMICOS is not concentrated in CJs but is rather spread throughout the cristae membrane. Hypothetically the reason is that discoidal cristae are formed by different mechanism than lamellar cristae of opisthokonts. The reasons why cristae have different shapes in different organisms and what proteins define these differences, is still unanswered. Also, it is not clear if cristae shape itself has any adaptive function.

Another MICOS feature conserved among opisthokonts and excavates, is close association with Sam50. Sam50 was co-immunoprecipitated with TbMICOS despite the fact that the protein we putatively designate as TbMic60 lacks a mitofilin domain, which is responsible for interaction with Sam50 in yeast and mammals. Presumably another subunit named TbMic34 may be mitofilin domain, but this hypothesis needs to be tested.

Similar to opisthokont MICOS, TbMICOS consists of two subcomplexes. The principles of their organization are different than in opisthokonts. One of TbMICOS subcomplexes is comprised of integral membrane subunits predominantly responsible for crista biogenesis. Another one consists of peripheral subunits facilitating protein import. In contrast, opisthokont MICOS subcomplexes are organized around the most conserved Mic10 and Mic60.

Among novel features of TbMICOS is an apparent direct participation in IMS protein import. A thioredoxin-like protein TbMic20 is responsible for the import of small proteins that require oxidative folding in the IMS. The TbMic20 depletome overlaps with the depletome of TbErv1, the only protein identified so far to perform IMS protein import in *T. brucei*. Mia40, the

oxidoreductase responsible for oxidative protein folding in opisthokonts, is missing in trypanosomatids. We demonstrated a role of TbMic20 in IMS protein import *in vivo* and *in vitro*. Furthermore, we demonstrated that TbMic20 can complement the bacterial protein DsbA, which has an established role in oxidative protein folding in the periplasm of alphaproteobacteria. The CIPC motif of TbMic20 resembles the CPC motif of Mia40. We demonstrated the importance of the CIPC motif for protein import made some initial steps in the direct detection of TbMic20 covalently bound to substrates. Successful purification of intermediates will prove with certainty that TbMic20 is the functional analog of opisthokont Mia40. Detailed description of the oxidative folding process is also missing, and further experiments are required. Whether protein folding and other novel TbMICOS features described in this study are restricted to closely related trypanosomatid species or whether they are found other excavates or even supergroups is a question to be addressed by further studies.

References

Aaltonen, M.J., Friedman, J.R., Osman, C., Salin, B., di Rago, J.-P., Nunnari, J., Langer, T., Tatsuta, T., 2016. MICOS and phospholipid transfer by Ups2–Mdm35 organize membrane lipid synthesis in mitochondria. J Cell Biol 213, 525–534. https://doi.org/10.1083/jcb.201602007

Adl, S.M., Bass, D., Lane, C.E., Lukeš, J., Schoch, C.L., Smirnov, A., Agatha, S., Berney, C., Brown, M.W., Burki, F., Cárdenas, P., Čepička, I., Chistyakova, L., del Campo, J., Dunthorn, M., Edvardsen, B., Eglit, Y., Guillou, L., Hampl, V., Heiss, A.A., Hoppenrath, M., James, T.Y., Karpov, S., Kim, E., Kolisko, M., Kudryavtsev, A., Lahr, D.J.G., Lara, E., Le Gall, L., Lynn, D.H., Mann, D.G., Massana i Molera, R., Mitchell, E.A.D., Morrow, C., Park, J.S., Pawlowski, J.W., Powell, M.J., Richter, D.J., Rueckert, S., Shadwick, L., Shimano, S., Spiegel, F.W., Torruella i Cortes, G., Youssef, N., Zlatogursky, V., Zhang, Q., 2018. Revisions to the Classification, Nomenclature, and Diversity of Eukaryotes. J. Eukaryot. Microbiol. jeu.12691. https://doi.org/10.1111/jeu.12691

Agier, V., Oliviero, P., Lainé, J., L'Hermitte-Stead, C., Girard, S., Fillaut, S., Jardel, C., Bouillaud, F., Bulteau, A.L., Lombès, A., 2012. Defective mitochondrial fusion, altered respiratory function, and distorted cristae structure in skin fibroblasts with heterozygous OPA1 mutations. Biochimica et Biophysica Acta (BBA) - Molecular Basis of Disease 1822, 1570–1580. https://doi.org/10.1016/j.bbadis.2012.07.002

Alkhaja, A.K., Jans, D.C., Nikolov, M., Vukotic, M., Lytovchenko, O., Ludewig, F., Schliebs, W., Riedel, D., Urlaub, H., Jakobs, S., Deckers, M., 2012. MINOS1 is a conserved component of mitofilin complexes and required for mitochondrial function and cristae organization. MBoC 23, 247–257. https://doi.org/10.1091/mbc.e11-09-0774

Allen, J.W.A., Ferguson, S.J., Ginger, M.L., 2008. Distinctive biochemistry in the trypanosome mitochondrial intermembrane space suggests a model for stepwise evolution of the MIA pathway for import of cysteine-rich proteins. FEBS Letters 582, 2817–2825. https://doi.org/10.1016/j.febslet.2008.07.015

Altmann, R., 1890. Die Elementarorganismen und ihre Beziehungen zu den Zellen. Leipzig, Verlag Von Veit & comp.

Altschul, S.F., Madden, T.L., Schäffer, A.A., Zhang, J., Zhang, Z., Miller, W., Lipman, D.J., 1997. Gapped BLAST and PSI-BLAST: a new generation of protein database search programs. Nucleic Acids Research 25, 3389–3402. https://doi.org/10.1093/nar/25.17.3389

Anand, R., Strecker, V., Urbach, J., Wittig, I., Reichert, A.S., 2016. Mic13 Is Essential for Formation of Crista Junctions in Mammalian Cells. PLoS ONE 11, e0160258. https://doi.org/10.1371/journal.pone.0160258

Anderson, S., Bankier, A.T., Barrell, B.G., de Bruijn, M.H.L., Coulson, A.R., Drouin, J., Eperon, I.C., Nierlich, D.P., Roe, B.A., Sanger, F., Schreier, P.H., Smith, A.J.H., Staden, R., Young, I.G., 1981. Sequence and organization of the human mitochondrial genome. Nature 290, 457–465.

Andersson, S.G.E., Zomorodipour, A., Andersson, J.O., Sicheritz-Pontén, T., Alsmark, U.C.M., Podowski, R.M., Näslund, A.K., Eriksson, A.-S., Winkler, H.H., Kurland, C.G., 1998. The genome sequence of Rickettsia prowazekii and the origin of mitochondria. Nature 396, 133–140. https://doi.org/10.1038/24094

Archibald, J.M., 2015. Endosymbiosis and Eukaryotic Cell Evolution. Current Biology 25, R911–R921. https://doi.org/10.1016/j.cub.2015.07.055

Ardail, D., Privat, J.P., Egret-Charlier, M., Levrat, C., Lerme, F., Louisot, P., 1990. Mitochondrial contact sites. Lipid composition and dynamics. J. Biol. Chem. 265, 18797–18802.

Bader, M., Muse, W., Ballou, D.P., Gassner, C., Bardwell, J.C.A., 1999. Oxidative Protein Folding Is Driven by the Electron Transport System. Cell 98, 217–227. https://doi.org/10.1016/S0092-8674(00)81016-8

Banci, L., Bertini, I., Cefaro, C., Cenacchi, L., Ciofi-Baffoni, S., Felli, I.C., Gallo, A., Gonnelli, L., Luchinat, E., Sideris, D., Tokatlidis, K., 2010. Molecular chaperone function of Mia40 triggers consecutive induced folding steps of the substrate in mitochondrial protein import. Proceedings of the National Academy of Sciences 107, 20190–20195. https://doi.org/10.1073/pnas.1010095107

Banci, L., Bertini, I., Cefaro, C., Ciofi-Baffoni, S., Gallo, A., Martinelli, M., Sideris, D.P., Katrakili, N., Tokatlidis, K., 2009. MIA40 is an oxidoreductase that catalyzes oxidative protein folding in mitochondria. Nat Struct Mol Biol 16, 198–206. https://doi.org/10.1038/nsmb.1553

Barbot, M., Jans, D.C., Schulz, C., Denkert, N., Kroppen, B., Hoppert, M., Jakobs, S., Meinecke, M., 2015. Mic10 Oligomerizes to Bend Mitochondrial Inner Membranes at Cristae Junctions. Cell Metabolism 21, 756–763. https://doi.org/10.1016/j.cmet.2015.04.006

Barbot, M., Meinecke, M., 2016. Reconstitutions of mitochondrial inner membrane remodeling. Journal of Structural Biology 196, 20–28. https://doi.org/10.1016/j.jsb.2016.07.014

Bardwell, J.C.A., McGovern, K., Beckwith, J., 1991. Identification of a protein required for disulfide bond formation in vivo. Cell 67, 581–589. https://doi.org/10.1016/0092-8674(91)90532-4

Bayrhuber, M., Meins, T., Habeck, M., Becker, S., Giller, K., Villinger, S., Vonrhein, C., Griesinger, C., Zweckstetter, M., Zeth, K., 2008. Structure of the human voltage-dependent anion channel. PNAS 105, 15370–15375.

Bazán, S., Mileykovskaya, E., Mallampalli, V.K.P.S., Heacock, P., Sparagna, G.C., Dowhan, W., 2013. Cardiolipin-dependent Reconstitution of Respiratory Supercomplexes from Purified *Saccharomyces cerevisiae* Complexes III and IV. J. Biol. Chem. 288, 401–411. https://doi.org/10.1074/jbc.M112.425876

Benda, C., 1898. Ueber die Spermatogenese der Vertebraten und höherer Evertebraten, II Theil: die Histiogenese der Spermien. Arch Anal Physiol. 1898; 73: 393–398.

Bensley, R.R., Hoerr, N.L., 1934. Studies on cell structure by the freezing-drying method VI. The preparation and properties of mitochondria. Anat. Rec. 60, 449–455. https://doi.org/10.1002/ar.1090600408

Beverly, K.N., Sawaya, M.R., Schmid, E., Koehler, C.M., 2008. The Tim8–Tim13 Complex Has Multiple Substrate Binding Sites and Binds Cooperatively to Tim23. Journal of Molecular Biology 382, 1144–1156. https://doi.org/10.1016/j.jmb.2008.07.069

Bohnert, M., Zerbes, R.M., Davies, K.M., Mühleip, A.W., Rampelt, H., Horvath, S.E., Boenke, T., Kram, A., Perschil, I., Veenhuis, M., Kühlbrandt, W., van der Klei, I.J., Pfanner, N., van der Laan, M., 2015. Central Role of Mic10 in the Mitochondrial Contact Site and Cristae Organizing System. Cell Metabolism 21, 747–755. https://doi.org/10.1016/j.cmet.2015.04.007

Brown, R.C., Evans, D.A., Vickerman, K., 1973. Changes in oxidative metabolism and ultrastructure accompanying differentiation of the mitochondrion in Trypanosoma brucei. International Journal for Parasitology 3, 691–704. https://doi.org/10.1016/0020-7519(73)90095-7

Campello, S., Scorrano, L., 2010. Mitochondrial shape changes: orchestrating cell pathophysiology. EMBO Rep 11, 678–684. https://doi.org/10.1038/embor.2010.115

Carrie, C., Giraud, E., Duncan, O., Xu, L., Wang, Y., Huang, S., Clifton, R., Murcha, M., Filipovska, A., Rackham, O., Vrielink, A., Whelan, J., 2010. Conserved and Novel Functions for *Arabidopsis thaliana* MIA40 in Assembly of Proteins in Mitochondria and Peroxisomes. J. Biol. Chem. 285, 36138–36148. https://doi.org/10.1074/jbc.M110.121202

Cavalier-Smith, T., 1997. Amoeboflagellates and mitochondrial cristae in eukaryote evolution: megasystematics of the new protozoan subkingdoms eozoa and neozoa. Archiv für Protistenkunde 147, 237–258. https://doi.org/10.1016/S0003-9365(97)80051-6

Chacinska, A., Koehler, C.M., Milenkovic, D., Lithgow, T., Pfanner, N., 2009. Importing Mitochondrial Proteins: Machineries and Mechanisms. Cell 138, 628–644. https://doi.org/10.1016/j.cell.2009.08.005

Chatzi, A., Sideris, D.P., Katrakili, N., Pozidis, C., Tokatlidis, K., 2013. Biogenesis of yeast Mia40 - uncoupling folding from import and atypical recognition features. FEBS J 280, 4960–4969. https://doi.org/10.1111/febs.12482

Chen, X.J., Clark-Walker, G.D., 1999. The Petite Mutation in Yeasts: 50 Years On, in: International Review of Cytology. Elsevier, pp. 197–238. https://doi.org/10.1016/S0074-7696(08)62397-9

Cogliati, S., Enriquez, J.A., Scorrano, L., 2016. Mitochondrial Cristae: Where Beauty Meets Functionality. Trends in Biochemical Sciences 41, 261–273. https://doi.org/10.1016/j.tibs.2016.01.001

Curran, S.P., Leuenberger, D., Leverich, E.P., Hwang, D.K., Beverly, K.N., Koehler, C.M., 2004. The Role of Hot13p and Redox Chemistry in the Mitochondrial TIM22 Import Pathway. J. Biol. Chem. 279, 43744–43751. https://doi.org/10.1074/jbc.M404878200

Daems, W.Th., Wisse, E., 1966. Shape and attachment of the cristae mitochondriales in mouse hepatic cell mitochondria. Journal of Ultrastructure Research 16, 123–140. https://doi.org/10.1016/S0022-5320(66)80027-8

Dailey, F.E., Berg, H.C., 1993. Mutants in disulfide bond formation that disrupt flagellar assembly in Escherichia coli. Proceedings of the National Academy of Sciences 90, 1043–1047. https://doi.org/10.1073/pnas.90.3.1043

Darshi, M., Mendiola, V.L., Mackey, M.R., Murphy, A.N., Koller, A., Perkins, G.A., Ellisman, M.H., Taylor, S.S., 2011. ChChd3, an Inner Mitochondrial Membrane Protein, Is Essential for Maintaining Crista Integrity and Mitochondrial Function. J. Biol. Chem. 286, 2918–2932. https://doi.org/10.1074/jbc.M110.171975

Davies, K.M., Daum, B., 2013. Role of cryo-ET in membrane bioenergetics research. Biochm. Soc. Trans. 41, 1227–1234. https://doi.org/10.1042/BST20130029

Davies, K.M., Strauss, M., Daum, B., Kief, J.H., Osiewacz, H.D., Rycovska, A., Zickermann, V., Kuhlbrandt, W., 2011. Macromolecular organization of ATP synthase and complex I in whole mitochondria. Proceedings of the National Academy of Sciences 108, 14121–14126. https://doi.org/10.1073/pnas.1103621108

de Brito, O.M., Scorrano, L., 2010. An intimate liaison: spatial organization of the endoplasmic reticulum–mitochondria relationship. EMBO J 29, 2715–2723. https://doi.org/10.1038/emboj.2010.177
Dekker, P.J.T., 1997. The Tim core complex defines the number of mitochondrial translocation contact sites and can hold arrested preproteins in the absence of matrix Hsp70-Tim44. The EMBO Journal 16, 5408–5419. https://doi.org/10.1093/emboj/16.17.5408
Deponte, M., Hell, K., 2009. Disulphide Bond Formation in the Intermembrane Space of Mitochondria. Journal of Biochemistry 146, 599–608. https://doi.org/10.1093/jb/mvp133
Dormeyer, M., 2001. Trypanothione-dependent Synthesis of Deoxyribonucleotides by Trypanosoma brucei Ribonucleotide Reductase. J Cell Biol 276, 10602–10606. https://doi.org/10.1074/jbc.M010352200
Dudek, J., Rehling, P., van der Laan, M., 2013. Mitochondrial protein import: Common principles and physiological networks. Biochimica et Biophysica Acta (BBA) - Molecular Cell Research 1833, 274–285. https://doi.org/10.1016/j.bbamcr.2012.05.028
Eble, K. S, Coleman, B., Hantgan, R.R., Cunningham, C., 1990. Tightly Associated Cardiolipin in the Bovine Heart Mitochondrial ATP Synthase as Analyzed by 31P Nuclear Magnetic Resonance Spectroscopy. J. Biol. Chem. 265, 19434–19440.
Eckers, E., Cyrklaff, M., Simpson, L., Deponte, M., 2012. Mitochondrial protein import pathways are functionally conserved among eukaryotes despite compositional diversity of the import machineries. Biological Chemistry 393. https://doi.org/10.1515/hsz-2011-0255
Eichenberger, C., Oeljeklaus, S., Bruggisser, J., Mani, J., Haenni, B., Kaurov, I., Niemann, M., Zuber, B., Lukeš, J., Hashimi, H., Warscheid, B., Schimanski, B., Schneider, A., 2019. The highly diverged trypanosomal MICOS complex is organized in a nonessential integral membrane and an essential peripheral module. Mol Microbiol mmi.14389. https://doi.org/10.1111/mmi.14389
Eme, L., Sharpe, S.C., Brown, M.W., Roger, A.J., 2014. On the Age of Eukaryotes: Evaluating Evidence from Fossils and Molecular Clocks. Cold Spring Harbor Perspectives in Biology 6, a016139–a016139. https://doi.org/10.1101/cshperspect.a016139
Entian, K.D., Barnett, J.A., 1992. Regulation of sugar utilization by Saccharomyces cerevisiae. Trends in Biochemical Sciences 17, 506–510.
Ernster, L., Schatz, G., 1981. Mitochondria: a historical review. J Cell Biol 91, 227s–255s. https://doi.org/10.1083/jcb.91.3.227s
Fairlamb, A.H., 1992. Metabolism and Functions of Trypanothione in the Kinetoplastida. Annu. Rev. Microbiol. 46, 695–729.
Fass, D., 2008. The Erv family of sulfhydryl oxidases. Biochimica et Biophysica Acta (BBA) - Molecular Cell Research 1783, 557–566. https://doi.org/10.1016/j.bbamcr.2007.11.009
Fawcett, D.W., 1981. The cell, 2d ed. ed. W. B. Saunders Co, Philadelphia.
Finn, R.D., Clements, J., Eddy, S.R., 2011. HMMER web server: interactive sequence similarity searching. Nucleic Acids Research 39, W29–W37. https://doi.org/10.1093/nar/gkr367
Flemming, W., 1882. Flemming, W. 1882 . Zellsubstanz, Kem-und Zellteilung. Leipzig.
Frey, T.G., Mannella, C.A., 2000. The internal structure of mitochondria. Trends in Biochemical Sciences 25, 319–324. https://doi.org/10.1016/S0968-0004(00)01609-1
Frezza, C., Cipolat, S., Martins de Brito, O., Micaroni, M., Beznoussenko, G.V., Rudka, T., Bartoli, D., Polishuck, R.S., Danial, N.N., De Strooper, B., Scorrano, L., 2006. OPA1

Controls Apoptotic Cristae Remodeling Independently from Mitochondrial Fusion. Cell 126, 177–189. https://doi.org/10.1016/j.cell.2006.06.025
Friedman, J.R., Lackner, L.L., West, M., DiBenedetto, J.R., Nunnari, J., Voeltz, G.K., 2011. ER Tubules Mark Sites of Mitochondrial Division. Science 334, 358–362. https://doi.org/10.1126/science.1207385
Friedman, J.R., Mourier, A., Yamada, J., McCaffery, J.M., Nunnari, J., 2015. MICOS coordinates with respiratory complexes and lipids to establish mitochondrial inner membrane architecture. eLife 4, e07739. https://doi.org/10.7554/eLife.07739
Gabriel, K., 2003. Tom40, the import channel of the mitochondrial outer membrane, plays an active role in sorting imported proteins. The EMBO Journal 22, 2380–2386. https://doi.org/10.1093/emboj/cdg229
Gabriel, K., Milenkovic, D., Chacinska, A., Müller, J., Guiard, B., Pfanner, N., Meisinger, C., 2007. Novel Mitochondrial Intermembrane Space Proteins as Substrates of the MIA Import Pathway. Journal of Molecular Biology 365, 612–620. https://doi.org/10.1016/j.jmb.2006.10.038
Gebert, N., Joshi, A.S., Kutik, S., Becker, T., McKenzie, M., Guan, X.L., Mooga, V.P., Stroud, D.A., Kulkarni, G., Wenk, M.R., Rehling, P., Meisinger, C., Ryan, M.T., Wiedemann, N., Greenberg, M.L., Pfanner, N., 2009. Mitochondrial Cardiolipin Involved in Outer-Membrane Protein Biogenesis: Implications for Barth Syndrome. Current Biology 19, 2133–2139. https://doi.org/10.1016/j.cub.2009.10.074
Gilkerson, R.W., Margineantu, D.H., Capaldi, R.A., Selker, J.M.L., 2000. Mitochondrial DNA depletion causes morphological changes in the mitochondrial reticulum of cultured human cells. FEBS Letters 474, 1–4. https://doi.org/10.1016/S0014-5793(00)01527-1
Glick, S., Brandt, A., Cunningham, K., Hallberg, R.L., 1992. Cytochromes cl and b2 Are Sorted to the Intermembrane Space of Yeast Mitochondria by a Stop-Transfer Mechanism. Cell 69, 809–822.
Gohil, V.M., Thompson, M.N., Greenberg, M.L., 2005. Synthetic Lethal Interaction of the Mitochondrial Phosphatidylethanolamine and Cardiolipin Biosynthetic Pathways in *Saccharomyces cerevisiae*. J. Biol. Chem. 280, 35410–35416. https://doi.org/10.1074/jbc.M505478200
Gray, M.W., 2012. Mitochondrial Evolution. Cold Spring Harbor Perspectives in Biology 4, a011403–a011403. https://doi.org/10.1101/cshperspect.a011403
Grumbt, B., Stroobant, V., Terziyska, N., Israel, L., Hell, K., 2007. Functional Characterization of Mia40p, the Central Component of the Disulfide Relay System of the Mitochondrial Intermembrane Space. J. Biol. Chem. 282, 37461–37470. https://doi.org/10.1074/jbc.M707439200
Guarani, V., McNeill, E.M., Paulo, J.A., Huttlin, E.L., Fröhlich, F., Gygi, S.P., Van Vactor, D., Harper, J.W., 2015. QIL1 is a novel mitochondrial protein required for MICOS complex stability and cristae morphology. eLife 4, e06265. https://doi.org/10.7554/eLife.06265
Hackenbrock, C.R., 1968. ULTRASTRUCTURAL BASES FOR METABOLICALLY LINKED MECHANICAL ACTIVITY IN MITOCHONDRIA: II. Electron Transport-Linked Ultrastructural Transformations in Mitochondria. The Journal of Cell Biology 37, 345–369. https://doi.org/10.1083/jcb.37.2.345
Haindrich, A.C., Boudová, M., Vancová, M., Diaz, P.P., Horáková, E., Lukeš, J., 2017. The intermembrane space protein Erv1 of Trypanosoma brucei is essential for mitochondrial

Fe-S cluster assembly and operates alone. Molecular and Biochemical Parasitology 214, 47–51. https://doi.org/10.1016/j.molbiopara.2017.03.009
Harner, M., Körner, C., Walther, D., Mokranjac, D., Kaesmacher, J., Welsch, U., Griffith, J., Mann, M., Reggiori, F., Neupert, W., 2011. The mitochondrial contact site complex, a determinant of mitochondrial architecture: Molecular architecture of mitochondria. The EMBO Journal 30, 4356–4370. https://doi.org/10.1038/emboj.2011.379
Harner, M.E., Unger, A.-K., Geerts, W.J., Mari, M., Izawa, T., Stenger, M., Geimer, S., Reggiori, F., Westermann, B., Neupert, W., 2016. An evidence based hypothesis on the existence of two pathways of mitochondrial crista formation. eLife 5, e18853. https://doi.org/10.7554/eLife.18853
Hatefi, Y., Haavik, A.G., Fowler, L.R., Griffiths, D.E., 1962. Studies on the Electron Transfer System. J. Biol. Chem. 237, 2661–2669.
Head, B.P., Zulaika, M., Ryazantsev, S., van der Bliek, A.M., 2011. A novel mitochondrial outer membrane protein, MOMA-1, that affects cristae morphology in *Caenorhabditis elegans*. MBoC 22, 831–841. https://doi.org/10.1091/mbc.e10-07-0600
Herrero, E., Ros, J., Tamarit, J., Bellí, G., 2006. Glutaredoxins in fungi. Photosynth Res 89, 127–140. https://doi.org/10.1007/s11120-006-9079-3
Herrmann, J.M., Riemer, J., 2010. The Intermembrane Space of Mitochondria. Antioxidants & Redox Signaling 13, 1341–1358. https://doi.org/10.1089/ars.2009.3063
Hessenberger, M., Zerbes, R.M., Rampelt, H., Kunz, S., Xavier, A.H., Purfürst, B., Lilie, H., Pfanner, N., van der Laan, M., Daumke, O., 2017. Regulated membrane remodeling by Mic60 controls formation of mitochondrial crista junctions. Nat Commun 8, 15258. https://doi.org/10.1038/ncomms15258
Hizukuri, Y., Yakushi, T., Kawagishi, I., Homma, M., 2006. Role of the Intramolecular Disulfide Bond in FlgI, the Flagellar P-Ring Component of Escherichia coli. Journal of Bacteriology 188, 4190–4197. https://doi.org/10.1128/JB.01896-05
Hofmann, S., Rothbauer, U., Mühlenbein, N., Neupert, W., Gerbitz, K.-D., Brunner, M., Bauer, M.F., 2002. The C66W Mutation in the Deafness Dystonia Peptide 1 (DDP1) Affects the Formation of Functional DDP1·TIM13 Complexes in the Mitochondrial Intermembrane Space. J. Biol. Chem. 277, 23287–23293. https://doi.org/10.1074/jbc.M201154200
Höhr, A.I.C., Straub, S.P., Warscheid, B., Becker, T., Wiedemann, N., 2015. Assembly of β-barrel proteins in the mitochondrial outer membrane. Biochimica et Biophysica Acta (BBA) - Molecular Cell Research 1853, 74–88. https://doi.org/10.1016/j.bbamcr.2014.10.006
Hoppins, S., Collins, S.R., Cassidy-Stone, A., Hummel, E., DeVay, R.M., Lackner, L.L., Westermann, B., Schuldiner, M., Weissman, J.S., Nunnari, J., 2011. A mitochondrial-focused genetic interaction map reveals a scaffold-like complex required for inner membrane organization in mitochondria. J Cell Biol 195, 323–340. https://doi.org/10.1083/jcb.201107053
Hoppins, S.C., Nargang, F.E., 2004. The Tim8-Tim13 Complex of *Neurospora crassa* Functions in the Assembly of Proteins into Both Mitochondrial Membranes. J. Biol. Chem. 279, 12396–12405. https://doi.org/10.1074/jbc.M313037200
Hu, J., Dong, L., Outten, C.E., 2008. The Redox Environment in the Mitochondrial Intermembrane Space Is Maintained Separately from the Cytosol and Matrix. J. Biol. Chem. 283, 29126–29134. https://doi.org/10.1074/jbc.M803028200

Huang, K.C., Ramamurthi, K.S., 2010. Macromolecules that prefer their membranes curvy: Curvature-dependent localization of macromolecules. Molecular Microbiology 76, 822–832. https://doi.org/10.1111/j.1365-2958.2010.07168.x

Huynen, M.A., Mühlmeister, M., Gotthardt, K., Guerrero-Castillo, S., Brandt, U., 2016. Evolution and structural organization of the mitochondrial contact site (MICOS) complex and the mitochondrial intermembrane space bridging (MIB) complex. Biochimica et Biophysica Acta 11.

Imachi, H., Nobu, M.K., Nakahara, N., Morono, Y., Ogawara, M., Takaki, Y., Takano, Y., Uematsu, K., Ikuta, T., Ito, M., Matsui, Y., Miyazaki, M., Murata, K., Saito, Y., Sakai, S., Song, C., Tasumi, E., Yamanaka, Y., Yamaguchi, T., Kamagata, Y., Tamaki, H., Takai, K., 2019. Isolation of an archaeon at the prokaryote-eukaryote interface (preprint). Microbiology. https://doi.org/10.1101/726976

Jaipargas, E.-A., Barton, K.A., Mathur, N., Mathur, J., 2015. Mitochondrial pleomorphy in plant cells is driven by contiguous ER dynamics. Front. Plant Sci. 6. https://doi.org/10.3389/fpls.2015.00783

Jans, D.C., Wurm, C.A., Riedel, D., Wenzel, D., Stagge, F., Deckers, M., Rehling, P., Jakobs, S., 2013. STED super-resolution microscopy reveals an array of MINOS clusters along human mitochondria. Proceedings of the National Academy of Sciences 110, 8936–8941. https://doi.org/10.1073/pnas.1301820110

Jedelský, P.L., Doležal, P., Rada, P., Pyrih, J., Šmíd, O., Hrdý, I., Šedinová, M., Marcinčiková, M., Voleman, L., Perry, A.J., Beltrán, N.C., Lithgow, T., Tachezy, J., 2011. The Minimal Proteome in the Reduced Mitochondrion of the Parasitic Protist Giardia intestinalis. PLoS ONE 6, e17285. https://doi.org/10.1371/journal.pone.0017285

Jensen, R.E., Dunn, C.D., 2002. Protein import into and across the mitochondrial inner membrane: role of the TIM23 and TIM22 translocons. Biochimica et Biophysica Acta (BBA) - Molecular Cell Research 1592, 25–34. https://doi.org/10.1016/S0167-4889(02)00261-6

John, G.B., Shang, Y., Li, L., Renken, C., Mannella, C.A., Selker, J.M.L., Rangell, L., Bennett, M.J., Zha, J., 2005. The Mitochondrial Inner Membrane Protein Mitofilin Controls Cristae Morphology□D. Molecular Biology of the Cell 16, 12.

Kallergi, E., Andreadaki, M., Kritsiligkou, P., Katrakili, N., Pozidis, C., Tokatlidis, K., Banci, L., Bertini, I., Cefaro, C., Ciofi-Baffoni, S., Gajda, K., Peruzzini, R., 2012. Targeting and Maturation of Erv1/ALR in the Mitochondrial Intermembrane Space. ACS Chem. Biol. 7, 707–714. https://doi.org/10.1021/cb200485b

Karnkowska, A., Vacek, V., Zubáčová, Z., Treitli, S.C., Petrželková, R., Eme, L., Novák, L., Žárský, V., Barlow, L.D., Herman, E.K., Soukal, P., Hroudová, M., Doležal, P., Stairs, C.W., Roger, A.J., Eliáš, M., Dacks, J.B., Vlček, Č., Hampl, V., 2016. A Eukaryote without a Mitochondrial Organelle. Current Biology 26, 1274–1284. https://doi.org/10.1016/j.cub.2016.03.053

Kaurov, I., Vancová, M., Schimanski, B., Cadena, L.R., Heller, J., Bílý, T., Potěšil, D., Eichenberger, C., Bruce, H., Oeljeklaus, S., Warscheid, B., Zdráhal, Z., Schneider, A., Lukeš, J., Hashimi, H., 2018. The Diverged Trypanosome MICOS Complex as a Hub for Mitochondrial Cristae Shaping and Protein Import. Current Biology 28, 3393-3407.e5. https://doi.org/10.1016/j.cub.2018.09.008

Keilin, D., King, T.E., 1958. Reconstitution of the Succinic Oxidase System from Soluble Succinic Dehydrogenase and a Particulate Cytochrome System Preparation. Nature 181, 1520–1522. https://doi.org/10.1038/1811520a0
Kojer, K., Bien, M., Gangel, H., Morgan, B., Dick, T.P., Riemer, J., 2012. Glutathione redox potential in the mitochondrial intermembrane space is linked to the cytosol and impacts the Mia40 redox state: E_{GSH} of the IMS is maintained by the cytosol. The EMBO Journal 31, 3169–3182. https://doi.org/10.1038/emboj.2012.165
Kojer, K., Peleh, V., Calabrese, G., Herrmann, J.M., Riemer, J., 2015. Kinetic control by limiting glutaredoxin amounts enables thiol oxidation in the reducing mitochondrial intermembrane space. MBoC 26, 195–204. https://doi.org/10.1091/mbc.E14-10-1422
Koonin, E.V., 2010. The origin and early evolution of eukaryotes in the light of phylogenomics. Genome Biol 11, 209. https://doi.org/10.1186/gb-2010-11-5-209
Körner, C., Barrera, M., Dukanovic, J., Eydt, K., Harner, M., Rabl, R., Vogel, F., Rapaport, D., Neupert, W., Reichert, A.S., 2012. The C-terminal domain of Fcj1 is required for formation of crista junctions and interacts with the TOB/SAM complex in mitochondria. MBoC 23, 2143–2155. https://doi.org/10.1091/mbc.e11-10-0831
Kozjak, V., Wiedemann, N., Milenkovic, D., Lohaus, C., Meyer, H.E., Guiard, B., Meisinger, C., Pfanner, N., 2003. An Essential Role of Sam50 in the Protein Sorting and Assembly Machinery of the Mitochondrial Outer Membrane. J. Biol. Chem. 278, 48520–48523. https://doi.org/10.1074/jbc.C300442200
Krauth-Siegel, R.L., Meiering, S.K., Schmidt, H., 2003. The Parasite-Specific Trypanothione Metabolism of Trypanosoma and Leishmania. Biological Chemistry 384. https://doi.org/10.1515/BC.2003.062
Kritsiligkou, P., Chatzi, A., Charalampous, G., Mironov, A., Grant, C.M., Tokatlidis, K., 2017. Unconventional Targeting of a Thiol Peroxidase to the Mitochondrial Intermembrane Space Facilitates Oxidative Protein Folding. Cell Reports 18, 2729–2741. https://doi.org/10.1016/j.celrep.2017.02.053
Kühlbrandt, W., 2015. Structure and function of mitochondrial membrane protein complexes. BMC Biol 13, 89. https://doi.org/10.1186/s12915-015-0201-x
Kuntzel, H., Noll, H., 1967. Mitochondrial and cytoplasmic polysomes from Neurospora crassa. Nature 215, 1340–1345.
Landeta, C., Boyd, D., Beckwith, J., 2018. Disulfide bond formation in prokaryotes. Nat Microbiol 3, 270–280. https://doi.org/10.1038/s41564-017-0106-2
Lindmark, D.G., Muller, M., 1973. Hydrogenosome, a Cytoplasmic Organelle of the Anaerobic Flagellate Tritrichomonas foetus, and Its Role in Piruvate Metabolism. J. Biol. Chem. 248, 7724–7728.
Lukeš, J., Basu, S., 2015. Fe/S protein biogenesis in trypanosomes — A review. Biochimica et Biophysica Acta (BBA) - Molecular Cell Research 1853, 1481–1492. https://doi.org/10.1016/j.bbamcr.2014.08.015
Lukeš, J., Skalický, T., Týč, J., Votýpka, J., Yurchenko, V., 2014. Evolution of parasitism in kinetoplastid flagellates. Molecular and Biochemical Parasitology 195, 115–122. https://doi.org/10.1016/j.molbiopara.2014.05.007
Mannella, C.A., Pfeiffer, D.R., Bradshaw, P.C., Moraru, I.I., Slepchenko, B., Loew, L.M., Hsieh, C., Buttle, K., Marko, M., 2001. Topology of the Mitochondrial Inner Membrane: Dynamics and Bioenergetic Implications. IUBMB Life (International Union of

Biochemistry and Molecular Biology: Life) 52, 93–100. https://doi.org/10.1080/15216540152845885
Matthews, K.R., 2015. 25 years of African trypanosome research: From description to molecular dissection and new drug discovery. Molecular and Biochemical Parasitology 200, 30–40. https://doi.org/10.1016/j.molbiopara.2015.01.006
Meeusen, S., DeVay, R., Block, J., Cassidy-Stone, A., Wayson, S., McCaffery, J.M., Nunnari, J., 2006. Mitochondrial Inner-Membrane Fusion and Crista Maintenance Requires the Dynamin-Related GTPase Mgm1. Cell 127, 383–395. https://doi.org/10.1016/j.cell.2006.09.021
Mesecke, N., Bihlmaier, K., Grumbt, B., Longen, S., Terziyska, N., Hell, K., Herrmann, J.M., 2008. The zinc-binding protein Hot13 promotes oxidation of the mitochondrial import receptor Mia40. EMBO Rep 9, 1107–1113. https://doi.org/10.1038/embor.2008.173
Michaud, M., Gros, V., Tardif, M., Brugière, S., Ferro, M., Prinz, W.A., Toulmay, A., Mathur, J., Wozny, M., Falconet, D., Maréchal, E., Block, M.A., Jouhet, J., 2016. AtMic60 Is Involved in Plant Mitochondria Lipid Trafficking and Is Part of a Large Complex. Current Biology 26, 627–639. https://doi.org/10.1016/j.cub.2016.01.011
Milenkovic, D., Ramming, T., Wenz, L.-S., Gebert, N., Schulze-Specking, A., Stojanovski, D., Rospert, S., Chacinska, A., 2009. Identification of the Signal Directing Tim9 and Tim10 into the Intermembrane Space of Mitochondria. Molecular Biology of the Cell 20, 10.
Mokranjac, D., Neupert, W., 2010. The many faces of the mitochondrial TIM23 complex. Biochimica et Biophysica Acta (BBA) - Bioenergetics 1797, 1045–1054. https://doi.org/10.1016/j.bbabio.2010.01.026
Mordas, A., Tokatlidis, K., 2015. The MIA Pathway: A Key Regulator of Mitochondrial Oxidative Protein Folding and Biogenesis. Acc. Chem. Res. 48, 2191–2199. https://doi.org/10.1021/acs.accounts.5b00150
Morgenstern, M., Stiller, S.B., Lübbert, P., Peikert, C.D., Dannenmaier, S., Drepper, F., Weill, U., Höß, P., Feuerstein, R., Gebert, M., Bohnert, M., van der Laan, M., Schuldiner, M., Schütze, C., Oeljeklaus, S., Pfanner, N., Wiedemann, N., Warscheid, B., 2017. Definition of a High-Confidence Mitochondrial Proteome at Quantitative Scale. Cell Reports 19, 2836–2852. https://doi.org/10.1016/j.celrep.2017.06.014
Muñoz-Gómez, S.A., Slamovits, C.H., Dacks, J.B., Baier, K.A., Spencer, K.D., Wideman, J.G., 2015a. Ancient Homology of the Mitochondrial Contact Site and Cristae Organizing System Points to an Endosymbiotic Origin of Mitochondrial Cristae. Current Biology 25, 1489–1495. https://doi.org/10.1016/j.cub.2015.04.006
Muñoz-Gómez, S.A., Slamovits, C.H., Dacks, J.B., Wideman, J.G., 2015b. The evolution of MICOS: Ancestral and derived functions and interactions. Communicative & Integrative Biology 8, e1094593. https://doi.org/10.1080/19420889.2015.1094593
Muñoz-Gómez, S.A., Wideman, J.G., Roger, A.J., Slamovits, C.H., 2017. The origin of mitochondrial cristae from alphaproteobacteria. Mol Biol Evol msw298. https://doi.org/10.1093/molbev/msw298
Murley, A., Lackner, L.L., Osman, C., West, M., Voeltz, G.K., Walter, P., Nunnari, J., 2013. ER-associated mitochondrial division links the distribution of mitochondria and mitochondrial DNA in yeast. eLife 2, e00422. https://doi.org/10.7554/eLife.00422
Murphy, M.P., 2009. How mitochondria produce reactive oxygen species. Biochem. J. 417, 1–13. https://doi.org/10.1042/BJ20081386

Nass, S., 1963. INTRAMITOCHONDRIAL FIBERS WITH DNA CHARACTERISTICS: II. Enzymatic and Other Hydrolytic Treatments. The Journal of Cell Biology 19, 613–629. https://doi.org/10.1083/jcb.19.3.613
Neupert, W., Herrmann, J.M., 2007. Translocation of Proteins into Mitochondria. Annu. Rev. Biochem. 76, 723–749. https://doi.org/10.1146/annurev.biochem.76.052705.163409
Osman, C., Voelker, D.R., Langer, T., 2011. Making heads or tails of phospholipids in mitochondria. J Cell Biol 192, 7–16. https://doi.org/10.1083/jcb.201006159
Ott, C., Ross, K., Straub, S., Thiede, B., Gotz, M., Goosmann, C., Krischke, M., Mueller, M.J., Krohne, G., Rudel, T., Kozjak-Pavlovic, V., 2012. Sam50 Functions in Mitochondrial Intermembrane Space Bridging and Biogenesis of Respiratory Complexes. Molecular and Cellular Biology 32, 1173–1188. https://doi.org/10.1128/MCB.06388-11
Pagliarini, D.J., Calvo, S.E., Chang, B., Sheth, S.A., Vafai, S.B., Ong, S.-E., Walford, G.A., Sugiana, C., Boneh, A., Chen, W.K., Hill, D.E., Vidal, M., Evans, J.G., Thorburn, D.R., Carr, S.A., Mootha, V.K., 2008. A Mitochondrial Protein Compendium Elucidates Complex I Disease Biology. Cell 134, 112–123. https://doi.org/10.1016/j.cell.2008.06.016
Palade, G. E., 1953. Palade, G. E. 1953. An electron microscope study of the mitochondrial structure. J. Histochem. Cytochem. 1. 188-211.
Palade, G.E., 1952. The fine structure of mitochondria. Anat. Rec. 114, 427–451. https://doi.org/10.1002/ar.1091140304
Panigrahi, A.K., Ogata, Y., Zíková, A., Anupama, A., Dalley, R.A., Acestor, N., Myler, P.J., Stuart, K.D., 2009. A comprehensive analysis of Trypanosoma brucei mitochondrial proteome. Proteomics 9, 434–450. https://doi.org/10.1002/pmic.200800477
Pedrajas, J.R., Kosmidou, E., Miranda-Vizuete, A., Gustafsson, J.-Å., Wright, A.P.H., Spyrou, G., 1999. Identification and Functional Characterization of a Novel Mitochondrial Thioredoxin System in *Saccharomyces cerevisiae*. J. Biol. Chem. 274, 6366–6373. https://doi.org/10.1074/jbc.274.10.6366
Peleh, V., Zannini, F., Backes, S., Rouhier, N., Herrmann, J.M., 2017. Erv1 of Arabidopsis thaliana can directly oxidize mitochondrial intermembrane space proteins in the absence of redox-active Mia40. BMC Biol 15, 106. https://doi.org/10.1186/s12915-017-0445-8
Perkins, G., Renken, C., Martone, M.E., Young, S.J., Ellisman, M., Frey, T., 1997. Electron Tomography of Neuronal Mitochondria: Three-Dimensional Structure and Organization of Cristae and Membrane Contacts. Journal of Structural Biology 119, 260–272. https://doi.org/10.1006/jsbi.1997.3885
Pfanner, N., van der Laan, M., Amati, P., Capaldi, R.A., Caudy, A.A., Chacinska, A., Darshi, M., Deckers, M., Hoppins, S., Icho, T., Jakobs, S., Ji, J., Kozjak-Pavlovic, V., Meisinger, C., Odgren, P.R., Park, S.K., Rehling, P., Reichert, A.S., Sheikh, M.S., Taylor, S.S., Tsuchida, N., van der Bliek, A.M., van der Klei, I.J., Weissman, J.S., Westermann, B., Zha, J., Neupert, W., Nunnari, J., 2014. Uniform nomenclature for the mitochondrial contact site and cristae organizing system. J Cell Biol 204, 1083–1086. https://doi.org/10.1083/jcb.201401006
Phillips, M.J., Voeltz, G.K., 2016. Structure and function of ER membrane contact sites with other organelles. Nat Rev Mol Cell Biol 17, 69–82. https://doi.org/10.1038/nrm.2015.8
Pittis, A.A., Gabaldón, T., 2016. Late acquisition of mitochondria by a host with chimaeric prokaryotic ancestry. Nature 531, 101–104. https://doi.org/10.1038/nature16941

Porcelli, A.M., Ghelli, A., Zanna, C., Pinton, P., Rizzuto, R., Rugolo, M., 2005. pH difference across the outer mitochondrial membrane measured with a green fluorescent protein mutant. Biochemical and Biophysical Research Communications 326, 799–804. https://doi.org/10.1016/j.bbrc.2004.11.105

Rabl, R., Soubannier, V., Scholz, R., Vogel, F., Mendl, N., Vasiljev-Neumeyer, A., Körner, C., Jagasia, R., Keil, T., Baumeister, W., Cyrklaff, M., Neupert, W., Reichert, A.S., 2009. Formation of cristae and crista junctions in mitochondria depends on antagonism between Fcj1 and Su *e* / *g*. J Cell Biol 185, 1047–1063. https://doi.org/10.1083/jcb.200811099

Rampelt, H., Wollweber, F., Gerke, C., de Boer, R., van der Klei, I.J., Bohnert, M., Pfanner, N., van der Laan, M., 2018. Assembly of the Mitochondrial Cristae Organizer Mic10 Is Regulated by Mic26–Mic27 Antagonism and Cardiolipin. Journal of Molecular Biology 430, 1883–1890. https://doi.org/10.1016/j.jmb.2018.04.037

Reddehase, S., Grumbt, B., Neupert, W., Hell, K., 2009. The Disulfide Relay System of Mitochondria Is Required for the Biogenesis of Mitochondrial Ccs1 and Sod1. Journal of Molecular Biology 385, 331–338. https://doi.org/10.1016/j.jmb.2008.10.088

Rehling, P., Brandner, K., Pfanner, N., 2004. Mitochondrial import and the twin-pore translocase. Nat Rev Mol Cell Biol 5, 519–530. https://doi.org/10.1038/nrm1426

Roesch, K., 2002. Human deafness dystonia syndrome is caused by a defect in assembly of the DDP1/TIMM8a-TIMM13 complex. Human Molecular Genetics 11, 477–486. https://doi.org/10.1093/hmg/11.5.477

Sagan, L., 1967. On the Origin of Mitosing Cells. J. Theoret. Biol 14, 225–274.

Sakowska, P., Jans, D.C., Mohanraj, K., Riedel, D., Jakobs, S., Chacinska, A., 2015. The Oxidation Status of Mic19 Regulates MICOS Assembly. Mol. Cell. Biol. 35, 4222–4237. https://doi.org/10.1128/MCB.00578-15

Santos, H.J., Makiuchi, T., Nozaki, T., 2018. Reinventing an Organelle: The Reduced Mitochondrion in Parasitic Protists. Trends in Parasitology 34, 1038–1055. https://doi.org/10.1016/j.pt.2018.08.008

Sato, Y., Inaba, K., 2012. Disulfide bond formation network in the three biological kingdoms, bacteria, fungi and mammals: Cellular network for disulfide bond formation. FEBS Journal 279, 2262–2271. https://doi.org/10.1111/j.1742-4658.2012.08593.x

Schafer, F.Q., Buettner, G.R., 2001. Redox environment of the cell as viewed through the redox state of the glutathione disulfide/glutathione couple. Free Radical Biology and Medicine 30, 1191–1212. https://doi.org/10.1016/S0891-5849(01)00480-4

Schlame, M., Haldar, D., 1993. Cardiolipin Is Synthesized on the Matrix Side of the Inner Membrane in Rat Liver Mitochondria. J. Biol. Chem. 268, 74–79.

Scorrano, L., Ashiya, M., Buttle, K., Weiler, S., Oakes, S.A., Mannella, C.A., Korsmeyer, S.J., 2002. A Distinct Pathway Remodels Mitochondrial Cristae and Mobilizes Cytochrome c during Apoptosis. Developmental Cell 2, 55–67. https://doi.org/10.1016/S1534-5807(01)00116-2

Sideris, D.P., Petrakis, N., Katrakili, N., Mikropoulou, D., Gallo, A., Ciofi-Baffoni, S., Banci, L., Bertini, I., Tokatlidis, K., 2009. A novel intermembrane space–targeting signal docks cysteines onto Mia40 during mitochondrial oxidative folding. J Cell Biol 187, 1007–1022. https://doi.org/10.1083/jcb.200905134

Simbeni, R., Pon, L., Zinser, E., Paltauf, F., Daum, G., 1991. Mitochondrial membrane contact sites of yeast. Characterization of lipid components and possible involvement in intramitochondrial translocation of phospholipids. J. Biol. Chem. 266, 10047–10049.

Simon, V.R., Theresa C. Swayne, Liza A. Port, 1995. Actin-dependent mitochondrial motility in mitotic yeast and cell-free systems: identification of a motor activity on the mitochondrial surface. The Journal of Cell Biology 130, 345–354. https://doi.org/10.1083/jcb.130.2.345

Sjostrand, F.S., 1953. Electron Mycroscopy of Mitochondria and Cytoplasmic Double Membranes. Nature 171, 30–31.

Smith, T.K., Bringaud, F., Nolan, D.P., Figueiredo, L.M., 2017. Metabolic reprogramming during the Trypanosoma brucei life cycle. F1000Research. https://doi.org/10.12688/f1000research.10342.1

Steverding, D., 2008. The history of African trypanosomiasis. Parasites Vectors 1, 3. https://doi.org/10.1186/1756-3305-1-3

Stojanovski, D., Bragoszewski, P., Chacinska, A., 2012. The MIA pathway: A tight bond between protein transport and oxidative folding in mitochondria. Biochimica et Biophysica Acta (BBA) - Molecular Cell Research 1823, 1142–1150. https://doi.org/10.1016/j.bbamcr.2012.04.014

Stojanovski, D., Müller, J.M., Milenkovic, D., Guiard, B., Pfanner, N., Chacinska, A., 2008. The MIA system for protein import into the mitochondrial intermembrane space. Biochimica et Biophysica Acta (BBA) - Molecular Cell Research 1783, 610–617. https://doi.org/10.1016/j.bbamcr.2007.10.004

Stoldt, S., Stephan, T., Jans, D.C., Brüser, C., Lange, F., Keller-Findeisen, J., Riedel, D., Hell, S.W., Jakobs, S., 2019. Mic60 exhibits a coordinated clustered distribution along and across yeast and mammalian mitochondria. Proc Natl Acad Sci USA 201820364. https://doi.org/10.1073/pnas.1820364116

Summerhayes, I.C., Wong, D., Chen, L.B., 1983. EFFECT OF MICROTUBULES AND INTERMEDIATE FILAMENTS ON MITOCHONDRIAL DISTRIBUTION. J Cell Sci 61, 87–105.

Szalai, G., Krishnamurthy, R., Hajnóczky, G., 1999. Apoptosis driven by IP3-linked mitochondrial calcium signals. EMBO J 18, 6349–6361. https://doi.org/10.1093/emboj/18.22.6349

Tang, J., Zhang, K., Dong, J., Yan, C., Hu, C., Ji, H., Chen, L., Chen, S., Zhao, H., Song, Z., 2019. Sam50–Mic19–Mic60 axis determines mitochondrial cristae architecture by mediating mitochondrial outer and inner membrane contact. Cell Death Differ. https://doi.org/10.1038/s41418-019-0345-2

Tarasenko, D., Barbot, M., Jans, D.C., Kroppen, B., Sadowski, B., Heim, G., Möbius, W., Jakobs, S., Meinecke, M., 2017. The MICOS component Mic60 displays a conserved membrane-bending activity that is necessary for normal cristae morphology. J. Cell Biol. 216, 889–899. https://doi.org/10.1083/jcb.201609046

Taylor, F.J., 1999. Ultrastructure as a Control for Protistan Molecular Phylogeny. The American Naturalist 154.

Terziyska, N., Grumbt, B., Bien, M., Neupert, W., Herrmann, J.M., Hell, K., 2007. The sulfhydryl oxidase Erv1 is a substrate of the Mia40-dependent protein translocation pathway. FEBS Letters 581, 1098–1102. https://doi.org/10.1016/j.febslet.2007.02.014

Tovar, J., León-Avila, G., Sánchez, L.B., Sutak, R., Tachezy, J., van der Giezen, M., Hernández, M., Müller, M., Lucocq, J.M., 2003. Mitochondrial remnant organelles of Giardia function in iron-sulphur protein maturation. Nature 426, 172–176. https://doi.org/10.1038/nature01945

Trindade, S., Rijo-Ferreira, F., Carvalho, T., Pinto-Neves, D., Guegan, F., Aresta-Branco, F., Bento, F., Young, S.A., Pinto, A., Van Den Abbeele, J., Ribeiro, R.M., Dias, S., Smith, T.K., Figueiredo, L.M., 2016. Trypanosoma brucei Parasites Occupy and Functionally Adapt to the Adipose Tissue in Mice. Cell Host & Microbe 19, 837–848. https://doi.org/10.1016/j.chom.2016.05.002

Truscott, K.N., Voos, W., Frazier, A.E., Lind, M., Li, Y., Geissler, A., Dudek, J., Müller, H., Sickmann, A., Meyer, H.E., Meisinger, C., Guiard, B., Rehling, P., Pfanner, N., 2003. A J-protein is an essential subunit of the presequence translocase–associated protein import motor of mitochondria. J Cell Biol 163, 707–713. https://doi.org/10.1083/jcb.200308004

Vafai, S.B., Mootha, V.K., 2012. Mitochondrial disorders as windows into an ancient organelle. Nature 491, 374–383. https://doi.org/10.1038/nature11707

van der Laan, M., Horvath, S.E., Pfanner, N., 2016. Mitochondrial contact site and cristae organizing system. Current Opinion in Cell Biology 41, 33–42. https://doi.org/10.1016/j.ceb.2016.03.013

van der Laan, M., Hutu, D.P., Rehling, P., 2010. On the mechanism of preprotein import by the mitochondrial presequence translocase. Biochimica et Biophysica Acta (BBA) - Molecular Cell Research 1803, 732–739. https://doi.org/10.1016/j.bbamcr.2010.01.013

Voelker, D. R., 1990. Characterization of phosphatidylserine synthesis and translocation in permeabilized animal cells. J. Biol. Chem. 265, 14340–14346.

Vogel, F., Bornhövd, C., Neupert, W., Reichert, A.S., 2006. Dynamic subcompartmentalization of the mitochondrial inner membrane. J Cell Biol 175, 237–247. https://doi.org/10.1083/jcb.200605138

von der Malsburg, K., Müller, J.M., Bohnert, M., Oeljeklaus, S., Kwiatkowska, P., Becker, T., Loniewska-Lwowska, A., Wiese, S., Rao, S., Milenkovic, D., Hutu, D.P., Zerbes, R.M., Schulze-Specking, A., Meyer, H.E., Martinou, J.-C., Rospert, S., Rehling, P., Meisinger, C., Veenhuis, M., Warscheid, B., van der Klei, I.J., Pfanner, N., Chacinska, A., van der Laan, M., 2011. Dual Role of Mitofilin in Mitochondrial Membrane Organization and Protein Biogenesis. Developmental Cell 21, 694–707. https://doi.org/10.1016/j.devcel.2011.08.026

Webb, C.T., Gorman, M.A., Lazarou, M., Ryan, M.T., Gulbis, J.M., 2006. Crystal Structure of the Mitochondrial Chaperone TIM9•10 Reveals a Six-Bladed α-Propeller. Molecular Cell 21, 123–133. https://doi.org/10.1016/j.molcel.2005.11.010

Weber, T.A., Koob, S., Heide, H., Wittig, I., Head, B., van der Bliek, A., Brandt, U., Mittelbronn, M., Reichert, A.S., 2013. APOOL Is a Cardiolipin-Binding Constituent of the Mitofilin/MINOS Protein Complex Determining Cristae Morphology in Mammalian Mitochondria. PLoS ONE 8, e63683. https://doi.org/10.1371/journal.pone.0063683

Wiedemann, N., Frazier, A.E., Pfanner, N., 2004a. The Protein Import Machinery of Mitochondria. J. Biol. Chem. 279, 14473–14476. https://doi.org/10.1074/jbc.R400003200

Wiedemann, N., Pfanner, N., 2017. Mitochondrial Machineries for Protein Import and Assembly. Annu. Rev. Biochem. 86, 685–714. https://doi.org/10.1146/annurev-biochem-060815-014352

Wiedemann, N., Truscott, K.N., Pfannschmidt, S., Guiard, B., Meisinger, C., Pfanner, N., 2004b. Biogenesis of the Protein Import Channel Tom40 of the Mitochondrial Outer Membrane: INTERMEMBRANE SPACE COMPONENTS ARE INVOLVED IN AN EARLY

STAGE OF THE ASSEMBLY PATHWAY. J. Biol. Chem. 279, 18188–18194. https://doi.org/10.1074/jbc.M400050200
Wrobel, L., Trojanowska, A., Sztolsztener, M.E., Chacinska, A., 2013. Mitochondrial protein import: Mia40 facilitates Tim22 translocation into the inner membrane of mitochondria. MBoC 24, 543–554. https://doi.org/10.1091/mbc.e12-09-0649
Wu, H., Carvalho, P., Voeltz, G.K., 2018. Here, there, and everywhere: The importance of ER membrane contact sites. Science 361, eaan5835. https://doi.org/10.1126/science.aan5835
Wurm, C.A., Jakobs, S., 2006. Differential protein distributions define two sub-compartments of the mitochondrial inner membrane in yeast. FEBS Letters 580, 5628–5634. https://doi.org/10.1016/j.febslet.2006.09.012
Xie, J., Marusich, M.F., Souda, P., Whitelegge, J., Capaldi, R.A., 2007. The mitochondrial inner membrane protein Mitofilin exists as a complex with SAM50, metaxins 1 and 2, coiled-coil-helix coiled-coil-helix domain-containing protein 3 and 6 and DnaJC11. FEBS Letters 581, 3545–3549. https://doi.org/10.1016/j.febslet.2007.06.052
Zapun, A., Cooper, L., Creighton, T.E., 1994. Replacement of the Active-Site Cysteine Residues of DsbA, a Protein Required for Disulfide Bond Formation in vivo. Biochemistry 33, 1907–1914. https://doi.org/10.1021/bi00173a038
Zaremba-Niedzwiedzka, K., Caceres, E.F., Saw, J.H., Bäckström, D., Juzokaite, L., Vancaester, E., Seitz, K.W., Anantharaman, K., Starnawski, P., Kjeldsen, K.U., Stott, M.B., Nunoura, T., Banfield, J.F., Schramm, A., Baker, B.J., Spang, A., Ettema, T.J.G., 2017. Asgard archaea illuminate the origin of eukaryotic cellular complexity. Nature 541, 353–358. https://doi.org/10.1038/nature21031
Zerbes, R.M., Höß, P., Pfanner, N., van der Laan, M., Bohnert, M., 2016. Distinct Roles of Mic12 and Mic27 in the Mitochondrial Contact Site and Cristae Organizing System. Journal of Molecular Biology 428, 1485–1492. https://doi.org/10.1016/j.jmb.2016.02.031
Zerbes, R.M., van der Klei, I.J., Veenhuis, M., Pfanner, N., van der Laan, M., Bohnert, M., 2012. Mitofilin complexes: conserved organizers of mitochondrial membrane architecture. Biological Chemistry 393, 1247–1261. https://doi.org/10.1515/hsz-2012-0239
Zhao, J., Lendahl, U., Nistér, M., 2013. Regulation of mitochondrial dynamics: convergences and divergences between yeast and vertebrates. Cell. Mol. Life Sci. 70, 951–976. https://doi.org/10.1007/s00018-012-1066-6
Zick, M., Rabl, R., Reichert, A.S., 2009. Cristae formation—linking ultrastructure and function of mitochondria. Biochimica et Biophysica Acta (BBA) - Molecular Cell Research 1793, 5–19. https://doi.org/10.1016/j.bbamcr.2008.06.013